ANALOG SIMULATION OF AUTOMATIC GLIDE SLOPE CONTROL USING LIFT SPOILERS AS DIRECT LIFT CONTROL

by

Robert Collins Lloyd
and
James Kenneth Swift

UNITED STATES NAVAL POSTGRADUATE SCHOOL

THESIS

ANALOG SIMULATION OF AUTOMATIC GLIDE SLOPE CONTROL USING WING LIFT SPOILERS AS DIRECT LIFT CONTROL

by

Robert Collins Lloyd

and

James Kenneth Swift

June 1968

[redacted]

ANALOG SIMULATION OF AUTOMATIC GLIDE SLOPE CONTROL

USING WING LIFT SPOILERS AS DIRECT LIFT CONTROL

by

Robert Collins Lloyd
Lieutenant, United States Navy
B.S., Texas Technological College, 1960

and

James Kenneth Swift
Lieutenant, United States Navy
B.S., University of Detroit, 1960

Submitted in partial fulfillment of the
requirements for the degree of

AERONAUTICAL ENGINEER

from the

NAVAL POSTGRADUATE SCHOOL
June 1968

ABSTRACT

The use of wing lift spoilers as a means of changing lift without changing angle of attack was studied for use in the landing approach task. The vehicle used was the F-8 type fighter. Automatic glide slope controllers were proposed using an elevator glide slope coupler in conjunction with an automatic power compensator for comparison with an automatic direct lift control system. The system gains were optimized for gust disturbances and initial offsets from glide slope. An analog computer simulation program including a manual control phase was used to determine arbitrary measures of effectiveness of the proposed systems.

TABLE OF CONTENTS

CHAPTER		PAGE
I.	INTRODUCTION	17
II.	DLC IMPLEMENTATION	21
III.	AUTOMATIC GLIDE SLOPE CONTROL	25
	System Description	25
	System Analysis	26
IV.	ANALOG SIMULATION PROGRAM	41
V.	RESULTS AND DISCUSSION	46
VI.	CONCLUSIONS	52
REFERENCES		54
APPENDIX		137

LIST OF TABLES

TABLE		PAGE
I.	Dimensional Stability Derivatives for the F-8 in Approach Configuration	56
II.	Analog Pot Settings	58
III.	Analog Scale Factors	60
IV.	Effectiveness of APC Compared with Basic Airplane and Manual Control	61
V.	Summary of Glide Slope Control Effectiveness . .	62
VI.	Comparison of Effectiveness of Manual and Automatic DLC Systems	64
VII.	Component Transfer Functions	65

[illegible]

[illegible]

[illegible]

[illegible]

[illegible]

[illegible]

[illegible]

[illegible]

[illegible]

[illegible]

LIST OF FIGURES

FIGURE PAGE

1. F-8 Wing Planform 66

2. NACA RM A54H26 Model 2 67

3. C_L vs α, Various Spoiler Deflections, from NACA RM A54H26 Model 2 68

4. C_L vs δ for Various α, NACA RM A54H26 Model 2 69

5. F-8 C_L vs α_W, Effect of Spoiler Deflection (Est.). 70

6. C_D vs α, Various Spoiler Deflections, NACA RM A54H26 Model 2 71

7. C_D vs α in DLC Range, Various Spoiler Deflections, NACA RM A54H26 Model 2 72

8. ΔC_D vs δ for Various α, NACA RM A54H26 73

9. F-8 C_D vs α_W, Effect of Spoiler Deflections (Est.), $C_{D\delta} = -0.07$. 74

10. $C_{M_{cg}}$ vs α_W, Effect of Spoiler Deflection 75

11. Axis System, Arrows Show Positive Direction . . . 76

12. Block Diagram-APC 77

13. Block Diagram-DLC (Auto). 78

14. Block Diagram-EGSC (Auto) 79

15. Root Locus Plot, APC Outer Loop 80

16. Root Locus Plot, DLC Feedback Loop 81

17. Root Locus Plot, DLC Outer Loop 82

18. Block Diagram-PCS System 37

19. Approach Geometry 83

20. Analog Diagram-Basic Airframe 84

FIGURE PAGE

21. Analog Diagram-DLC (AUTO) 85

22. Analog Diagram-APC 86

23. Analog Diagram-EGSC (AUTO) 87

24. Analog Diagram-Pitch Control System 88

25. APC Gain Optimization, u Response to 5 kt Tail Gust, K_u = 400, K_uK_i = Various, K_α = 10,000 89

26. APC Gain Optimization, u Response to . . . . 5 kt Tail Gust, K_u = Various, K_uK_i = .12, K_α = 10,000 90

27. APC Gain Optimization, u Response to 5 kt Tail Gust, K_u = 400, K_uK_i = .12, K_α = Various 91

28. DLC Gain Optimization, h Response to 10 ft Command, $K_{\dot h}$ = - .0073, K_h = Various, K_hK_i = 10^{-5} 92

29. DLC Gain Optimization, h Response to 10 ft Command, $K_{\dot h}$ = Various, K_h = .005, K_hK_i = 10^{-5} 93

30. DLC Gain Optimization, h Response to 10 ft Command, $K_{\dot h}$ = - .0073, K_h = .005, K_hK_i = Various 94

31. EGSC + APC Gain Optimization, Response to 10 ft Command, $K_{\dot h}$ = 4.4 x 10^{-4}, K_h = 5.2 K_hK_i = Various 95

32. EGSC + APC Gain Optimization, Response to 10 ft Command, $K_{\dot h}$ = Various, K_hK_i = 1.73 x 10^{-6} 96

33. APC + EGSC Gain Optimization, h Response to 10 ft Command, K_h = Various, $K_{\dot h}$ = 4.4 x 10^{-4} , K_hK_i = 1.73 97

FIGURE PAGE

34. General Arrangement 98

35. Throttle and Control Stick 99

36. Analog Computer Patch Board 100

37. Pilots Visual Display 101

38. Basic Airframe Response to 5 kt Tail Gust 102

39. Basic Airframe Response to 5 kt Up Gust 103

40. Basic Airframe Response to 5 kt Tail + 5 kt Up Gust 104

41. Basic Airframe Response to 0.01 Step Spoiler 105

42. Basic Airframe Response to 0.05° Step Stabilator 106

43. Airplane + DLC Response to 5 kt Tail Gust 107

44. Airplane + DLC Response to 5 kt Up Gust 108

45. Airplane + DLC Response to 5 kt Tail + 5 kt Up Gust 109

46. Airplane + DLC Response to 10 ft h Command 110

47. Airplane + APC Response to 5 kt Tail Gust 111

48. Airplane + APC Response to 5 kt Up Gust 112

49. Airplane + APC Response to 5 kt Tail + 5 kt Up Gust 113

50. Airplane + DLC + APC Response to 5 kt Tail Gust 114

FIGURE PAGE

51. Airplane + DLC + APC Response to 5 kt Up Gust 115

52. Airplane + DLC + APC Response to 5 kt Tail + 5 kt Up Gust 116

53. Airplane + DLC + APC Response to 10 ft h Command 117

54. Airplane + DLC + APC Response to 10 ft h Command and 5 kt Tail Gust 118

55. Airplane + APC + EGSC Response to 5 kt Tail Gust 119

56. Airplane + APC + EGSC Response to 5 kt Up Gust 120

57. Airplane + APC + EGSC Response to 5 kt Tail Gust and 5 kt Up Gust 121

58. Airplane + APC + EGSC Response to 10 ft h Command 122

59. Airplane + APC + EGSC Response to 5 kt Tail Gust and 10 ft h Command 123

60. Airplane + Pitch Control Response to 1^o Pitch Command 124

61. Manual Throttle + Manual Stabilator Response to 10 ft h Command 125

62. Manual Throttle + Manual Stabilator Response to 5 kt Up Gust 126

63. Manual Throttle + Manual Stabilator Response to 5 kt Tail Gust 127

64. APC + Manual Stabilator Response to 10 ft h Command 128

65. APC + Manual Stabilator Response to 5 kt Up Gust 129

FIGURE		PAGE

66. APC + Manual Stabilator Response to 5 kt Tail Gust 130

67. Manual Throttle + Manual Spoilers Response to 10 ft h Command 131

68. Manual Throttle + Manual Spoilers Response to 5 kt Up Gust 132

69. Manual Throttle + Manual Spoilers Response to 5 kt Tail Gust 133

70. APC + Manual Spoilers Response to 10 ft h Command 134

71. APC + Manual Spoilers Response to 5 kt Up Gust 135

72. APC + Manual Spoilers Response to 5 kt Tail Gust 136

73. Inner Loop, APC System 137

74. Outer Loop, APC System 138

75. Inner Loop, DLC System 140

76. Outer Loop, DLC System 141

77. Simplified PCS System 142

78. Simplified Block Diagram, PCS Outer Loop 143

79. Root Locus Plot, Pitch Control Outer Loop 145

TABLE OF SYMBOLS

Latin Symbols

a_x	Analog scale factor for parameter x
b	Wing span, ft
$\bar{c}$	Mean geometric chord, ft
C_D	Drag coefficient, dimensionless
$C_{D\delta}$	Spoiler drag effectiveness, $\left.\frac{\partial C_D}{\partial \delta}\right)_\alpha$
CE	Characteristic equation
cg	Center of gravity, fraction of $\bar{c}$
C_L	Lift coefficient, dimensionless
$C_{L\delta}$	Spoiler lift effectiveness, $\left.\frac{\partial C_L}{\partial \delta}\right)_\alpha$
$C_{M_{cg}}$	Pitching moment coefficient about cg, dimensionless
g	Acceleration of gravity, ft/sec^2
h	Deviation from glide path, ft
h_c	Glide slope command, ft
h_s	Spoiler projection, ft
K_h	h loop gain constant, 1/ft
$K_{\dot{h}}$	$\dot{h}$ loop gain constant, sec/ft
K_i	Integration loop gain constant, 1/ft
K_u	u loop gain constant, lb sec/ft
K_α	α loop gain constant, lb/rad
K_θ	θ loop gain constant, rad/rad
$K_{\dot{\theta}}$	$\dot{\theta}$ loop gain constant, sec
l_t	Tail lever arm, ft
m	Mass, slugs

N_i	Inboard spoiler location, fraction of b/2
N_o	Outboard spoiler location, fraction of b/2
q	Angular velocity in pitch, rad/sec
s	Laplace operator
T	Thrust perturbation, lbs
T_c	Command thrust perturbation, lbs
T_u	Thrust commanded by u loop, lbs
$T_{\int u}$	Thrust commanded by integration loop, lbs
T_α	Thrust commanded by α loop, lbs
U	Approach airspeed, ft/sec
u	Airspeed perturbation, ft/sec
u_c	Command airspeed perturbation, ft/sec
u_e	Airspeed error, ft/sec
u_g	Airspeed gust, ft/sec
w	Vertical velocity perturbation, ft/sec
W	Gross weight, lbs
x_s	Spoiler chordwise location, ft
X	Force parallel to flight path, lbs
z_T	Thrust lever arm, ft
Z	Force perpendicular to flight path, lbs

Greek Symbols

α	Angle of attack perturbation, rad
α_e	Angle of attack error, rad
α_g	Angle of attack gust, rad
α_w	Wing angle of attack, rad
γ	Glide path angle, rad
δ	Spoiler deflection, fraction of $\bar{c}$
δ_h	Spoiler deflection commanded by h loop, fraction of $\bar{c}$
$\delta_{\int h}$	Spoiler deflection commanded by integration loop, fraction of $\bar{c}$
$\delta_{\dot{h}}$	Spoiler deflection commanded by $\dot{h}$ loop, fraction of $\bar{c}$
ϵ	Thrust angle, rad
ζ	Damping ratio, fraction of critical (dimensionless)
η	Elevator deflection, rad
η_h	Elevator deflection commanded by h loop, rad
$\eta_{\int h}$	Elevator deflection commanded by integration loop, rad
$\eta_{\dot{h}}$	Elevator deflection commanded by $\dot{h}$ loop, rad
η_θ	Elevator deflection commanded by θ loop, rad
$\eta_{\dot{\theta}}$	Elevator deflection commanded by $\dot{\theta}$ loop, rad
Θ	Reference pitch angle, rad
θ	Pitch angle perturbation, rad
θ_c	Pitch angle command, rad
θ_e	Pitch angle error, rad
λ	Wing taper ratio, tip chord/root chord
ρ	Atmospheric density, slugs/ft
τ_e	Engine time lag, sec

Abbreviations

APC	Automatic Power Compensator
AR	Aspect Ratio
AUTO	Automatic
B	Basic airplane, no control inputs
DLC	Direct Lift Control System
EGSC	Elevator Glide Slope Coupler
MAN	Manual
PCS	Pitch Control System

CHAPTER I

INTRODUCTION

Since low aspect ratio, swept wing airplanes exhibit a relative insensitivity to change in lift with angle of attack and a sharp increase in drag with increasing angle of attack, a means of varying lift at constant angle of attack is desirable. Such a method is called Direct Lift Control (DLC) because the airplane is given a near instantaneous vertical acceleration, whereas changing lift by elevator control has an inherent time lag followed by an overshoot due to the airplane's moment of inertia about the pitch axis.

Various forms of DLC are:

1. Lift jets
2. Rotary wings
3. Fast acting wing flaps
4. Wing lift spoilers

Forms 1 and 2 are not applicable here. Form 3, fast acting wing flaps, is treated in References 1 through 5.

Form 4, wing lift spoilers, was first used as DLC on assault gliders in WW II (6). More recently, Bray and Drinkwater of NASA Ames Research Center have flight tested wing lift spoilers as DLC in a large subsonic jet transport; their work is awaiting publication. It is expected that Boeing Airplane Company will employ spoiler DLC on the B2707 SST. The implementation of wing spoilers as DLC is discussed in Chapter II.

At first glance, spoilers seem a negative approach to the problem of close glide slope control; however, one must note that an overall increase in the level of lift is not the intent for which DLC is employed in this context. What is sought here is rapid and precise control of the level of lift in order to maintain an instrument approach glide slope. Lift control is accomplished by trimming the airplane with spoilers extended to some base position; then retraction or further extension from this datum produces the required change in lift. An increase of stall speed is expected when the airplane is trimmed with the spoilers extended. The resulting increase in approach speed may be offset by use of an automatic power compensator which allows lower approach speeds. Also, more precise control of speed enables the approach to be made at a shallower glide slope angle which reduces the rate of descent. Objectionable airframe buffeting caused by extended spoilers may be reduced by venting the spoilers. Of great importance is the favorable drag change when a lift increase is commanded. This is not the case when wing flaps are used as DLC and is certainly not true when elevator control is used. This decrease in drag with increase in lift shows its full importance in the discussion of automatic systems in Chapter V.

In anticipation of Category III operations (zero ceiling-zero visibility landings), very precise glide slope sensors and transmitters are being designed. The Navy has recently developed an Automatic Carrier Landing System (ACLS) (7) which can bring airplanes aboard ship in zero-zero weather. Obviously tight glide slope control is of paramount importance under these circumstances. Automatic glide slope control, discussed in Chapter III, is needed to provide this capability.

The problem of automatic glide slope control is twofold; glide slope must be maintained and airspeed held constant. Automatic control of airspeed through the use of an Automatic Power Compensator (APC) is discussed in References 6, 8, 9, and 10. Automatic glide slope control using DLC with and without APC, Pitch Control System (PCS) without APC, and an Elevator Glide Slope Coupler (EGSC) with APC are proposed in Chapter III.

The linearized, longitudinal equations of motion for small perturbations were used in conjunction with concepts from elementary feedback control theory. Numerical values of the stability derivatives for the Chance Vought F-8 from Reference 9 are used in the equations of motion and are listed in Table I. Loop gains for the systems were approximated by the root locus method using a digital computer program. The gains thus obtained were optimized for various disturbances using the analog components of a Comcor Incorporated Ci 5000 Hybrid Computer.

In Chapter IV a man replaced the automatic systems in the control loop. Potentiometers were affixed to an aircraft type stick and throttle to provide control input signals. Real time display of deviation from trim airspeed and programmed glide slope was accomplished through a single channel 12 inch oscilloscope. A time sharing program was used to present two independent traces simultaneously.

The effectiveness of the various systems was determined from the simulated response of the airplane to horizontal and vertical gusts and to an initial glide slope deviation of 10 feet. Discussion of the results appears in Chapter V. A summary of conclusions and recommendations is found in Chapter VI.

CHAPTER II

DLC IMPLEMENTATION

General

Spoilers were used for DLC in this study because of their near instantaneous response and favorable drag characteristics. A flow separation device such as a spoiler is impossible to analyze using potential flow theory. There are, however, empirical means presented in the literature for the prediction of rolling effectiveness of spoilers in high speed flight (11, 12, 13). When these methods are extended beyond their limits to the high angles of attack used by swept wing aircraft in the landing approach, the results vary greatly. The predicted spoiler lift effectiveness from various sources is as follows:

Reference 11, $C_{L_\delta} = 1.4$

Reference 12, $C_{L_\delta} = 1.6$

Reference 13, $C_{L_\delta} = 2.1$

Reference 14, $C_{L_\delta} = 2.4$

Spoiler Analysis

Since analysis was next to impossible and empirical methods yielded inconsistent results, wind tunnel data were relied upon. A search of available data revealed a case which closely approximated the design in question. Reference (14) includes a remarkably similar wing planform to that of the F-8 aircraft. See Figures 1 and 2. The model was full size and was tested with a fuselage in place.

In the approach configuration, the angle of attack, α_w, range is 11 to 16 degrees for the F-8 (15). Hence the angle of attack range for DLC operation was established.

Pilots use vertical accelerations of order $\pm$ 0.1g to maintain a given glide slope (15). Therefore, the system was called upon to provide ΔC_L of $\pm$ 0.1 in the DLC range.

Reference 16 states that spoilers have little or no lag in operation when located at the 0.7 $\bar{c}$ position. Since ailerons at or near the wing tip are used for lateral control, the spoiler must not extend past the 0.6 b/2 location. The following configuration provides the required ΔC_L and meets the above position constraints.

$$X_s = 0.7\,\bar{c} \qquad N_i = 0.2\ b/2 \qquad N_o = 0.6\ b/2$$

For this configuration, C_L vs α curves were plotted from data in Reference 14 and appear in Figure 3 for various spoiler deflections. Spoiler deflection, δ, is measured in units of non-dimensional spoiler projection normal to the wing surface, $h_s/\bar{c}$. The sense of δ was considered positive for spoiler retraction since this action causes an increase in lift. Spoiler lift effectiveness, C_{L_δ}, is a positive quantity in that an increase in lift is caused by positive spoiler deflection. This is not the case when the system is used. Conversion to the X-Z system is shown in Table I.

Changes in C_L at constant α_w for various δ were plotted in Figure 4. The curves of ΔC_L vs α in Figure 4 do not pass through the origin. The effect was attributed to the re-attachment of the boundary layer when spoiler extensions are small.

The slopes of ΔC_L vs α in the $12.5° < \alpha < 14.6°$ range yielded $C_{L_\delta} = 2.4$. Applying C_{L_δ} to the C_L vs α curve for the F-8 (15), Figure 5, gave the required ΔC_L in the DLC range.

Drag curves (14) are shown in Figure 6. It was noted that virtually all of the drag in the DLC range is due to α, and there is surprisingly little change due to spoiler deflection. Since the drag change due to spoiler deflection is so small, an expanded scale plot of C_D vs α for the DLC range is given in Figure 7. Spoiler drag effectiveness, C_{D_δ}, was computed from the ΔC_D vs δ curve in Figure 8. For $\alpha = 14°$, $C_{D_\delta} = -0.07$. Results of applying C_{D_δ} to the F-8 C_D vs α_W curve (15) are shown in Figure 9 where the steep increase in drag with α is readily apparent.

The pitching moment curves are shown in Figure 10. Negative static stability of the NACA model in the $10° < \alpha_W < 17°$ range was due to the absence of a horizontal tail. When the effect of the tail is added, the system is statically stable at all α_W, as shown in the F-8 C_M vs α curve.

Equations of Motion

The effect of DLC on the dynamics of the airplane is shown in the longitudinal equations of motion. The controls fixed case was applicable here because of the assumption of power operated, irreversible controls.

In anticipation of real time analog flight simulation where a human pilot would be used, the equations of motion were used in dimensional form. All time derivatives were taken with respect to real time as opposed to non-dimensional time which is common practice in stability and control work.

The dimensional equations of motion for the longitudinal, controls fixed case were taken from Reference 17 and altered to include DLC terms. The equations are:

$$\dot{u} = X_u u + U X_w \alpha - g \cos\Theta\, \theta + X_\eta \eta + X_T T + X_\delta \delta$$

$$\dot{\alpha} = \frac{Z_u}{U} u + Z_w \alpha + \dot{\theta} - \frac{g \sin\Theta}{U} \theta + \frac{Z_\eta}{U} \eta + \frac{Z_T}{U} T + \frac{Z}{U} \delta \qquad (1)$$

$$\ddot{\theta} = M_u u + U M_w \alpha + U M_{\dot{w}} \dot{\alpha} + M_q \dot{\theta} + M_\eta \eta + M_T T + M_\delta \delta$$

where the axis system and angle convention is shown in Figure 11. The quantities on the right hand sides of Equations 1 are first order terms of a Taylor's series expansion. The spoiler effectiveness terms $X_\delta \delta$ and $Z_\delta \delta$ were added to the basic equations to represent an input from DLC. A suitable elevator-DLC interconnect was assumed to compensate for trim changes due to spoiler deflection; therefore, $M_\delta \delta$ was not introduced into the control equations.

CHAPTER III

AUTOMATIC GLIDE SLOPE CONTROL

I. SYSTEM DESCRIPTION

APC

In order to provide speed stability for the EGSC and to increase the speed stability of the DLC system, an APC was incorporated in this study. The APC investigated in Reference 9 was used. This system incorporates an automatic throttle controlled by feedbacks of u and α. In anticipation of restrictions on the number of operational amplifiers available on the Ci 5000 analog computer, the system was modified slightly. All time delays were deleted except for the engine acceleration time lag.

Automatic DLC

An automatic DLC system was considered without APC in order to investigate the ability of the system to maintain a given glide slope without the artificial speed stability supplied by the APC system. This step was prompted by the favorable drag characteristics mentioned in Chapter I. The automatic DLC controller used incorporates both position and rate feedback.

Automatic DLC and APC

The automatic DLC was coupled with the APC in order to determine if system performance could be improved by increasing the speed stability of the automatic DLC.

EGSC and APC

The conventional method of controlling attitude, and thus glide path, is with the elevator. The EGSC was selected to provide a basis for the evaluation of the DLC systems mentioned above. As shown in Chapter V, the automatic control of glide slope with an EGSC is impossible without some form of artificial speed stability.

II. SYSTEM ANALYSIS

APC

The block diagram for the modified APC system is shown in Figure 12. With the exception of system time lags, the controller is the same as the one described in Reference 9. The speed of the aircraft is sampled and compared with the desired approach speed. If an error exists, a variation in thrust is commanded to eliminate the error. A parallel control loop samples variations in α and commands a thrust variation in a similar manner. These thrust variations are summed and fed into the airplane aerodynamics. The blocks indicate individual transfer functions which will be derived later. Standard block diagram algebra (18) was used to obtain the APC system transfer function. The result was:

$$\frac{u}{u_c} = \frac{\frac{T_c}{u_e}\frac{u}{T}\frac{T}{T_c}}{1 + \frac{T}{u_e}\frac{u}{T}\frac{T}{T_c} - \frac{T}{T_c}\frac{T_c}{\alpha}\frac{\alpha}{T}} \qquad (2)$$

Automatic DLC

The block diagram for the automatic DLC system is shown in Figure 13. The system consists of an outer loop which incorporates position control with position feedback. The position controller itself consists of a proportional control and an integration term which is supplied to eliminate steady state error. The integral term may be thought of as memory since its effect is to make the actions of the controller depend upon the history of the error. The restoring force is proportional to the product of the average value of the error and time. If a small error continues to exist, the restoring force continues to increase with time.

The inner loop of the automatic DLC system incorporates rate, or derivative, feedback. Rate feedback has the effect of giving the controller the ability to anticipate errors and thus increase the effectiveness of the controller. Thus the output signal of the spoiler controller depends upon both position error and the rate at which position is changing.

An acceleration type feedback was considered for the inner loop but was discarded in favor of the rate feedback system because of the roughness encountered by higher derivative controls.

As in the case of the APC, standard block diagram algebra was used to obtain the overall system transfer function. The result was:

$$\frac{h}{h_c} = \frac{\frac{\delta}{h_e}\frac{\gamma}{\delta}\frac{\dot{h}}{\gamma}\frac{h}{\dot{h}}}{1 + \frac{\delta}{h_e}\frac{\gamma}{\delta}\frac{\dot{h}}{\gamma}\frac{h}{\dot{h}} - \frac{\gamma}{\delta}\frac{\dot{h}}{\gamma}\frac{\delta}{\dot{h}}} \tag{3}$$

<u>EGSC</u>

The block diagram for the EGSC is shown in Figure 14. The controller is identical to that used for the automatic DLC system except that inputs to the airplane aerodynamics are elevator deflections instead of spoiler deflections.

The closed loop transfer function for the EGSC is, from an analysis similar to the above:

$$\frac{h}{h_c} = \frac{\frac{\eta}{h_e}\frac{\gamma}{\eta}\frac{\dot h}{\gamma}\frac{h}{\dot h}}{1 + \frac{\eta}{h_e}\frac{\gamma}{\eta}\frac{\dot h}{\gamma}\frac{h}{\dot h} - \frac{\gamma}{\eta}\frac{\dot h}{\gamma}\frac{\eta_{\dot h}}{\dot h}} \tag{4}$$

Transfer Functions

Basically a transfer function is the ratio of the Laplace transforms of the output of a system to the input. The overall transfer functions of the systems, Equations 2, 3, and 4, are made up of the individual component transfer functions.

In the block diagrams of the various glide slope control systems and the APC, the airframe can be thought of as a plant which produces u, α, and Θ for inputs of T and δ or η. The airframe transfer functions of interest in this study were: $\frac{u}{T}$, $\frac{\alpha}{T}$, and $\frac{\gamma}{T}$ where γ is the glide slope angle perturbation.

In order to derive the airframe transfer functions, Equations 1 were recast into matrix form and use was made of Laplace transform notation. Equations 1 are then:

$$\begin{bmatrix} s - X_u & -UX_w & g\cos\Theta \\ -\frac{Z_u}{U} & (s - Z_w) & -s + g\frac{\sin\Theta}{U} \\ -M_w & -U(M_w + sM_{\dot w}) & s^2 - M_q s \end{bmatrix} \begin{bmatrix} u \\ \alpha \\ \Theta \end{bmatrix} = \begin{bmatrix} X_T & X_\delta & X_\eta \\ \frac{Z_T}{U} & \frac{Z_\delta}{U} & \frac{Z_\eta}{U} \\ M_T & M_\delta & M_\eta \end{bmatrix} \begin{bmatrix} T \\ \delta \\ \eta \end{bmatrix}$$

where the forcing functions are grouped on the right hand side. The individual functions were obtained by Cramer's rule. For example, $\frac{u}{T}$, the airframe's response in airspeed to a change in thrust at constant control deflection is:

$$\frac{u}{T} = \frac{\begin{vmatrix} X_T & -UX_w & g\cos\Theta \\ \frac{Z_T}{U} & s - Z_w & -s + g\frac{\sin\Theta}{U} \\ M_T & -U(M_w + sM_{\dot{w}}) & s^2 - M_q s \end{vmatrix}}{\begin{vmatrix} s - X_u & -UX_w & g\cos\Theta \\ -\frac{Z_u}{U} & s - Z_w & -s + g\frac{\sin\Theta}{U} \\ -M_w & -U(M_w + sM_{\dot{w}}) & s^2 - M_q s \end{vmatrix}} \tag{5}$$

where the denominator is the characteristic equation (CE) of the airframe and is common to all airframe transfer functions. The others are:

$$\frac{\alpha}{T} = \frac{\begin{vmatrix} s - X_u & X_T & g\cos\Theta \\ -\frac{Z_u}{U} & \frac{Z_T}{U} & -s + g\frac{\sin\Theta}{U} \\ -M_w & M_T & s^2 - M_q s \end{vmatrix}}{CE} \tag{6}$$

$$\frac{\alpha}{\delta} = \frac{\begin{vmatrix} s - X_u & X_\delta & g\cos\Theta \\ -\frac{Z_u}{U} & \frac{Z_\delta}{U} & -s + g\frac{\sin\Theta}{U} \\ -M_w & M_\delta & s^2 - M_q s \end{vmatrix}}{CE} \tag{7}$$

$$\frac{\theta}{\delta} = \frac{\begin{vmatrix} s - X_u & -UX_w & X_\delta \\ -\frac{Z_u}{U} & s - Z_w & \frac{Z_\delta}{U} \\ -M_w & -U(M_w + sM_{\dot{w}}) & M_\delta \end{vmatrix}}{CE} \qquad (8)$$

But

$$\gamma = \theta - \alpha \qquad (9)$$

hence

$$\frac{\gamma}{\delta} = \frac{\theta}{\delta} - \frac{\alpha}{\delta} \qquad (10)$$

The reader is reminded that the above relations are but four of the component transfer functions in Equations 2, 3, and 4. Although an analog computer was ultimately used to determine gains for the systems, an estimate of the magnitude of the gains was necessary so that an iteration process could be used. Accordingly, certain well known assumptions were used in the simplification of Equations 5, 6, 7, and 8.

The purpose of the u loop in the APC is to control long period oscillations of airspeed. The well known assumption that the longitudinal motion of the airplane can be separated into long period and short period oscillations was employed here. Long period oscillations in u were assumed to occur at constant α. Equations 1 then become:

$$\begin{bmatrix} s - X_u & g \\ -\frac{Z_u}{U} & -s \end{bmatrix} \begin{bmatrix} u \\ \theta \end{bmatrix} = \begin{bmatrix} X_T \\ 0 \end{bmatrix} \begin{bmatrix} T \end{bmatrix} \qquad (1b)$$

thus

$$\frac{u}{T} = \frac{s X_T}{s^2 - X_u s - g \frac{Z_u}{U}} \tag{5a}$$

The α loop in the APC is provided so that drag due to angle of attack perturbation is compensated by thrust. In accordance with the assumption above, variation in α occurs in the short period oscillation where u is assumed constant. For the short period case Equations 1 become:

$$\begin{bmatrix} s - Z_w & -s \\ -U(M_w + sM_{\dot{w}}) & s^2 - M_q s \end{bmatrix} \begin{bmatrix} \alpha \\ \theta \end{bmatrix} = \begin{bmatrix} 0 \\ M_T \end{bmatrix} [T] \tag{1c}$$

thus

$$\frac{\alpha}{T} = \frac{M_T}{s^2 - (Z_w + M_q + UM_{\dot{w}})s + Z_w M_q - UM_w} \tag{6a}$$

The automatic DLC controls short period deviations from the glide slope, hence, the constant airspeed assumption is used for the DLC transfer function. Equations 1 for the DLC under the short period assumption become

$$\begin{bmatrix} s - Z_w & -s \\ -U(M_w + sM_{\dot{w}}) & s^2 - M_q s \end{bmatrix} \begin{bmatrix} \alpha \\ \theta \end{bmatrix} = \begin{bmatrix} \frac{Z_\delta}{U} \\ 0 \end{bmatrix} [\delta] \tag{1d}$$

thus

$$\frac{\theta}{\delta} = \frac{Z_\delta (M_w + s M_{\dot{w}})}{s[s^2 - (Z_w + M_q + U M_{\dot{w}})s + M_q Z_w - U M_w]} \tag{8a}$$

$$\frac{\alpha}{\delta} = \frac{-\frac{Z_\delta}{U}(s^2 - M_q s)}{s[s^2 - (Z_w + M_q + U M_{\dot{w}})s + M_q Z_w - U M_w]} \tag{7a}$$

hence

$$\frac{\gamma}{\delta} = \frac{\frac{Z_\delta}{U}[s^2 - (U M_{\dot{w}} + M_q)s + U M_w}{s[s^2 - (Z_w + M_q + U M_{\dot{w}})s + M_q Z_w - U M_w]} \tag{11}$$

Rate of deviation from glide slope is given by Reference 3

$$\dot{h} = U\gamma \tag{12}$$

hence

$$\frac{\dot{h}}{\delta} = \frac{Z_\delta [s^2 - (U M_{\dot{w}} + M_q)s + U M_w]}{s[s^2 - (Z_w + M_q + U M_{\dot{w}})s + M_q Z_w - U M_w} \tag{13}$$

From Equation 12

$$h = \int U \gamma \, dt$$

then

$$\frac{h}{\delta} = \frac{Z_\delta [s^2 - (U M_{\dot{w}} + M_q)s + U M_w]}{s^2[s^2 - (Z_w + M_q + U M_{\dot{w}})s + M_q Z_w - U M_w} \tag{14}$$

The remaining component transfer functions are given in Reference 9 and presented here for clarity. The controller transfer functions relate thrust commands to deviations in α or u from desired values. The u loop controller transfer function is

$$\frac{T_c}{u_e} = K_u\left(1 + \frac{K_i}{s}\right)$$

where the $\frac{K_i}{s}$ term is the integral term discussed above. K_u and K_i are the gains which must be determined. The α loop controller transfer function is

$$\frac{T_c}{\alpha_e} = K_\alpha$$

where K_α is another undetermined gain. The engine is approximated by a first order time lag

$$\frac{T}{T_c} = \frac{1}{1+\tau_e s}$$

where τ_e is the spin up lag for the engine and is assumed here to be 1.15 seconds (9). Other lags such as servo lags and airspeed and angle of attack sensing lags were neglected for the reason mentioned earlier.

The remaining component transfer functions in the DLC overall transfer function, Equation 3 and Figure 13, are $\frac{\delta}{h}$, $\frac{h}{\dot{h}}$ and $\frac{\delta_{\dot{h}}}{\dot{h}}$. The position controller, referred to as the glide slope deviation controller, has the following transfer function

$$\frac{\delta}{h_e} = K_h\left(1 + \frac{K_i}{s}\right)$$

where the $\frac{K_i}{s}$ term is provided so that steady state errors in glide slope are eliminated. K_h and K_i are gains to be determined. The deviation rate controller transfer function is

$$\frac{\delta_{\dot{h}}}{\dot{h}} = K_{\dot{h}}$$

where $K_{\dot{h}}$ is another gain to be determined later. The rate of deviation from glide slope is integrated to produce glide slope error. The error in glide slope is fed back to the glide slope deviation controller which commands a corrective spoiler deflection. This spoiler deflection command is summed with the command from the rate controller and then fed into the airplane aerodynamics.

The component transfer functions for the EGSC system are analagous to those for the automatic DLC system.

Estimation of Gains

In each of the foregoing systems there are three unknown gains to be determined. Due to the relative ease with which system parameters can be varied on the analog computer, its use was highly desirable in the selection of loop gains. As stated earlier a reasonable estimation of the gains was needed as a basis for gain optimization. Since the inner loop on each system involved only one unknown gain, the inner loops were analyzed independently and gains were selected for a damping ratio of $\zeta = 0.8$. This procedure is customary in control engineering for the analysis of multiloop systems. The selected gains were inserted into the individual transfer functions, and the inner loops were incorporated into the overall transfer function for each system. The integration gain, K_i, was neglected in the overall transfer function analysis since its presence rather than its value is important in the steady state operation of the system. The outer loops were analyzed and gains were selected as close as possible to $\zeta = 0.5$. The reason for selecting a higher damping ratio for the inner loop was that addition of the outer loop tends to decrease inner loop damping. A more complete analysis than the one shown below can be found in the Appendix.

The transfer function for the inner loop of the APC system is

$$\frac{T_c}{T} = \frac{\frac{T}{T_c}}{1 - \frac{T}{T_c}\frac{T_c}{\alpha_e}\frac{\alpha_e}{T}}$$

Introducing Equations 6a, 16, and 17 along with the numerical values of the stability derivatives from Table I the transfer function becomes

$$\frac{T_c}{T} = \frac{s^2 + 0.806s + 1.281}{s^2 + 0.806s + 1.281 + 4.55 \times 10^{-6} K_\alpha}$$

in which the engine time lag has been neglected to allow a simple second order analysis. The characteristic equation for the inner loop is

$$s^2 + 0.806s + 1.281 + 4.55 \times 10^{-6} K_\alpha = 0$$

from which

$$K_\alpha = -148{,}500 \text{ lb/rad}$$

Using this value for K_α, the inner loop transfer function becomes

$$\frac{T_c}{T} = \frac{s^2 + 0.806s + 1.281}{s^2 + 0.806s + 0.65}$$

With the inner loop transfer function determined, the APC transfer function was found to be

$$\frac{u}{u_c} = \frac{K_u \frac{T_c}{T}\frac{u}{T}}{1 + K_u \frac{T_c}{T}\frac{\alpha}{T}}$$

Inserting the transfer functions and stability derivative values as above, the APC transfer function is

$$\frac{u}{u_c} = \frac{s(0.00145K_u s^2 + 0.00117K_u s + 0.00186K_u)}{s^4 + (0.866 + 0.00145K_u)s^3 + (0.734 + 0.00117K_u)s^2 + (0.07 + 0.001K_u)s}$$

A root locus plot was made for the above system using a digital computer program. The value for K_u found from Figure 15 was

$$K_u = 42 \text{ lb sec/ft}$$

The APC transfer function then becomes

$$\frac{u}{u_c} = \frac{0.06s^3 + 0.049s^2 + 0.078s}{s^4 + 0.926s^3 + 0.783s^2 + 0.146s + 0.023}$$

The gains thus selected were used as initial values in the gain optimization procedure.

In a similar manner, the inner loop transfer function for the automatic DLC system was found to be

$$\frac{\dot{h}}{\delta_h} = \frac{234(0.36s^2 + 0.134s + 0.41)}{s^3 + (0.806 - 84.3K_{\dot{h}})s^2 + (1.281 - 31.4K_{\dot{h}})s - 96K_{\dot{h}}}$$

Root locus analysis of this transfer function, Figure 16, yielded

$$K_{\dot{h}} = -0.003 \text{ sec/ft}$$

from which

$$\frac{\dot{h}}{\delta_h} = \frac{234(0.36s^2 + 0.134s + 0.41)}{s^3 + 1.06s^2 + 1.38s + 0.288}$$

Analysis of the outer loop of the automatic DLC system then yielded

$$\frac{h}{h_c} = \frac{234K_h(0.36s^2 + 0.134s + 0.41}{s^4 + 1.06s^3 + (1.38 + 84.3K_h)s^2 + (0.288 + 31.4K_h)s + 96K_h}$$

From a root locus plot of the above system, Figure 17,

$$K_h = 0.005$$

The overall transfer function for the automatic DLC system is

$$\frac{h}{h_c} = \frac{0.409s^2 + 0.157s + 0.48}{s^4 + 1.06s^3 + 1.8s^2 + 0.445s + 0.48}$$

Since the EGSC system is useless without automatic speed control, and since the analysis of the EGSC system coupled with the APC system would involve a seventh order transfer function, it was decided to attempt gain optimization for this system without estimated values of the gains. The iteration procedure involved is discussed in the next section, Gain Optimization.

In order to demonstrate the lack of feasibility of conventional elevator without APC as an automatic glide slope controller, a simple Pitch Control System (PCS) was devised, Figure 18.

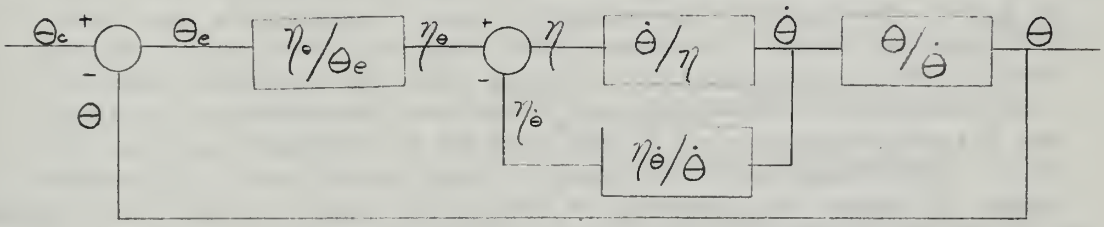

FIGURE 18
BLOCK DIAGRAM-PCS SYSTEM

The inner loop transfer function was found to be

$$\frac{\dot{\theta}}{\eta} = \frac{-(2.25s + 0.867)}{s^2 + (0.806 - 2.25K_\theta)s + (1.281 - 0.867K_\theta)}$$

from which, for $\zeta = 0.8$,

$$K_{\dot{\theta}} = -0.667 \text{ sec}$$

Inserting this value, the overall transfer function was found to be

$$\frac{\theta}{\theta_c} = \frac{-(2.25K_\theta s + 0.867K_\theta)}{s^3 + 2.362s^2 + (1.858 - 2.25K_\theta)s - 0.867K_\theta}$$

From the root locus plot of this transfer function for $\zeta = 0.5$

$$K_\theta = -1.3 \text{ rad/sec}$$

Gain Optimization

Within the framework of the feasible gains determined above, it is possible to find the best values of the gains to give optimum response to various disturbances. To this end a systematic iteration process was employed through the use of the Ci 5000 analog computer and a fast response machine plotter.

The disturbances used were: 1) initial glide slope error of 10 feet low (fly up command), 2) 5 knot tail gust, and 3) 5 knot up gust. The reasons for choosing these disturbances were the difficulties encountered when flying into the turbulent wake of the island structure and flight deck of an aircraft carrier (7). Figure 19 shows the geometry of the mirror approach and the relative location of the airplane when wake turbulence is encountered. The 10 foot error corresponds to a full low deflection on the mirror landing system at 800 feet from touch down. The gusts and glide slope deviations are of necessity small so that the small perturbation assumption is not violated. Relatively small disturbances, however, can produce divergent oscillations if the systems are unstable. It was decided that the glide slope systems would be more sensitive to an h command disturbance, while the APC would be susceptible to a tail gust. The plan was then to optimize the systems for the critical disturbance while maintaining stable response to the other disturbances.

The airplane and the systems were patched into the Ci 5000 according to Figures 20 through 24. Individual potentiometer settings are listed in Table II. The scaling equations are shown in Table III. Gains for the APC, DLC, and EGSC were initially set as determined from the root locus analysis.

In the above analysis of the APC, the integration gain, Ki, was assumed zero. For optimization purposes, a small value of Ki on the order of .01, was used as an initial setting. A feasible value of K_α from the analysis was set; then various values of the u loop gain, K_u, were tried until a stable system with an acceptable rise time of less than, say, 4 seconds was determined. This intermediate value of Ku was then held constant. Then, K_α was varied until an intermediate value of K_α was determined. Finally, the product $K_u K_i$ was varied until steady error was minimized. With $K_u K_i$ set at .12, Ku was varied about its intermediate value using overshoot, rise time, and damping as criteria for choosing a K_u of 400 as optimum. A similar procedure using overshoot as a standard optimized K_α at -10,000. The gains thus obtained are quite different from those predicted by the analysis. This was expected since the loops were assumed independent which they obviously were not. However, a starting point was all that was desired from the analysis. Figures 25, 26, and 27 each show three values of the gains used in optimizing the APC system.

The procedure for optimizing the gains for the DLC system was similar to the above. Values of K_h, $K_{\dot{h}}$, and $K_h K_i$ equal to .005, -.0073, and 10^{-5} respectively, were determined. Figures 28, 29, and 30 show the effect on the system of varying the gains from the optimum. Of particular interest is Figure 28 which confirms what was said earlier, that increasing outer loop gain, K_h, decreases the damping of the whole system. Figure 29 illustrates a divergent response when the rate loop gain, $K_{\dot{h}}$, is decreased in an effort to obtain a shorter rise time. As expected, the integration gain K_i had little effect on the damping of the system.

Gain optimization for the EGSC APC combination was performed directly on the analog computer. It was found that a gross estimation of the gains was all that was necessary if a few more iterations were used. Thus the somewhat lengthy root locus analysis was avoided in this case. Optimum gains for $K_h K_i$, $K_{\dot{h}}$ and K_h were found to be 1.73×10^{-6}, 4.4×10^{-4}, and 5.2×10^{-4}. Effects of varying loop gains are depicted on Figures 31, 32, and 33. An interesting effect is noted on Figure 32 where an increase in $K_{\dot{h}}$ produces separate motion superimposed on the basic oscillation. The source of this motion was not determined, but it was noted that the trace became more erratic as $K_{\dot{h}}$ was increased. This effect established an upper boundary on the inner loop gain. When overshoot is limited to, say, 20 per cent of the initial displacement, the rise times for the EGSC APC combination were twice as long as rise times for the DLC system. This was the first indication of the superiority of the DLC system over the EGSC APC combination.

CHAPTER IV

ANALOG SIMULATION PROGRAM

General

The Analog Simulation was accomplished in three phases. The first phase involved the analog solution of Equations 1 to establish the responses of the basic airplane without control as a standard. Automatic control was introduced in phase two. In the third phase a man was placed in the control loop.

The Comcor Inc. Ci 5000 analog computer was used in this study. A photograph of the control console is provided in Figure 34. The computer has 52 operational amplifiers installed with space provided for 84 more. Of these 52 amplifiers, 20 may be used as integrators. The machine incorporates 48 servo set potentiometers along with 32 manual pots. The servo setting feature allows rapid changing of system parameters. Time scaling for the speeding up or slowing down of the solution is readily accomplished on the logic patch board. The analog computer combined with a SDS 930 digital computer comprise the NPGS Hybrid Computer.

Basic Airplane

The linearized longitudinal equations of motion for small perturbations were used in the Analog Simulation. Numerical values of the stability derivatives for the F-8 were substituted in Equations 1. The equations were then scaled for the 100 volt Ci 5000 according to the scaling equations and scale factors in Table IV. After substitution, scaling and rearrangement, Equations 1 appear as:

$$\dot{\tilde{u}} = -0.101\tilde{u} - 0.0116\tilde{\alpha} - 0.111\tilde{\theta} - 0.292\tilde{T} - 0.006\tilde{\eta} + 0.005\tilde{\delta}$$

$$\dot{\tilde{\alpha}} = -0.544\tilde{u} - 0.43\tilde{\alpha} + \dot{\tilde{\theta}} - 0.01935\tilde{\theta} + 0.082\tilde{\eta} - 0.202\tilde{\delta}$$

$$\ddot{\tilde{\theta}} = 0.031\tilde{u} - 0.398\tilde{\alpha} - 0.015\dot{\tilde{\alpha}} - 0.118\dot{\tilde{\theta}} - 0.785\tilde{\eta} - 0.091\tilde{T}$$

where $\sim$ indicates scaled variables.

The analog circuit diagram for the basic airplane is seen in Figure 20. All such diagrams used herein employ standard symbology; the reader is referred to any good text on analog computer techniques such as References 17, 18, or 19. Although the diagrams are not as concise as they might be, it was felt that clarity was more important than style. Potentiometer settings are found in Table II.

In phase one no control was provided; hence the basic airplane's inherent dynamic stability was relied upon to close the loop. The basic airplane was perturbed from the trimmed state by the following gust disturbances:

1) Tail gust of 5 kt magnitude

2) Up gust of 5 kt

3) Combined 5 kt tail and 5 kt up gust

As stated earlier these disturbances are representative of conditions astern an aircraft carrier making 35 knots in still air. Due to separated flow from the angled deck and the island structure there is turbulence and a defect in velocity extending about 800 to 1000 feet aft of the ship (7, 15). The reader is referred again to Figure 19.

The basic airplane was also subjected to step control inputs of stabilator and DLC spoiler in order to compare their effects.

Automatic control systems introduced in phase two were: 1) APC, 2) DLC, 3) DLC plus APC, 4) EGSC plus APC, and 5) PCS. Circuit diagrams for each component system are provided in Figures 21 through 24. Scale factors are found in Table III, and potentiometer settings are in Table II.

The APC is used to augment the speed stability of the basic airplane and cannot be considered by itself as a means for glide slope control. Therefore, the APC system was subjected to the same gust disturbances as was the basic airplane. In this case the task for the APC was to maintain trimmed airspeed in the influence of a gust.

The glide slope controllers were required to maintain glide slope in the influence of gusts. Additional required tasks were that of returning the airplane to the glide slope from an initial offset of 10 feet low and the combination of initial 10 feet low offset and 5 knots slow.

The PCS system was checked only for its response to a step pitch command. Its inclusion was for the purpose of showing the infeasibility of using automatic elevator without an APC for glide slope control.

Phase three of the simulation used a man in the control loop assisted in some cases by the APC. The pilot was provided with a stick and throttle (Figure 35). Visual cues were provided by traces on a 12 inch oscilloscope pictured in Figure 34. Photographs of the analog and logic patching used for the manned simulation are shown in Figure 36.

Potentiometers were affixed to the stick and throttle through gear trains to assure adequate amplification of the small control movements anticipated. Ten turn potentiometers required an elaborate transmission to effectively use the resolution they provided; hence, the use of these was discarded in favor of one turn pots with a simple gear train. The gear trains and pots were located at the base of the stick and inside the throttle assembly.

Artificial feel was provided by centering springs on the stick. The throttle assembly included a friction control to suit the pilot's preference.

At first, visual display was tried using the multiple channel oscilloscope which is part of the analog computer accessories. It was found that by increasing the time scale, oscillations in pitch were displayed as a vertically translating horizontal line analogous to the attitude gyro in an airplane. It was not possible to differentiate between traces of airspeed and glide slope deviation so another method was tried.

The single channel 12 inch oscilloscope mentioned earlier was used in conjunction with a time sharing and blanking program. Thus a one amplifier scope was used to give the appearance of two independent and recognizable traces. The blanking circuit eliminated unwanted portions of the trace. A dot was chosen to represent airspeed deviation from trim where a "fast" is above the datum and a "slow" is below.

Glide slope information was displayed as a horizontal line. The line was beneath datum for a below glide slope signal and above for a "high." This was opposite to the standard Instrument Landing System, "fly to the needle," display. Full scale on airspeed was four knots while full scale on glide slope deviation was eight feet. Photographs of the actual display are in Figure 37.

The tasks required of the pilot were essentially the same as for the automatic systems. He was required to maintain glide slope and airspeed in the influence of gust disturbances. The additional task of responding to a "fly up 10 feet" command was also required.

The pilot was thoroughly briefed before each task and allowed to practice until he was satisfied with his performance. He was told when and what kind of disturbance to expect on each test. The best of his efforts was retained. Thus the pilot was given every favorable chance to compete with the automatic system.

The results of this Analog Simulation Program are presented in Chapter V.

CHAPTER V

RESULTS AND DISCUSSION

General

Data from the analog simulation program in Chapter IV were obtained from the computer in the form of time histories. The traces were produced by a six channel Brush Recorder and are presented as Figures 38 through 72. Scales for the perturbations were kept uniform wherever possible for ease in comparison with the basic airplane. The basic airplane plus all automatic systems were calculated in time scale on the computer in order to speed up the solution. The traces, Figures 38 through 60, were run at 10 mm per second, but in real time this is 1 mm per second. The manual simulation was accomplished in real time, and the records, Figures 61 through 72, were run at 5 mm per second in order to smooth out the appearance of the control inputs.

Due to equipment malfunctions, the recording channels available were reduced to four by the time manual simulation was begun. Unfortunately the channels available were not grouped together, thus making it necessary to cut out each trace and fix the collection together with rubber cement. This was at best a tedious task. Nevertheless, a formidable amount of data was produced, and some manner of summarizing the important features was needed.

Measures of Effectiveness

It was decided to group the data into responses to gusts and commands. The gusts were 1) 5 kt tail gust, 2) 5 kt up gust, and 3) combination of 1) and 2). The various commands were: 1) step stabilator, 2) step spoiler, 3) one degree pitch, and 4) fly up 10 feet. Thus grouped, there were obvious desirable quantities apparent. Such summaries of data are presented in Tables IV, V, and VI.

The measures of effectiveness of a system in response to a gust disturbance were taken to be: 1) first time u = 0, 2) percentage overshoot in u, 3) maximum h, and 4) value of h at 5 seconds after disturbance. "First time u = 0" is a measure of the rise time of the system. This time is to be minimized but not at the expense of "Percentage overshoot in u." The overshoot is a measure of system damping. An arbitrary range of values from 15 to 25 per cent is considered optimum for overshoot. It is evident that maximum glide slope deviation should be minimized. Of vital importance to the pilot is deviation from glide slope 5 seconds after disturbance. It takes about 5 seconds to traverse the last 900 feet of glide path at a closure rate of 105 knots. The disturbance is assumed to occur at this point (Recall Figure 19) and could well mean the difference between a successful arrestment or a catastrophic collision with the flight deck ramp of the carrier.

An evaluation of the responses to commands indicated the following measures of effectiveness: 1) time for h = 10 feet,

2) percentage overshoot in h, 3) maximum deviation in airspeed, and 4) peak values of α .

The maximum allowable deviation from glide slope at 900 feet out is 10 feet. This is the lower limit of the mirror landing system cone at this range. Any deviation lower than 10 feet will probably result in a ramp strike while 10 feet high could cause the airplane to "bolt," i.e., miss all the arresting wires. The time to eliminate this error obviously must be within the time envelope of 5 seconds mentioned above. Hence "time for h = 10 feet" must be minimized. Again this time must not be minimized at the expense of overshoot since correction for a "high" could result in a "scooping out" at the ramp. The next measure was maximum deviation in airspeed; this is to be minimized. Excursions in angle of attack are also to be minimized.

Gust Response

Figures 38, 39, and 40 show the basic airplane response to gust disturbances. The phugoid oscillation is a readily apparent long period variation in pitch and airspeed while α_w remains practically constant. The motion is lightly damped, and the period is 36 seconds. This result confirms the well known assumption employed earlier. The short period is characterized by a heavily damped oscillation in α . Here the period is six seconds and the motion is damped out after one cycle. The basic airplane results are important not only because they are used to compare the effects of adding control, but they also provide a means to check the analog model.

Reference 15 shows essentially the same results as shown in Figures 38 and 39. This favorable comparison was made even though Chance-Vought includes some non-linear effects in their analog model of the F-8.

APC lightens the pilot's load during a carrier landing approach by allowing him to concentrate more on glide slope and line up. The result is a more precise, and thus safer, carrier approach. APC is not and was not intended to be glide slope control.

The performance of the APC was best determined from its gust response. Measures of effectiveness for the APC were taken from Reference 9 and are listed in Table IV. Here the APC shows the expected improvement over the basic airplane (configuration B) and the conventionally controlled airplane. Of interest is the case where the elevator is manually controlled but APC is used. Here it seems the pilot's performance would have improved if he had not used the stick at all because the APC alone outperformed him in all measures. However, the APC plus pilot is better in performance than manual power compensation.

Tail gusts cause the airplane to sink below glide slope while up gusts tend to make the airplane go high. Thus one test for the glide slope controller was gust performance. Summaries of glide slope controller effectiveness in gust conditions are presented in Tables V and VI.

Inspection of the manual control records for the gust conditions yielded an average time lag for the pilot. The disturbance was presented to the pilot by warning him, then suddenly illuminating his display scope. The time from disturbance to first control movement can be measured on the manual control record. The pilot's average time lag was found to be 0.5 seconds.

Another test for the glide slope controllers was the response to a fly up command. This task was meant to test the system's recovery from a 10 foot low condition. These results are summarized in Tables IV and V.

On the basis of the measures of effectiveness the best glide slope controllers were judged to be the DLC controllers. The DLC controllers were then compared with each other in Table V. The results showed that automatic DLC was superior to manual DLC, but the latter was a feasible means of control.

The best DLC system was determined from gust and command performance. The best controller was, as expected, the DLC and APC system.

The step commands, Figures 41 and 42, gave interesting though intuitive results. While step elevator initially caused the airplane to climb, the steady state result was a rate of descent; see Table V. The opposite was true for the suddenly retracted spoiler. An initial climb was followed by steady state rate of climb, Figure 41, Table V.

Automatic glide slope control cannot be achieved by means of EGSC without the use of an APC. In fact, any control of glide slope, automatic or not, is impossible with elevator control only. The stick and throttle must be skillfully coordinated in order to maintain or recapture glide slope. Thus the automatic systems currently being tested by the Navy (7) are ineffective without a functioning APC.

Figures 42 and 60 substantiated this intuition. Step stabilator for the intention of climbing results in steady state descent due to the increase in drag. A Pitch Control System also yielded a rate of descent after nose up pitch was commanded. Hence the glide slope controller using pitch control without APC initially corrected in the proper sense for a low, but the steady state response was improper. As the nose came up, airspeed decreased due to increased drag and decreased kinetic energy. The steady state value of α became greater than pitch angle, θ. Hence from Equation 9, a negative glide slope angle resulted.

Figure 60 also emphasizes the importance of the integration term used in all the other controllers in this context. Recall that the integration term was used to wash out steady state error. The PCS, Figure 18, did not incorporate this feature; hence, a steady state error in θ appears in Figure 60. One degree of pitch angle was commanded, but only 0.6 degree was produced.

CHAPTER VI

CONCLUSIONS AND RECOMMENDATIONS

Conclusions

This study encompassed three areas of investigation: 1) implementation of wing lift spoilers as a DLC system, 2) automatic control of glide slope, and 3) the analog simulation program.

Conclusions from the DLC implementation are as follows. First, wind tunnel data, preferably full scale, are needed when dealing with wing lift spoilers. Second, spoilers provide a means of rapidly increasing lift while decreasing drag.

In the study of automatic glide slope control the following conclusions were made: First, not only position feedback but rate feedback as well, must be used in automatic glide slope control. Second, increasing the gain of the outer loop of the automatic glide slope controllers results in decreasing the system damping. Third, recourse to an analog computer for determination of gain constants is easier than the root locus method.

First, the analog simulation program indicated that a DLC system using spoilers could be used for glide slope control without an APC. Second, an elevator glide slope coupler (EGSC) system incorporating an APC was not as effective as a DLC or APC system. Third, EGSC system cannot control glide slope automatically without a functioning APC. Fourth, a man controls glide slope remarkably well but is not as effective as the automatic systems.

Recommendations

The work involved, during this investigation, in gathering data on spoiler effectiveness was almost insurmountable. Data were at best sparse and inconsistent. It is therefore recommended that a meaningful investigation be made of the characteristics of spoiler systems.

The hybrid computer which is available at the Naval Postgraduate School opens the door for a wealth of simulation studies. The high speed digital retrieval of data will allow simulation to be accomplished using non-linear equations of motion and random disturbances.

REFERENCES

1. "Simulator Study of Direct Lift Control During Landing Approaches," Douglas Aircraft Division Report No. LB-31253, Long Beach: 1963.

2. Klein, D. G., A Preliminary Investigation of the Use of Lift Control in Maneuvering Flight. M.S.E. Thesis, Princeton University School of Engineering and Applied Science, Princeton University: 1967.

3. Mazza, C. J., "A Performance and Mechanical Design Analysis of Direct Lift Control for Improving the Carrier Landing Characteristics of Five Naval Airplanes," Naval Air Development Center NADC-ED-6460, Johnsville: 1965.

4. Etheridge, J. D., "Direct Lift Control as a Landing Approach Aid in the F-8C Airplane-Simulator and Flight Tests," LTV, Vought Aeronautics Division Report No. 2-53310/4R-175. Dallas: 1964.

5. Gralow, R. T., "Evaluation of the Direct Lift Control System in the F-8C Airplane," Naval Air Test Center Technical Report FT-51R-65, Patuxent River: 1965.

6. Andrews, E. John, "Automatic Throttle-Control for Deck Recovery of Carrier Based Airplanes," Unpublished paper presented to the Royal Aeronautical Society, London: 1965.

7. Kelly, William P., "Automatic Carrier Landing System Developmental Testing," The Society of Experimental Test Pilots Eleventh Annual Report, Beverly Hills: 1967.

8. Bell, Gerald R., An Investigation of the Effect of Auto-Throttle Devices on Aircraft Control in the Carrier Landing Approach. M.S. Thesis, Naval Postgraduate School, Monterey: 1963.

9. McConnel, Richard A., A Study of an Automatic Power Compensator with Airspeed and Angle of Attack as Controlling Inputs. M.S. Thesis, Naval Postgraduate School, Monterey: 1966.

10. Hodgkins, P. D., "Flight Test of Specialties Incorporated Approach Power Compensator in F-8U Type Aircraft," Naval Air Test Center Report FT 2221-180, Patuxent River: 1962.

11. Jones, Arthur L., Lamb, Owen P., Cronk, Alfred E., "A Method for Predicting Lift Effectiveness of Spoilers at Subsonic Speeds," Journal of the Aeronautical Sciences, 23 (April, 1956) 330.

12. Hoak, D. E., "USAF Stability and Control DATCOM," Air Force Flight Dynamics Laboratory AF 33 (616)-6460, Wright Patterson AFB: 1965.

13. Franks, Ralph W., "The Application of a Simplified Lifting Surface Theory to the Prediction of the Rolling Effectiveness of Plain Spoiler Ailerons at Subsonic Speeds," NACA RM A54H26a, Washington: 1954.

14. Franks, Ralph W., "Tests in the Ames 40-by 80-Foot Wind Tunnel of the Aerodynamic Characteristics of Airplane Models with Plain Spoiler Ailerons," NACA RM A54H26, National Advisory Committee for Aeronautics, Washington: 1954.

15. Eberle, R. B., Schoelerman, D. B., Smykacz, N. A., "Criteria for Predicting Landing Approach Speed Based on an Analog Computer Analysis of 21 Jet-Propelled Aircraft," Chance-Vought Report EOR-13202. Chance-Vought,Inc., Texas: 1960.

16. Weick, F. E., "Development of the NACA Slot Tip Aileron," NACA TN547, Washington: 1935.

17. Etkin, Bernard, Dynamics of Flight Stability and Control. John Wiley and Sons, Inc., New York: 1959.

18. Raven, Francis H., Automatic Control Engineering. McGraw-Hill Book Company, Inc., New York: 1967.

19. Johnson, Clarence L., Analog Computer Techniques. McGraw-Hill Book Company, Inc., New York: 1963.

TABLE I

DIMENSIONAL STABILITY DERIVATIVES
FOR THE F-8 IN APPROACH CONFIGURATION

DATA:

S_w	= Wing area	= 375 ft^2
z_t	= Thrust arm	= - .437 ft
l_t	= Tail arm	= 14.08 ft
c	= Mean chord	= 11.8 ft
B	= Moment of inertia	= 96000 slug ft^2
U	= 1.3 x stall speed	= 234 ft/sec
cg	= Center of gravity	= .24c
W	= Gross weight	= 22000 lb
Θ	= Pitch reference	= 8.1 deg
ϵ	= Thrust angle	= .85 deg

SYMBOL	DEFINITION	DIMENSIONALIZER	VALUE
X_u =	$\frac{1}{m}\frac{\partial X}{\partial u}$ =	$\frac{\rho S U}{2m}(-C_D - C_{D_u})$	= - .060 1/sec
X_w =	$\frac{1}{m}\frac{\partial X}{\partial w}$ =	$\frac{\rho S U}{2m}(C_L - C_{D_\alpha})$	= -.01419 1/sec
X_δ =	$\frac{1}{m}\frac{\partial X}{\partial \delta}$ =	$\frac{\rho S U^2}{2m}(-C_{D_\delta})$	= 2.48 ft/sec^2
X_η =	$\frac{1}{m}\frac{\partial X}{\partial \eta}$ =	$\frac{\rho S U^2}{2m}(-C_{D_\eta})$	= - .1.64 $ft/sec^2 rad$
X_T =	$\frac{1}{m}\frac{\partial X}{\partial T}$ =	$\frac{\cos \epsilon}{m}$	= .00145 $ft/lb\ sec^2$
Z_u =	$\frac{1}{m}\frac{\partial Z}{\partial u}$ =	$\frac{\rho S U^2}{2m}(-C_{L_\delta})$	= - .2655 1/sec

TABLE I (CONTINUED)

SYMBOL	DEFINITION	DIMENSIONALIZER	VALUE
Z_w =	$\frac{1}{m}\frac{\partial Z}{\partial w}$	= $\frac{\rho S U}{2m}(-C_{L_\alpha} - C_D)$	= - .4265 1/sec
Z_δ =	$\frac{1}{m}\frac{\partial Z}{\partial \delta}$	= $\frac{\rho S U^2}{2m}(-C_{L_\delta})$	= - 85 ft/sec^2
Z_η =	$\frac{1}{m}\frac{\partial Z}{\partial \eta}$	= $\frac{\rho S U^2}{2m}(-C_{L_\eta})$	= - 19.1 ft/sec^{2}rad
Z_T =	$\frac{1}{m}\frac{\partial Z}{\partial T}$	= $\frac{\sin \epsilon}{m}$	= - 2.17 x 10^{-5} ft/sec^{2}rad
M_u =	$\frac{1}{B}\frac{\partial M}{\partial u}$	= $\frac{\rho S U}{B}(-C_T\ z_T)$	= .000185 1/sec ft
M_w =	$\frac{1}{B}\frac{\partial M}{\partial w}$	= $\frac{\rho S U \bar{c}}{2B}(C_{M_\alpha})$	= - .004858 1/sec ft
$M_{\dot{w}}$ =	$\frac{1}{B}\frac{\partial M}{\partial \dot{w}}$	= $\frac{\rho S \bar{c}^2}{4B}(C_{M_{\dot{\alpha}}})$	= - 1.772 x 10^{-4} 1/ft
M_q =	$\frac{1}{B}\frac{\partial M}{\partial q}$	= $\frac{\rho S U \bar{c}^2}{4B}(C_{M_q})$	= - .3384 1/sec rad
M_η =	$\frac{1}{B}\frac{\partial M}{\partial \eta}$	= $\frac{\rho S U^2 \bar{c}}{2B}(C_{M_\eta})$	= - 2.25 1/rad sec^2
M_T =	$\frac{1}{B}\frac{\partial M}{\partial T}$	= $\frac{-Z_T}{B}$	= - 4.55 x 10^{-6} 1/lb sec

TABLE II

ANALOG POT SETTINGS

Pot	Represents	Setting	Gain
1	$.060\ a_{\dot u}/a_u$	.1011	1
2	$.332\ a_{\dot u}/a_\alpha$	.0116	1
3	$31.85\ a_{\dot u}/a_\theta$	.111	1
4	$2.5\ a_{\dot u}/a_\delta$	.0051	1
5	$.00145\ a_{\dot u}/a_\tau$	.0292	10
6	$a_u/a_{\dot u}$	.593	1
7	$.00113\ a_{\dot\alpha}/a_u$	.547	1
8	$.4265\ a_{\dot\alpha}/a_\alpha$	.4265	1
9	$.01935\ a_{\dot\alpha}/a_\theta$	.01935	1
10	$a_{\dot\alpha}/a_{\dot\theta}$	.1	10
11	$.0815\ a_{\dot\alpha}/a_\eta$	.00815	10
12	$.353\ a_{\dot\alpha}/a_\delta$	.202	1
13	$a_{\dot\theta}/a_{\ddot\theta}$	.286	10
14	$1.85 \times 10^{-4}\ a_{\ddot\theta}/a_u$	.0312	1
15	$.338\ a_{\ddot\theta}/a_{\dot\theta}$	.118	1
16	$.0415\ a_{\ddot\theta}/a_{\dot\alpha}$	.0415	1
17	$1.14\ a_\theta/a_\alpha$	.0398	10
18	$4.55 \times 10^{-6}\ a_{\ddot\theta}/a_\tau$	.0091	10
19	$2.25\ a_{\ddot\theta}/a_\eta$	.0786	10
20	u_g	Various	1
21	α_g	Various	1
22	$U\ a_\eta/a_\gamma$	.409	1

TABLE II (CONTINUED)

Pot	Represents	Setting	Gain
23	$U\ K_{\dot{h}}\ a_{\delta}/a_{\gamma}$	.300	10
24	$K_{h}\ a_{\delta}/a_{h}$	.500	10
25	$K_{h} K_{i} a_{\delta}/a_{h}$	.001	1
26	h_c	Various	1
27	$K_{u}\ a_{T}/a_{u}$	.337	10
28	$K_{u} K_{i}\ a_{T}/a_{u}$	.0336	1
29	$K_{\alpha}\ a_{T}/a_{\alpha}$	.1745	1
30	τ_e	.8711	1
31	τ_e	.8711	1
32	$U\ a_{h}/a_{\gamma}$	.409	1
33	$U\ K_{\dot{h}} a_{\eta}/a_{\gamma}$	.250	1
34	h_c	Various	1
35	$K_{h}\ a_{\eta}/a_{h}$	.300	1
36	$K_{h} K_{i} a_{\eta}/a_{h}$	.0025	1
37	θ_c	Various	1
38	$K_{\theta} a_{\theta}/a_{\eta}$	.13	10
39	$K_{\dot{\theta}}\ a_{\dot{\theta}}/a_{\eta}$	.677	1

TABLE III

ANALOG SCALE FACTORS

Parameter	Maximum Value	Scale Factor (a_x)
$\dot{u}$	50 ft/sec^2	2 volts/ft/sec^2
u, u_c, u_g	84.3 ft/sec 5 kts	1.189 volts/ft/sec 2 volts/kt
$\alpha, \alpha_g, \gamma, \theta, \theta_c, \eta, \eta_c$	10 deg .1745 rad	10 volts/deg 573 volts/rad
$\dot{\alpha}, \dot{\theta}$	10 deg/sec .1745 rad/sec	10 volts/deg/sec 573 volts/rad/sec
$\ddot{\theta}$	.5 rad/sec^2	200 volts/rad/sec^2
T	1000 lbs	.01 volts/lb
h, h_c	100 ft	1 volt/ft
δ	$.1\bar{c}$	1000 volts/$\bar{c}$

TABLE IV

EFFECTIVENESS OF APC COMPARED
WITH BASIC AIRPLANE AND MANUAL CONTROL

Disturbance	5 Knot Tail Gust			
Figure Number	38	47	63	66
Thrust Control Type	B	AUTO	MAN	AUTO
Glide Slope Control System	B	B	EGSC	EGSC
Glide Slope Control Type	B	B	MAN	MAN
First Time u = 0, Sec.	8	2.5	6.5	3
Time for $-1 < u < 1$, Sec.	102	2	5.2	2.5
u Overshoot, %	85	33	50	40
Maximum Thrust Change, Lbs.	---	1800	-600	2600

Disturbance	5 Knot Up Gust			
Figure Number	39	48	62	65
Thrust Control Type	B	AUTO	MAN	AUTO
Glide Slope Control System	B	B	EGSC	EGSC
Glide Slope Control Type	B	B	MAN	MAN
First Time u = 0, Sec.	12	20	17	8
Time for $-1 < u < 1$, Sec.	10	0	11	5
u Overshoot, %	80	0	0	0
Maximum Thrust Change, Lbs.	---	300	-600	-650

Disturbance	Combination Gust	
Figure Number	40	49
Thrust Control Type	B	AUTO
Glide Slope Control System	B	B
Glide Slope Control Type	B	B
First Time u = 0, Sec.	9	3
Time for $-1 < u < 1$, Sec.	102	2.5
Maximum Thrust Change, Lbs.	---	2000

TABLE V

SUMMARY OF GLIDE SLOPE CONTROL EFFECTIVENESS

Disturbance	5 Knot Tail Gust				
Figure Number	38	43	50	55	63
Thrust Control Type	B	B	AUTO	AUTO	MAN
Glide Slope Control System	B	DLC	DLC	EGSC	EGSC
Glide Slope Control Type	B	AUTO	AUTO	AUTO	MAN
First Time u = 0, Sec.	8	60	3	3	6.5
u Overshoot, %	85	0	20	14	50
h Maximum, Ft.	-115	-6	-4	-7	3
h at 5 Sec., Ft.	-20	-6	-4	-6	-2
Disturbance	5 Knot Up Gust				
Figure Number	39	44	51	56	62
Thrust Control Type	B	B	AUTO	AUTO	MAN
Glide Slope Control System	B	DLC	DLC	EGSC	EGSC
Glide Slope Control Type	B	AUTO	AUTO	AUTO	MAN
First Time u = 0, Sec.	14	7	5	15	17
u Overshoot, %	80	50	---	0	0
h Maximum, Ft.	27	3	3	5	5.5
h at 5 Sec., Ft.	15	0	4	5	1
Disturbance	Combination Gust				
Figure Number	48	45	52	57	
Thrust Control Type	B	B	AUTO	AUTO	
Glide Slope Control System	B	DLC	DLC	EGSC	
Glide Slope Control Type	B	AUTO	AUTO	AUTO	
First Time u = 0, Sec.	9	60	3	3	
u Overshoot, %	80	0	20	20	
h Maximum, Ft.	-105	-6	-4	-3	
h at 5 Sec., Ft.	-5	5	-3	-1	

TABLE V (CONTINUED)

Command	Fly Up 10 Feet				
Figure Number	46	53	58	61	64
Thrust Control Type	B	AUTO	AUTO	MAN	AUTO
Glide Slope Control System	DLC	DLC	EGSC	EGSC	EGSC
Glide Slope Control Type	AUTO	AUTO	AUTO	MAN	MAN
Time to 10 Ft., Sec.	3.5	3.8	7	5.3	5
h Overshoot, %	20	25	25	25	20
u Maximum, Kts.	---	.75	-.8	-1	-.6
α Peak, Deg.	1.1	.5	.5	---	---

Command	Low/Slow (10 Ft./5 Knots)	
Figure Number	54	59
Thrust Control Type	AUTO	AUTO
Glide Slope Control System	DLC	EGSC
Glide Slope Control Type	AUTO	AUTO
Time to 10 Ft., Sec.	6	12
h Overshoot, %	25	30
u Maximum, Kts.	.3	-1
α Peak, Deg.	-.5	1

Command	Step Control Input		
Figure Number	42	41	60
Thrust Control Type	B	B	B
Glide Slope Control System	EGSC	DLC	PCS
Type Input	η	δ	θ
γ Initial	+	+	+
γ Steady, Deg.	-1.75	2	-2
θ Peak, Deg.	2.4	1.3	.9
α Peak, Deg.	1.2	-.2	2.1

TABLE VI

COMPARISON OF EFFECTIVENESS OF
MANUAL AND AUTOMATIC DLC SYSTEMS

Disturbance	5 Knot Tail Gust			
Figure Number	69	72	43	50
Thrust Control Type	MAN	AUTO	B	AUTO
Glide Slope Control System	DLC	DLC	DLC	DLC
Glide Slope Control Type	MAN	MAN	AUTO	AUTO
First Time u = 0, Sec.	7.2	3	60	3
u Overshoot, %	50	20	0	20
h Maximum, Ft.	7.5	-7	-6	-4
h at 5 Sec., Ft.	-5	-7	-6	-4

Disturbance	5 Knot Up Gust			
Figure Number	68	71	44	51
Thrust Control Type	MAN	AUTO	B	AUTO
Glide Slope Control System	ELC	DLC	DLC	DLC
Glide Slope Control Type	MAN	MAN	AUTO	AUTO
First Time u = 0, Sec.	13	6	7	5
u Overshoot, %	25	0	50	0
h Maximum, Ft.	5	4	3	3
h at 5 Sec., Ft.	-1	0	0	4

Command	Fly Up 10 Feet			
Figure Number	67	70	46	53
Thrust Control Type	MAN	AUTO	B	AUTO
Glide Slope Control System	DLC	DLC	DLC	DLC
Glide Slope Control Type	MAN	MAN	AUTO	AUTO
Time to 10 Ft., Sec.	11	6	3.5	3.8
h Overshoot, %	15	30	20	25
u Maximum, Kts.	-2	-1	-1	.75
α Peak, Deg.	---	---	$\pm.5$	$\pm.5$

TABLE VII

COMPONENT TRANSFER FUNCTIONS

$\frac{T}{T_c} = \frac{1}{1 + 1.15s}\ \frac{\text{lb}}{\text{lb}}$	$\frac{\eta_\theta}{\theta_e} = -1.3\ \frac{\text{rad}}{\text{rad}}$
$\frac{T_c}{\alpha} = -10{,}000\ \frac{\text{lb}}{\text{rad}}$	$\frac{\eta_{\dot\theta}}{\dot\theta} = -0.667\ \text{sec}$
$\frac{\alpha}{T} = \frac{-4.55 \times 10^{-6}}{s^2 + 0.806s + 1.281}\ \frac{\text{rad}}{\text{lb}}$	$\frac{\theta}{\dot\theta} = \frac{1}{s}\ \text{sec}$
$\frac{T_c}{u_e} = 400\left(1 + \frac{0.003}{s}\right)\ \frac{\text{lb sec}}{\text{ft}}$	$\frac{\theta}{\eta} = \frac{-(2.25s + 0.867)}{s(s^2 + 0.806s + 1.281)}\ \frac{\text{rad}}{\text{rad}}$
$\frac{u}{T} = \frac{0.00145s}{s^2 + 0.06s + 0.036}\ \frac{\text{ft}}{\text{sec lb}}$	$\frac{\dot\theta}{\eta} = \frac{-(2.25s + 0.867)}{s^2 + 0.806s + 1.281}\ \frac{\text{rad}}{\text{rad}}$
$\frac{\delta_h}{\dot h} = -0.0073\ \frac{\text{sec}}{\text{ft}}$	$\frac{\alpha}{\delta} = \frac{-(0.36s^2 + 0.122s)\ \text{rad}}{s(s^2 + 0.806s + 1.281)}$
$\frac{\delta_h}{h_e} = -0.005\left(1 + \frac{0.002}{s}\right)\ \frac{1}{\text{ft}}$	$\frac{\theta}{\delta} = \frac{0.014s + 0.409}{s(s^2 + 0.806s + 1.281)}\ \text{rad}$
$\frac{h}{\dot h} = \frac{1}{s}\ \text{sec}$	$\frac{\gamma}{\delta} = \frac{0.36s^2 + 0.136s + 0.409}{s(s^2 + 0.806s + 1.281)}\ \text{rad}$

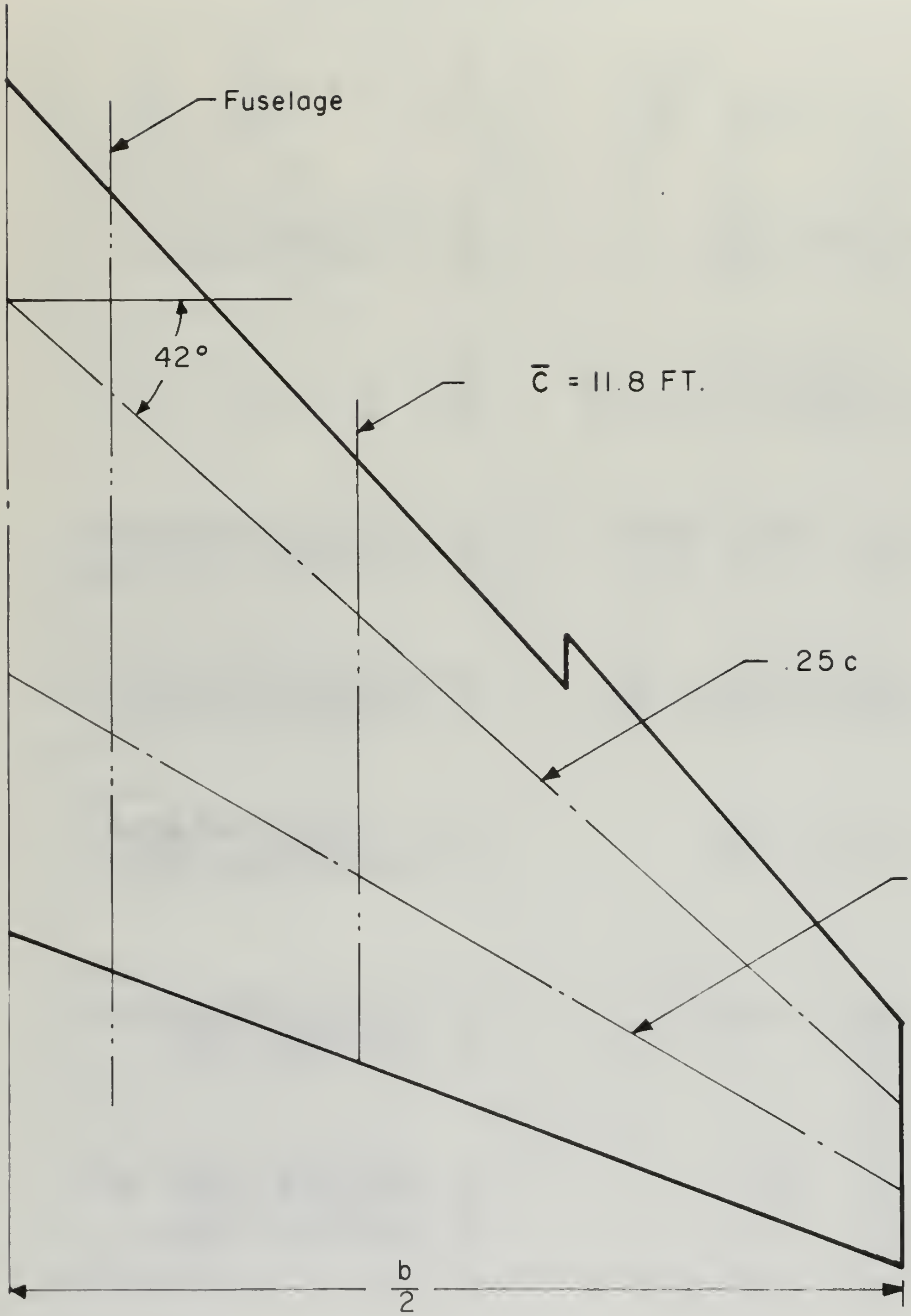

FIGURE 1
F8 WING PLANFORM
S_w = 375 FT^2 b = 35.6 FT
AR = 3.3 λ = .28

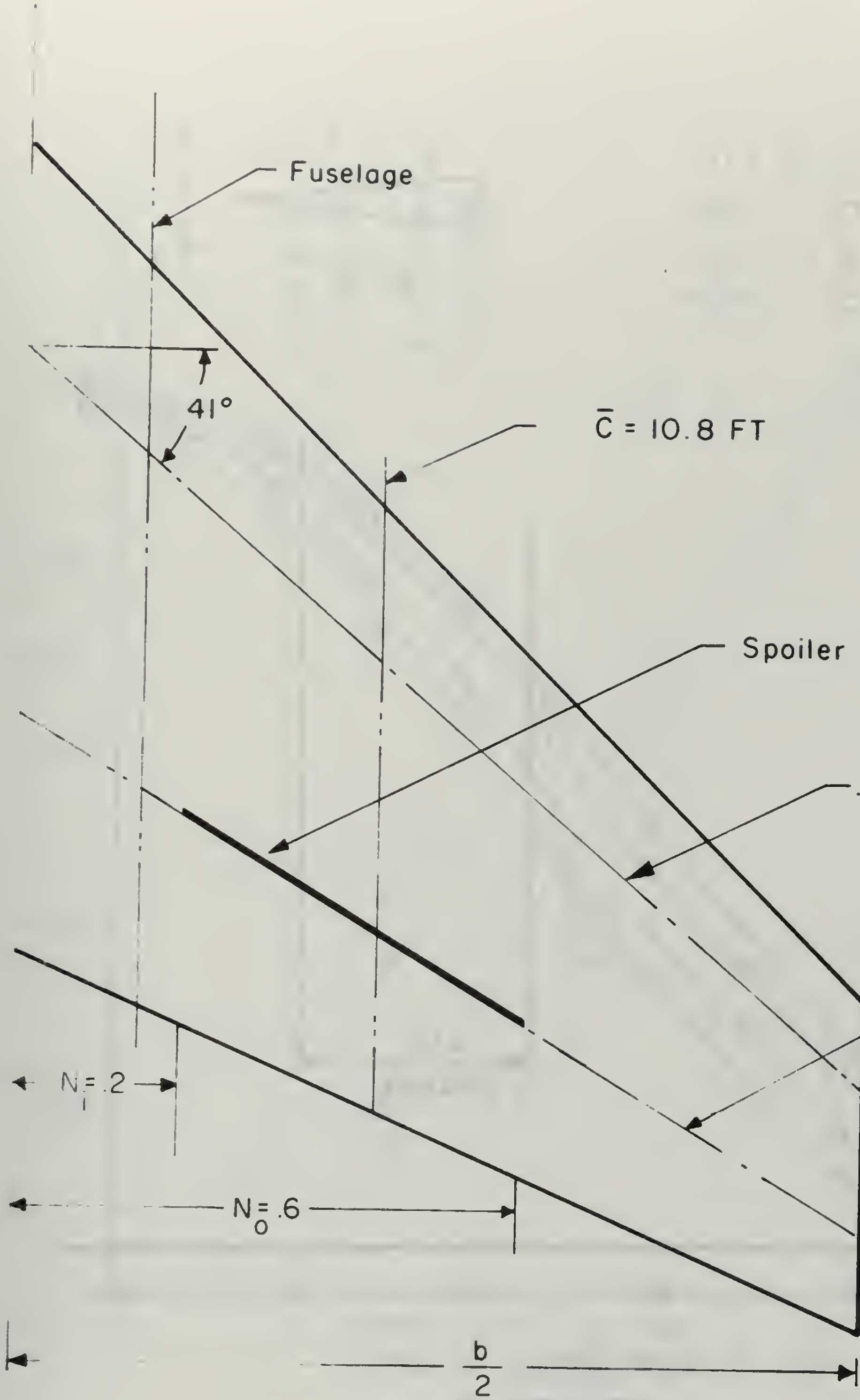

FIGURE 2
NACA RM A54H26 MODEL 2
S = 312.5 $FT.^2$ b = 30.6 FT
AR = 3.0 λ = .4

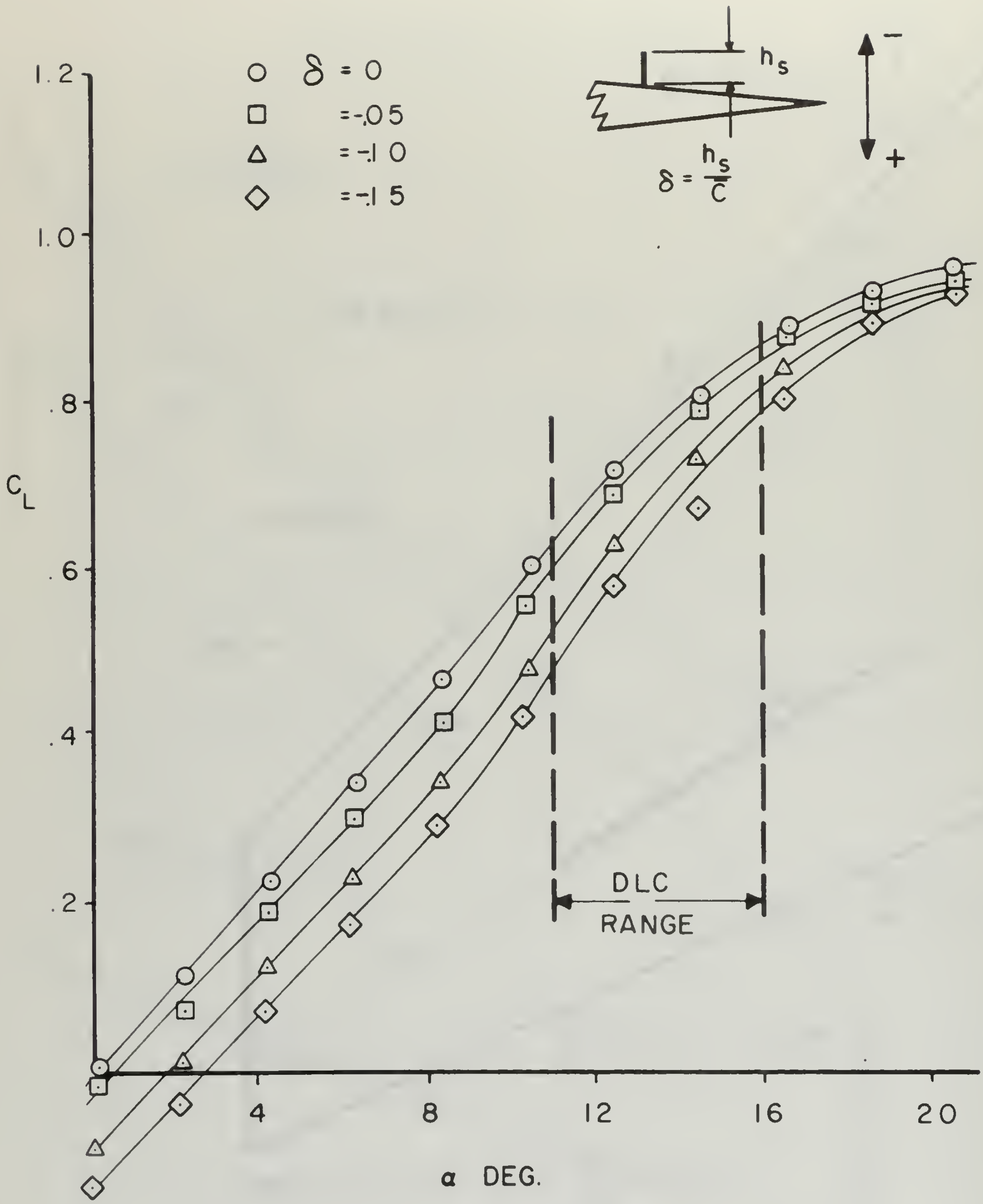

FIGURE 3

C_L vs. α

VARIOUS SPOILER DEFLECTIONS
NACA RM A54H26 MODEL 2

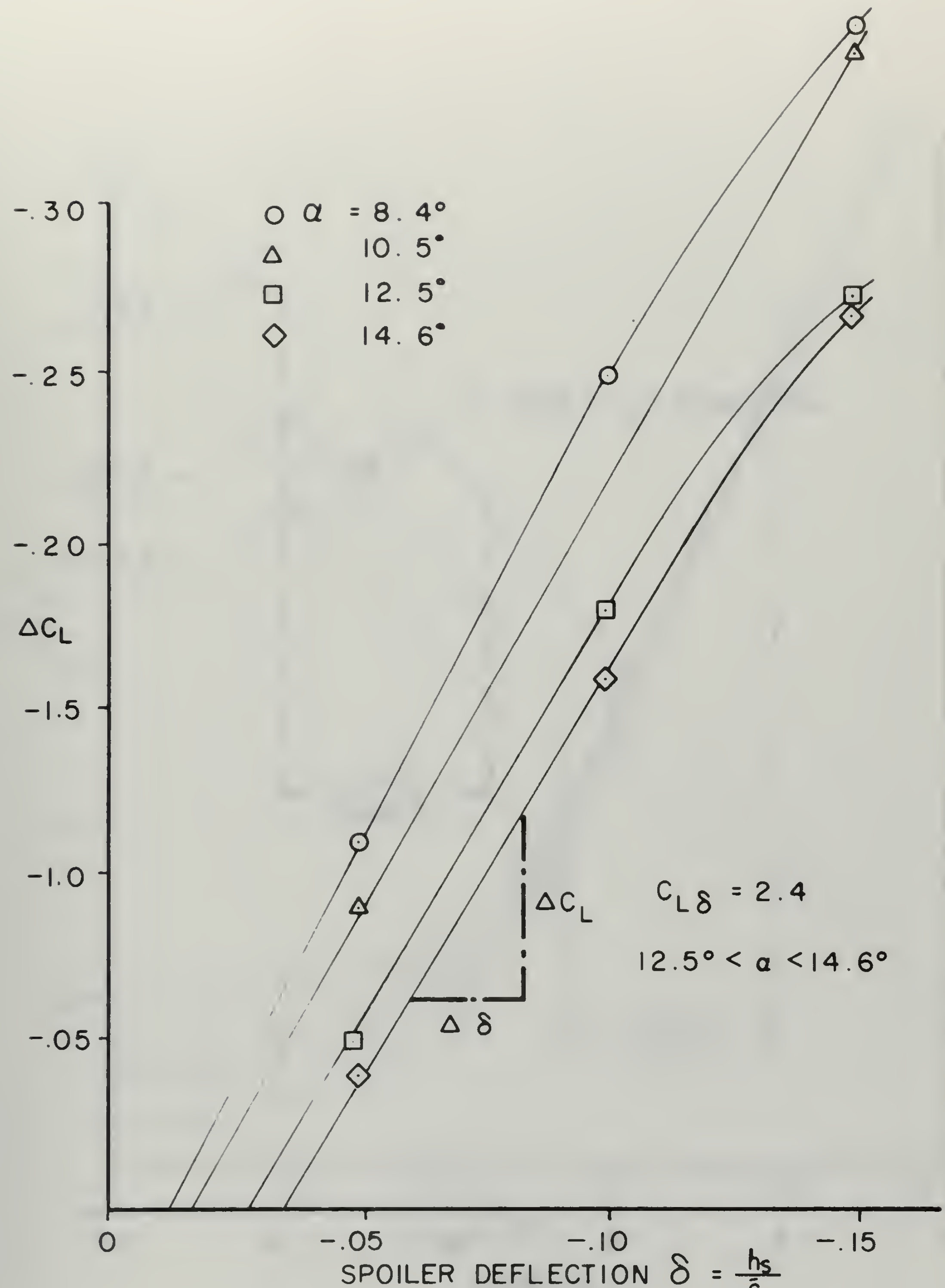

FIGURE 4

ΔC_L VS. δ FOR VARIOUS α

NACA RM A54H26 MODEL 2

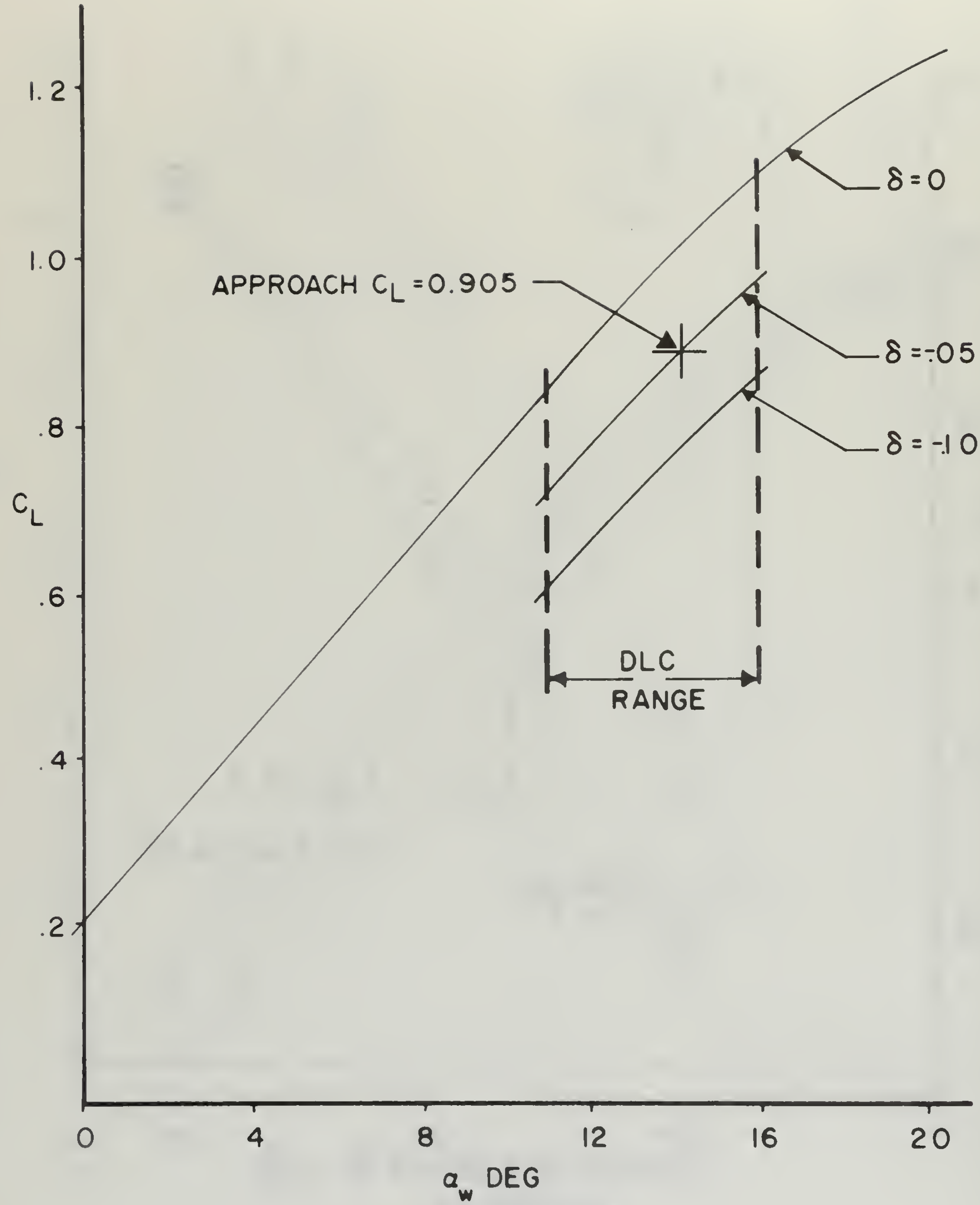

FIGURE 5

F8 - C_L vs. α_W

EFFECT OF SPOILER DEFLECTION (EST.)

$C_{L\delta}=2.4$

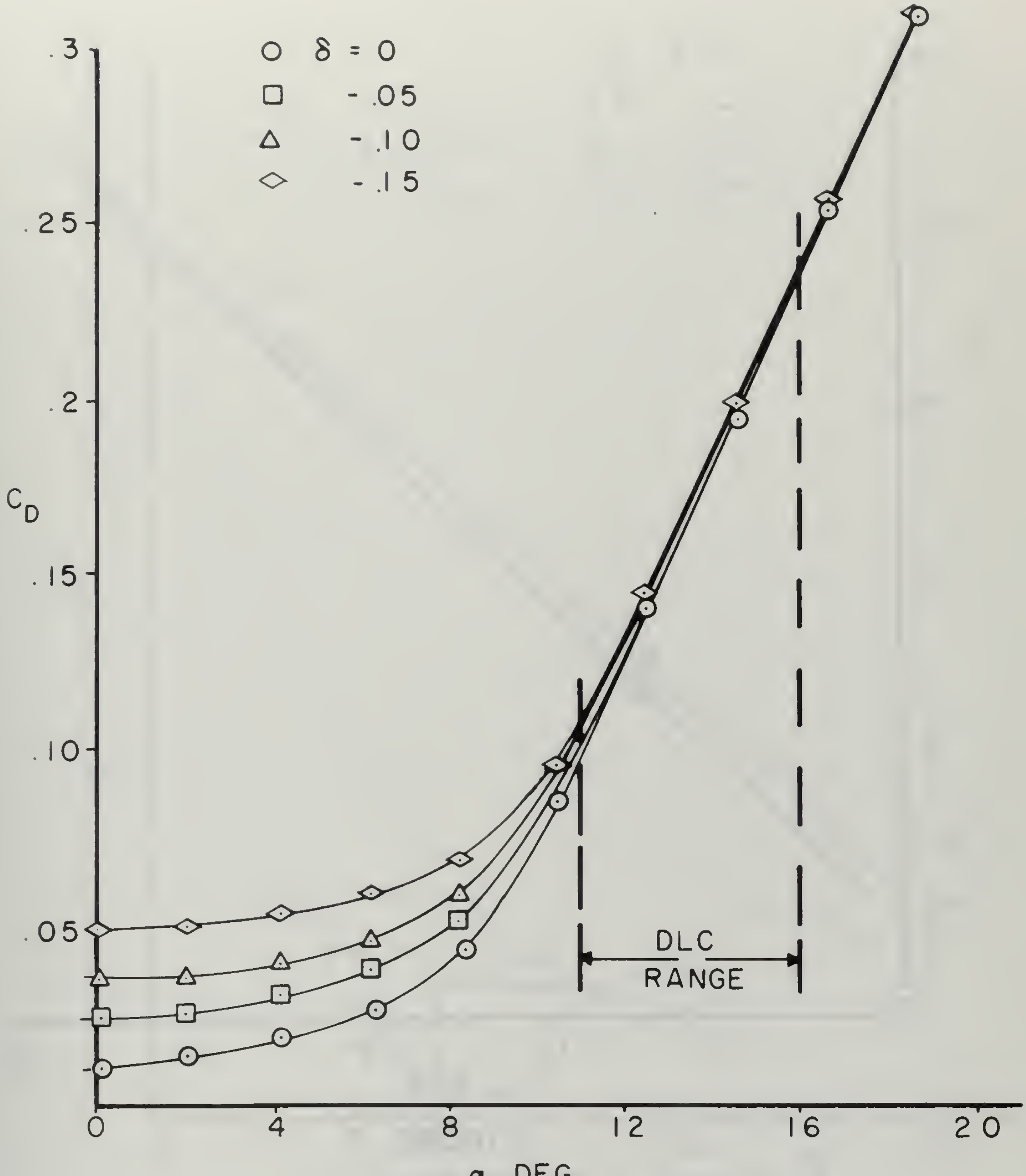

FIGURE 6

C_D vs. α

VARIOUS SPOILER DEFLECTIONS

NACA RM A54H26 MODEL 2

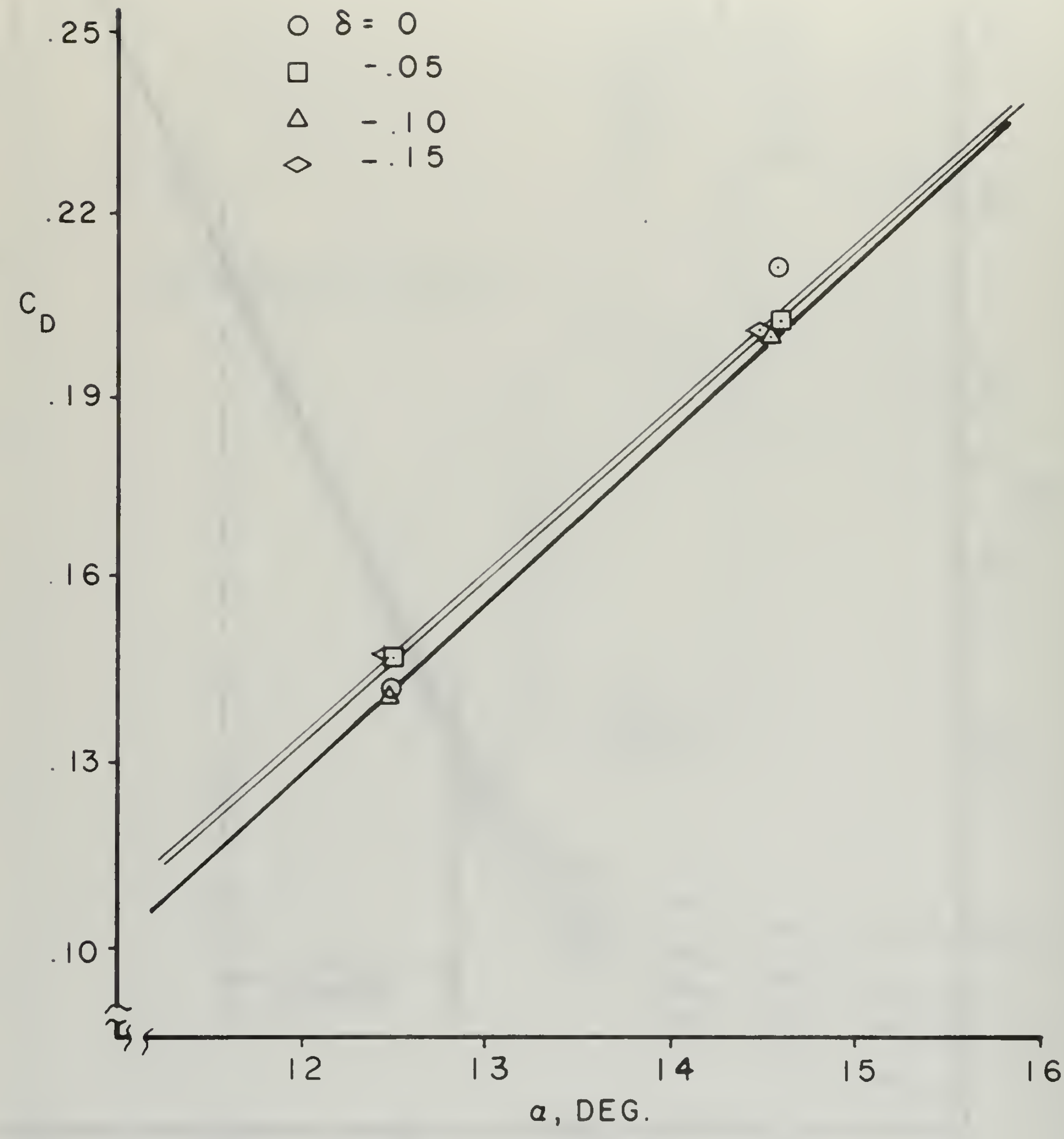

FIGURE 7

C_D vs. α IN DLC RANGE
VARIOUS SPOILER DEFLECTIONS
NACA RM A54H26 MODEL 2

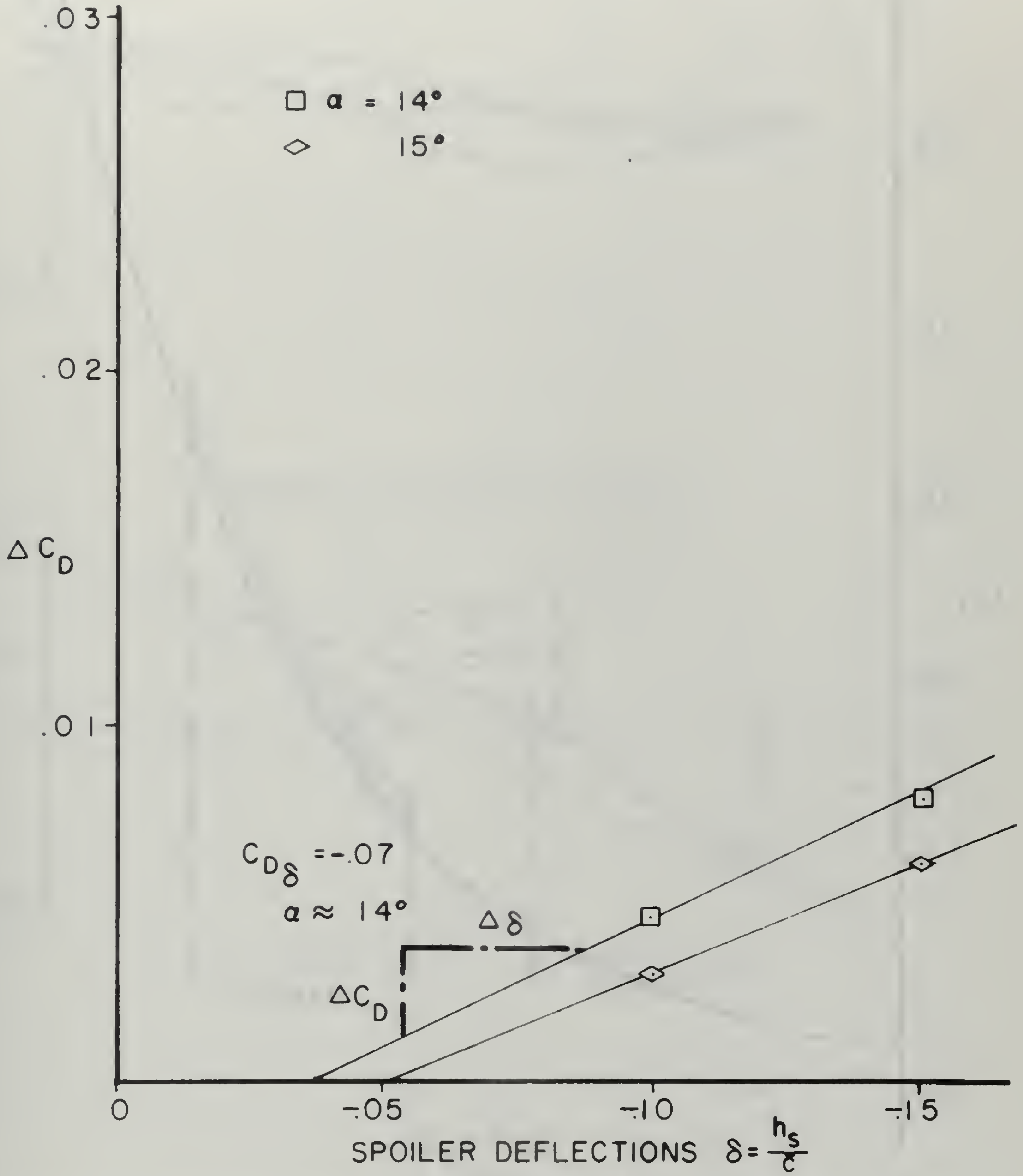

FIGURE 8

ΔC_D vs. δ FOR VARIOUS α

NACA RM A54H26 MODEL 2

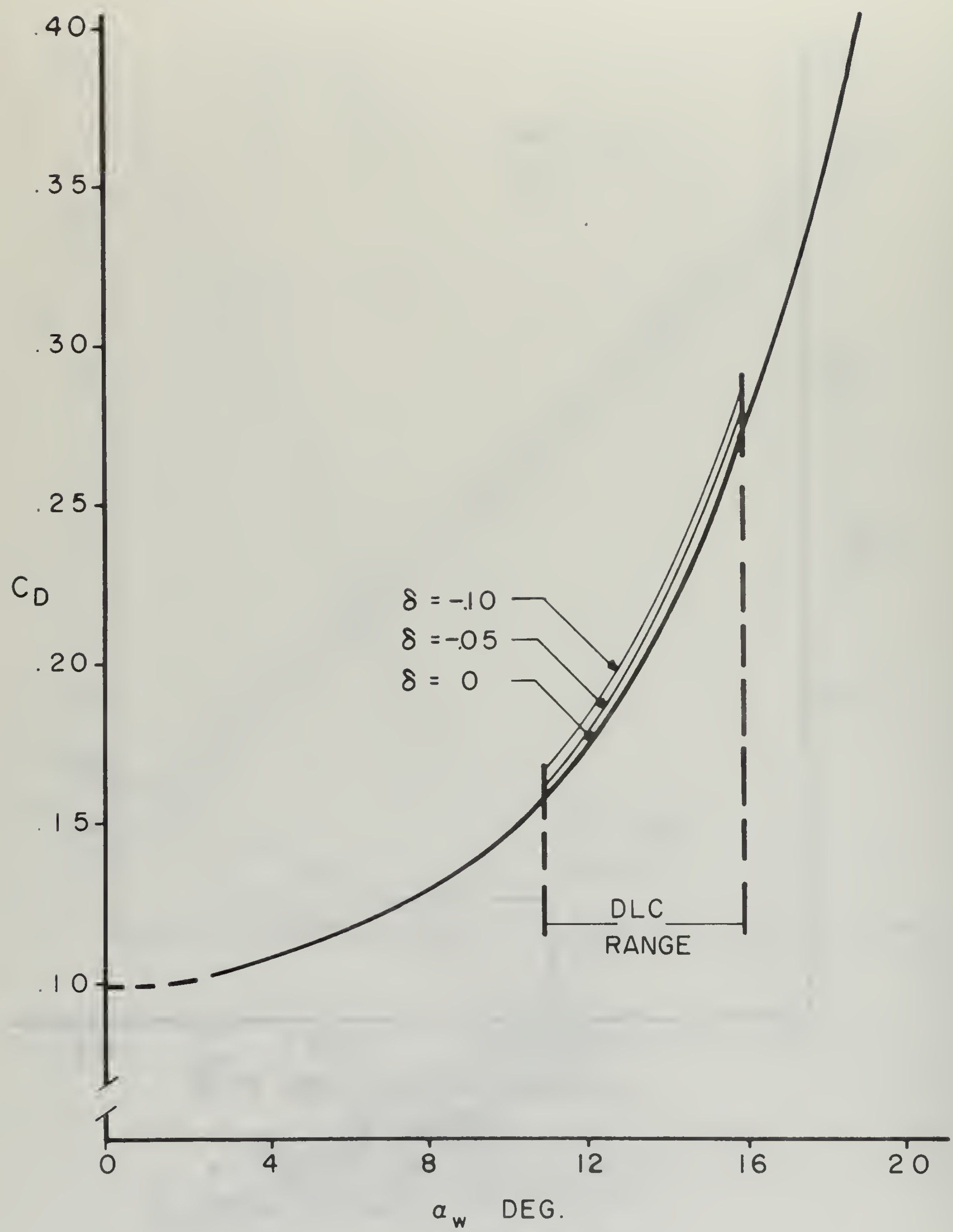

FIGURE 9

F8 C_D vs. α_w

EFFECT OF SPOILER DEFLECTIONS (EST.)

$C_{D\delta} = -.07$

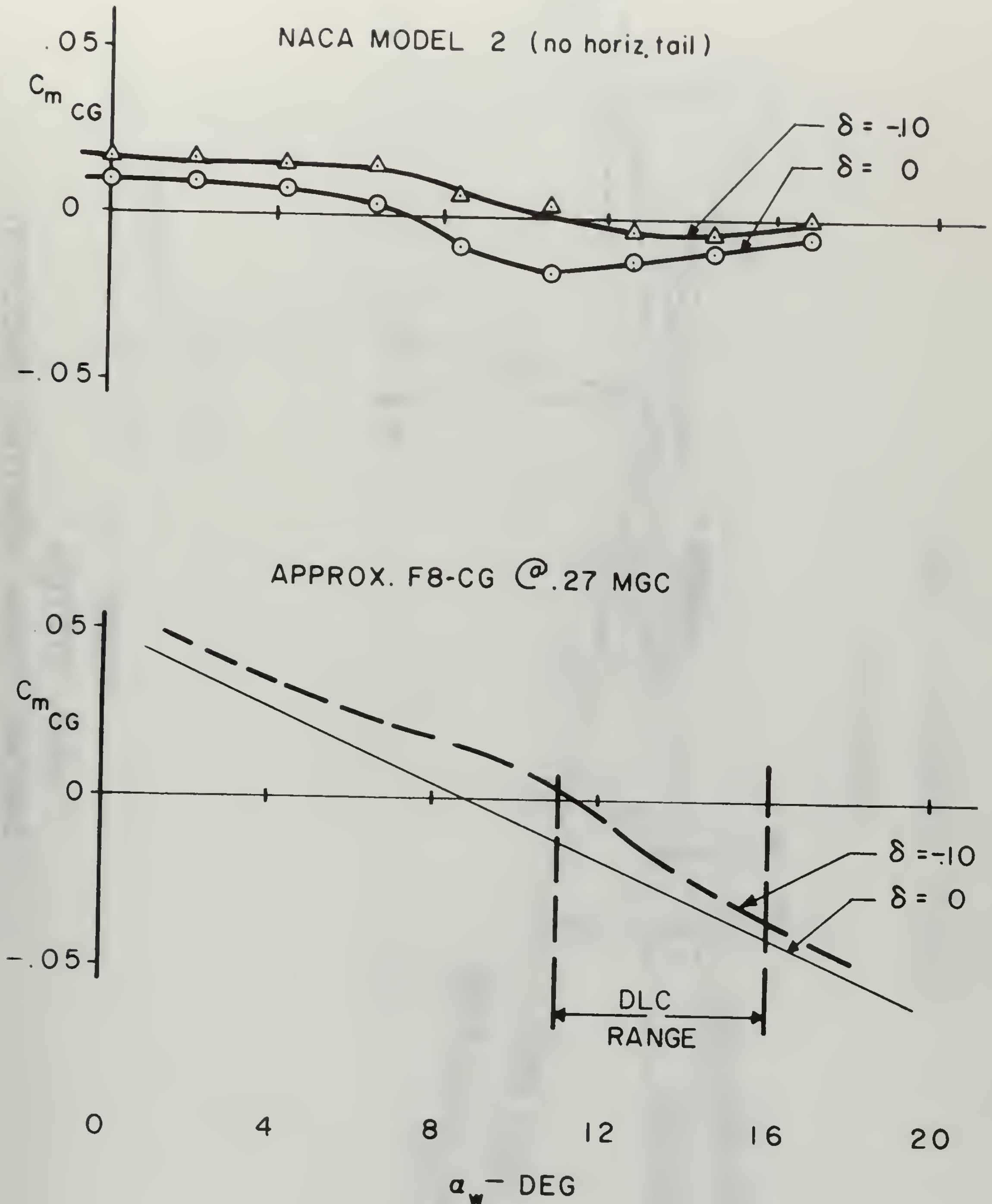

FIGURE 10

$C_{m_{CG}}$ vs. α_w

EFFECT OF SPOILER DEFLECTION

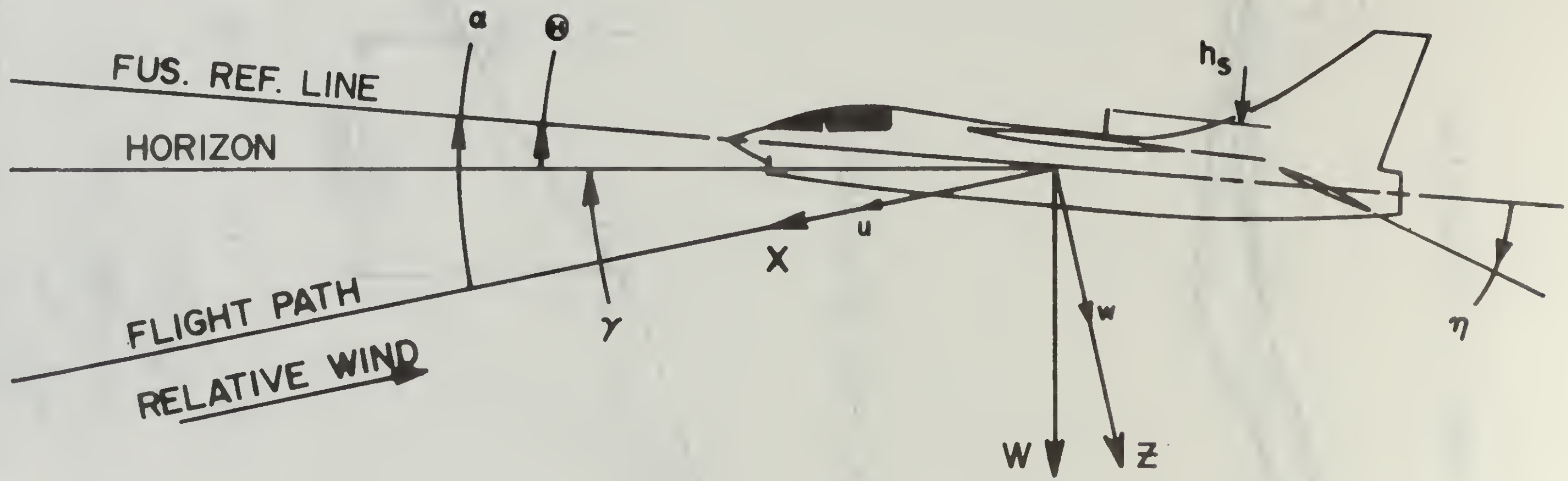

FIGURE 11
AXIS SYSTEM
ARROWS SHOW POSITIVE DIRECTION

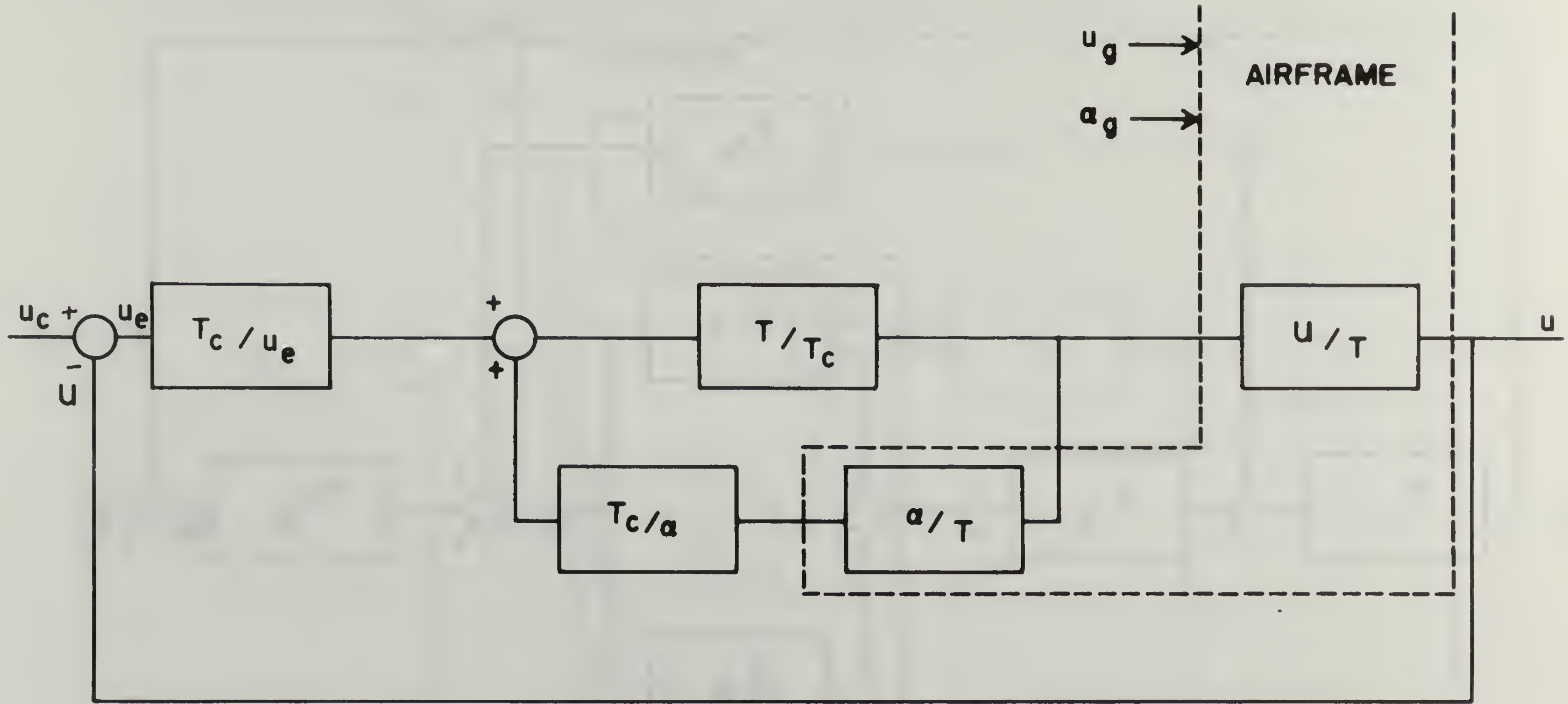

FIGURE 12

BLOCK DIAGRAM — APC

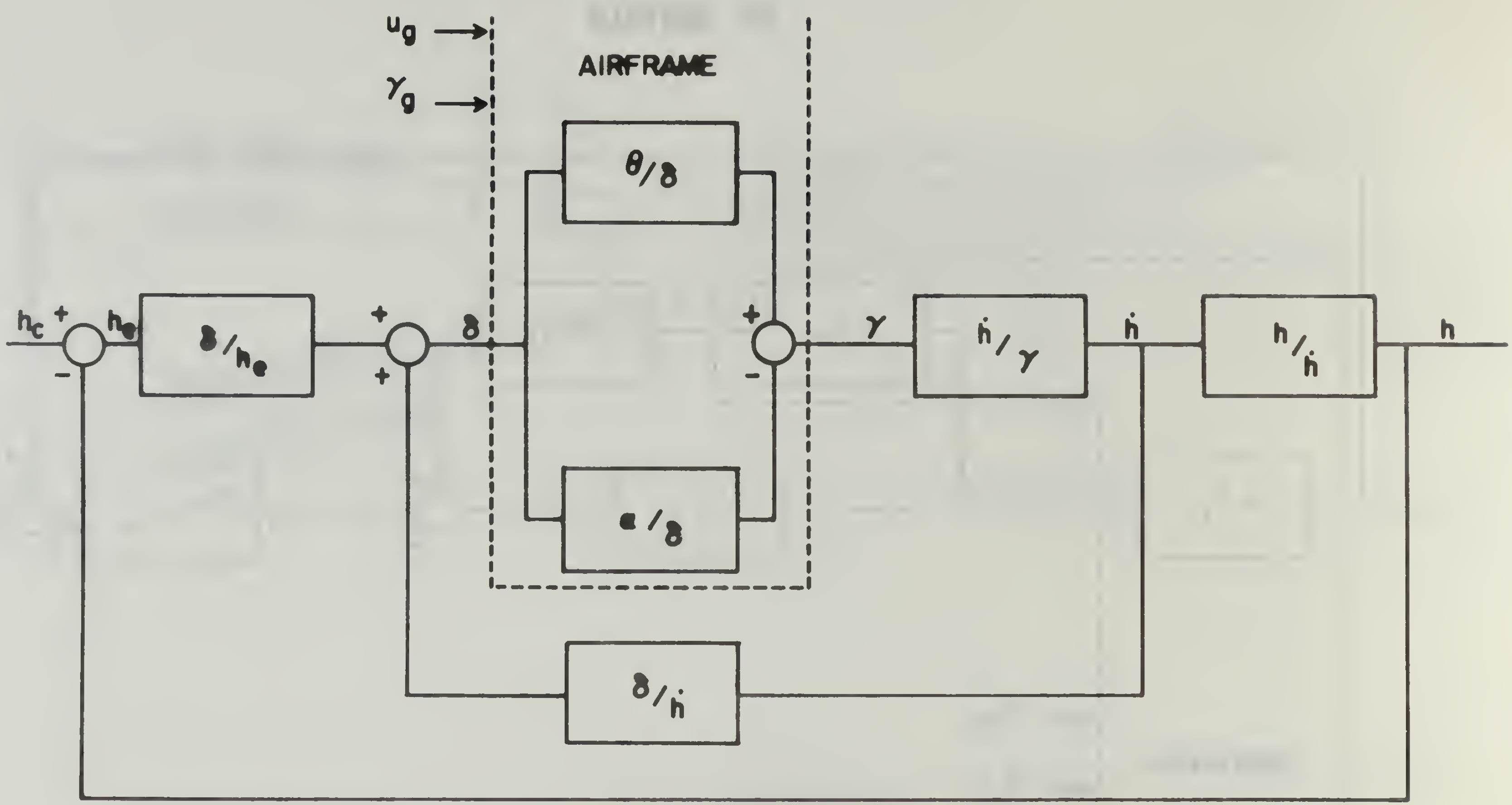

FIGURE 13 BLOCK DIAGRAM - DLC (AUTO)

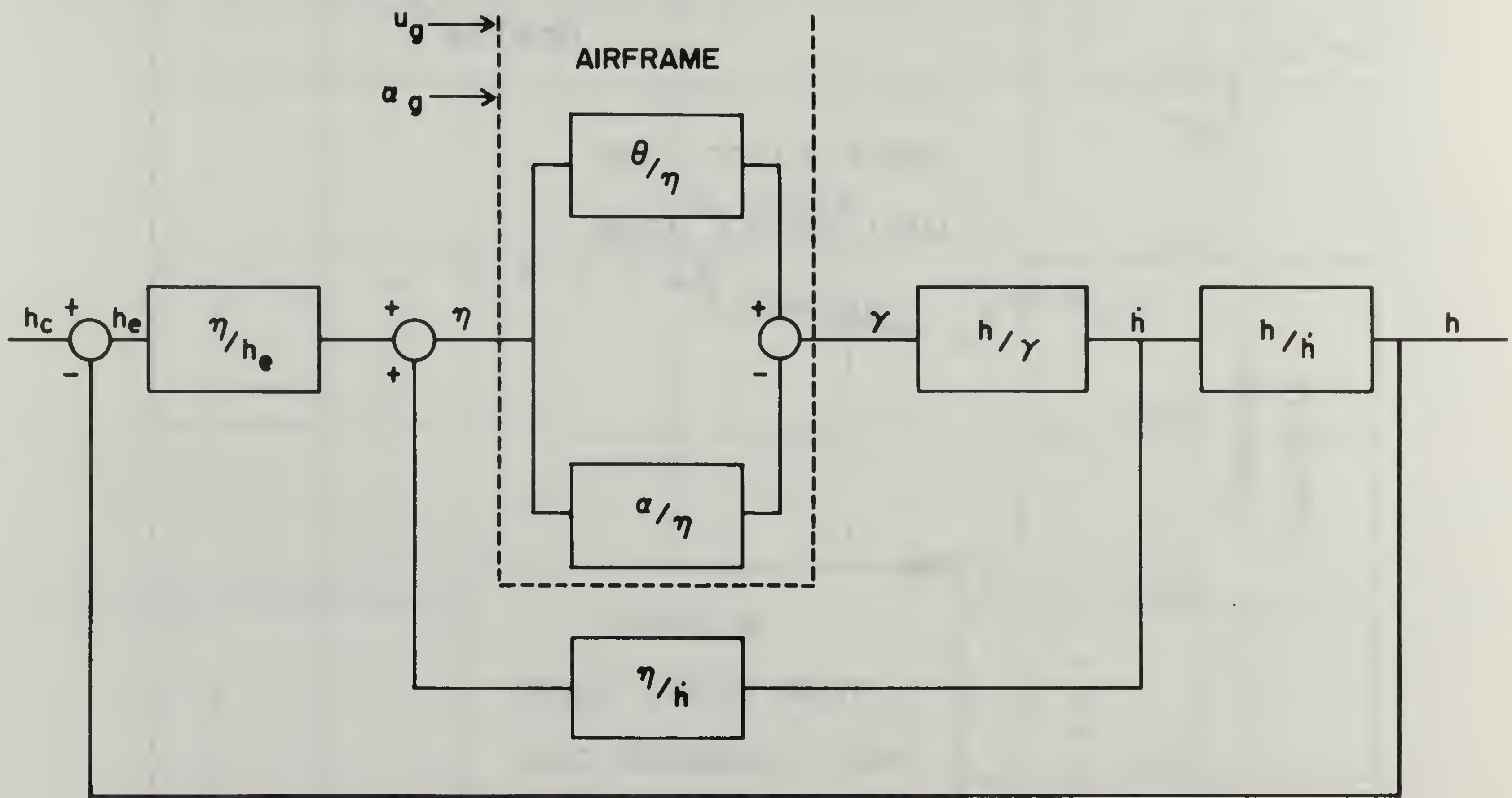

FIGURE 14 BLOCK DIAGRAM - EGSC (AUTO)

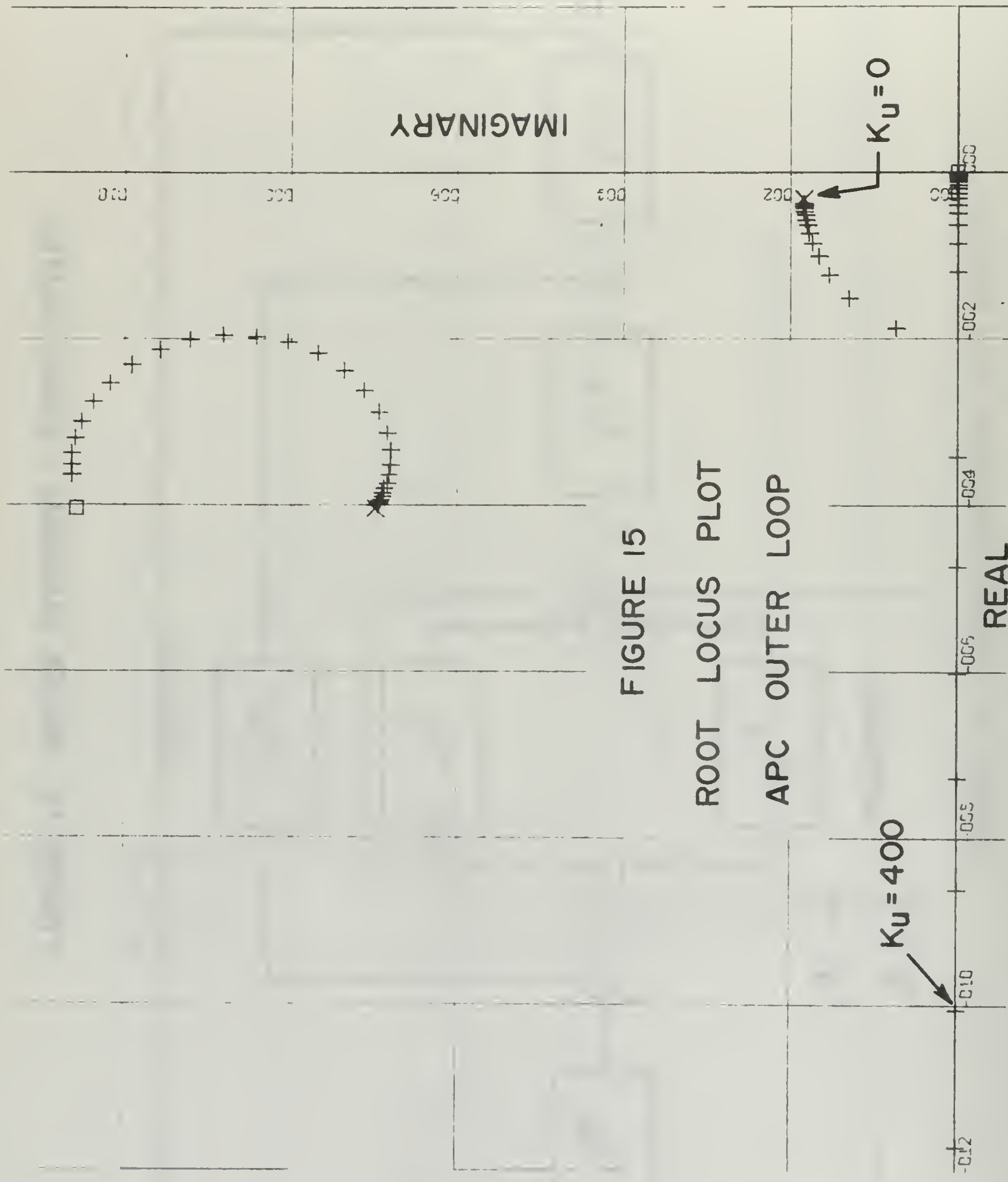

FIGURE 15

ROOT LOCUS PLOT

APC OUTER LOOP

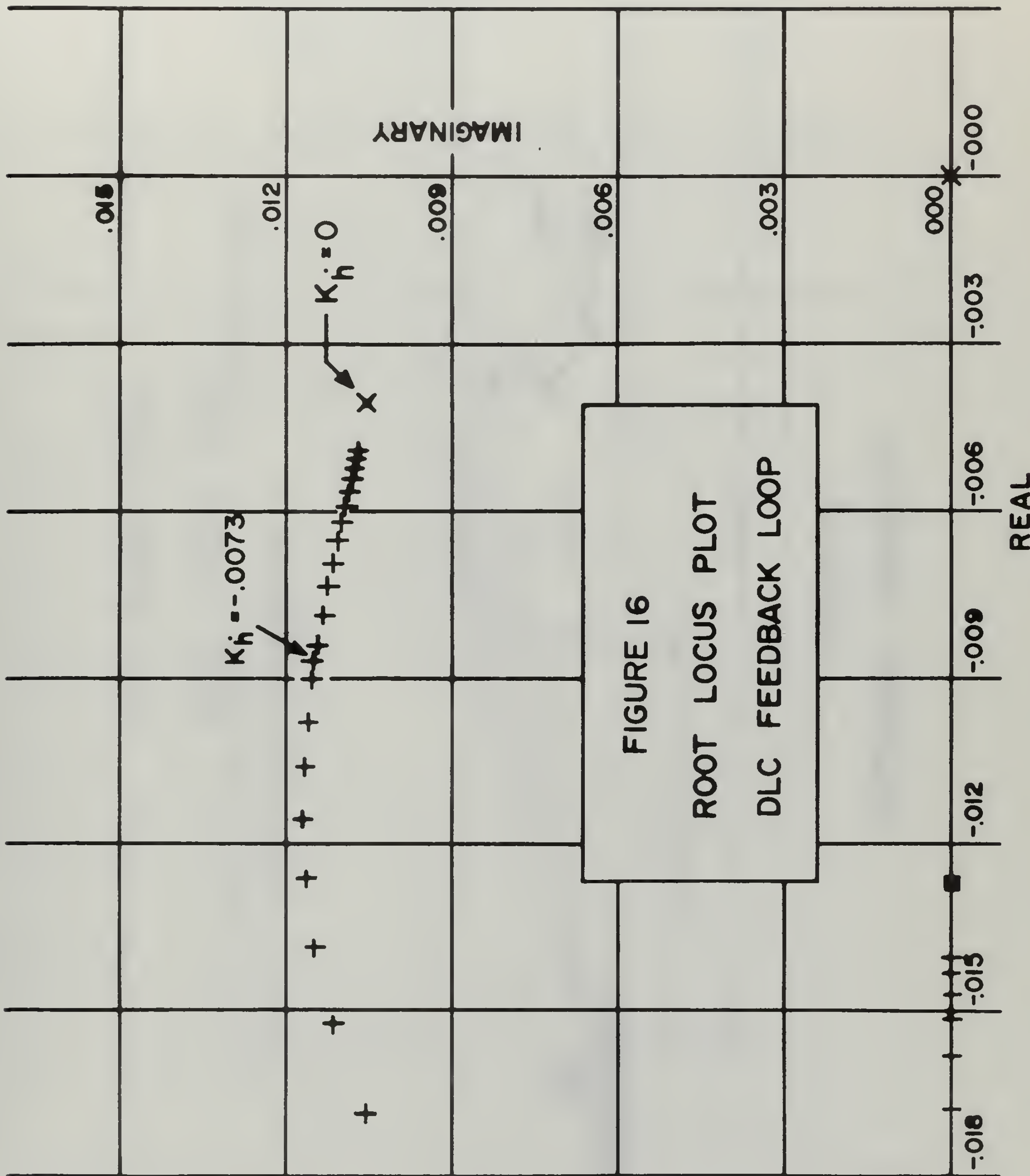

FIGURE 16
ROOT LOCUS PLOT
DLC FEEDBACK LOOP

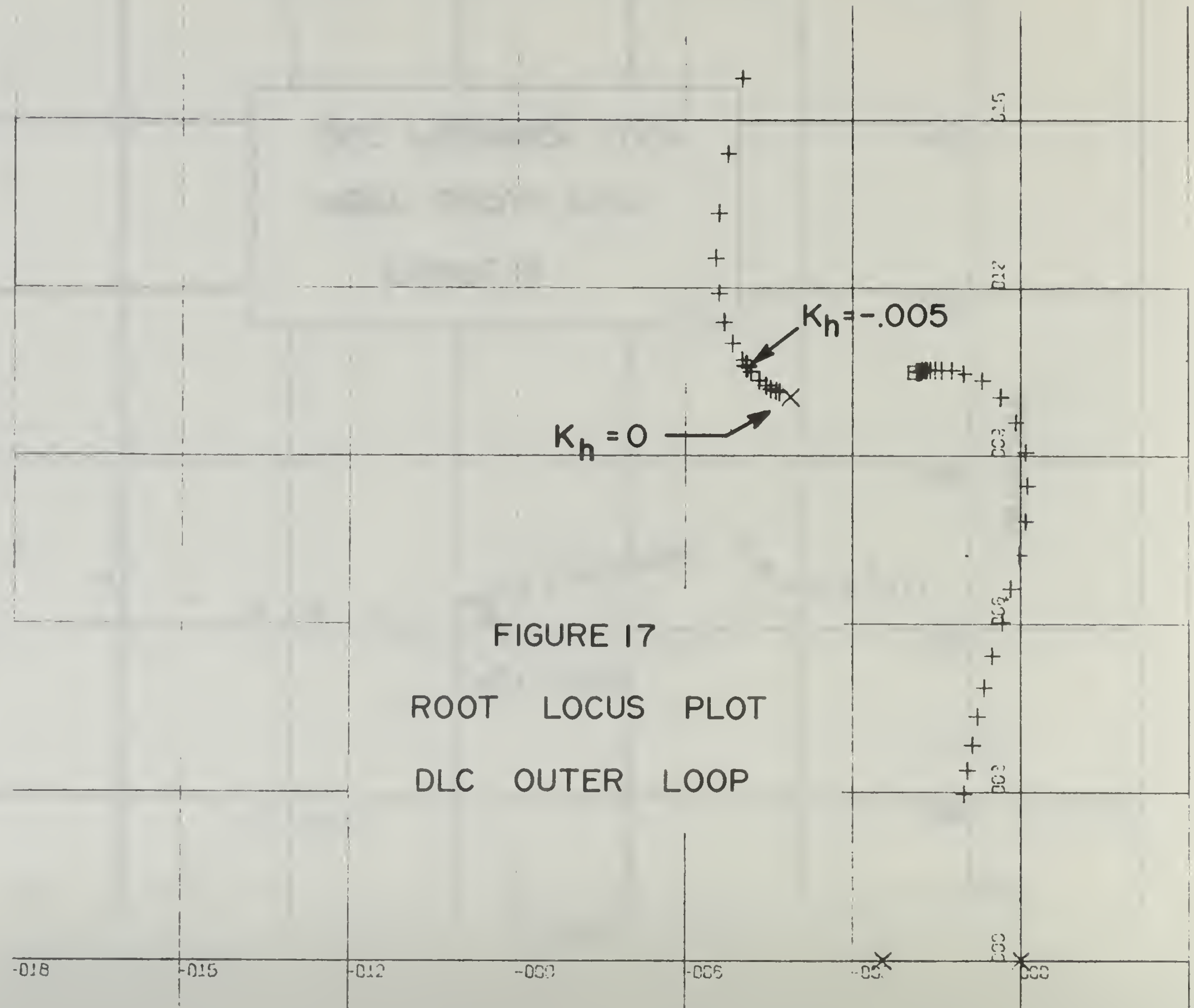

FIGURE 17

ROOT LOCUS PLOT

DLC OUTER LOOP

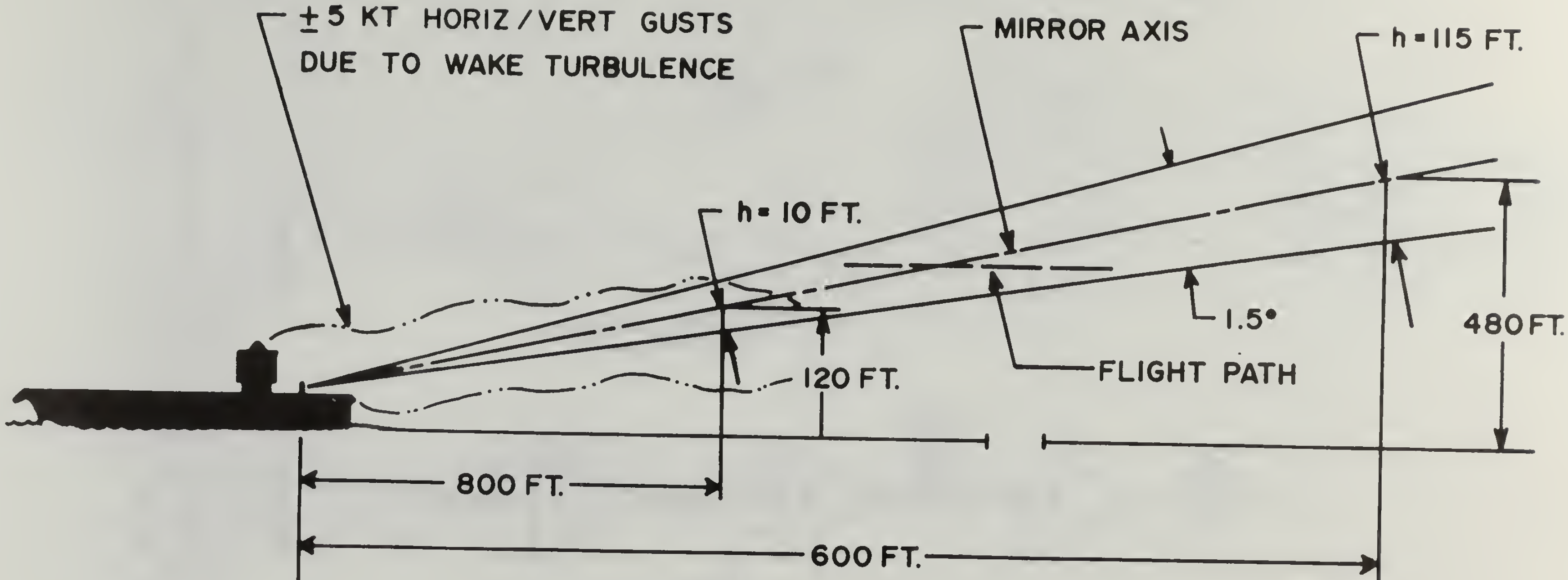

FIGURE 19

APPROACH GEOMETRY

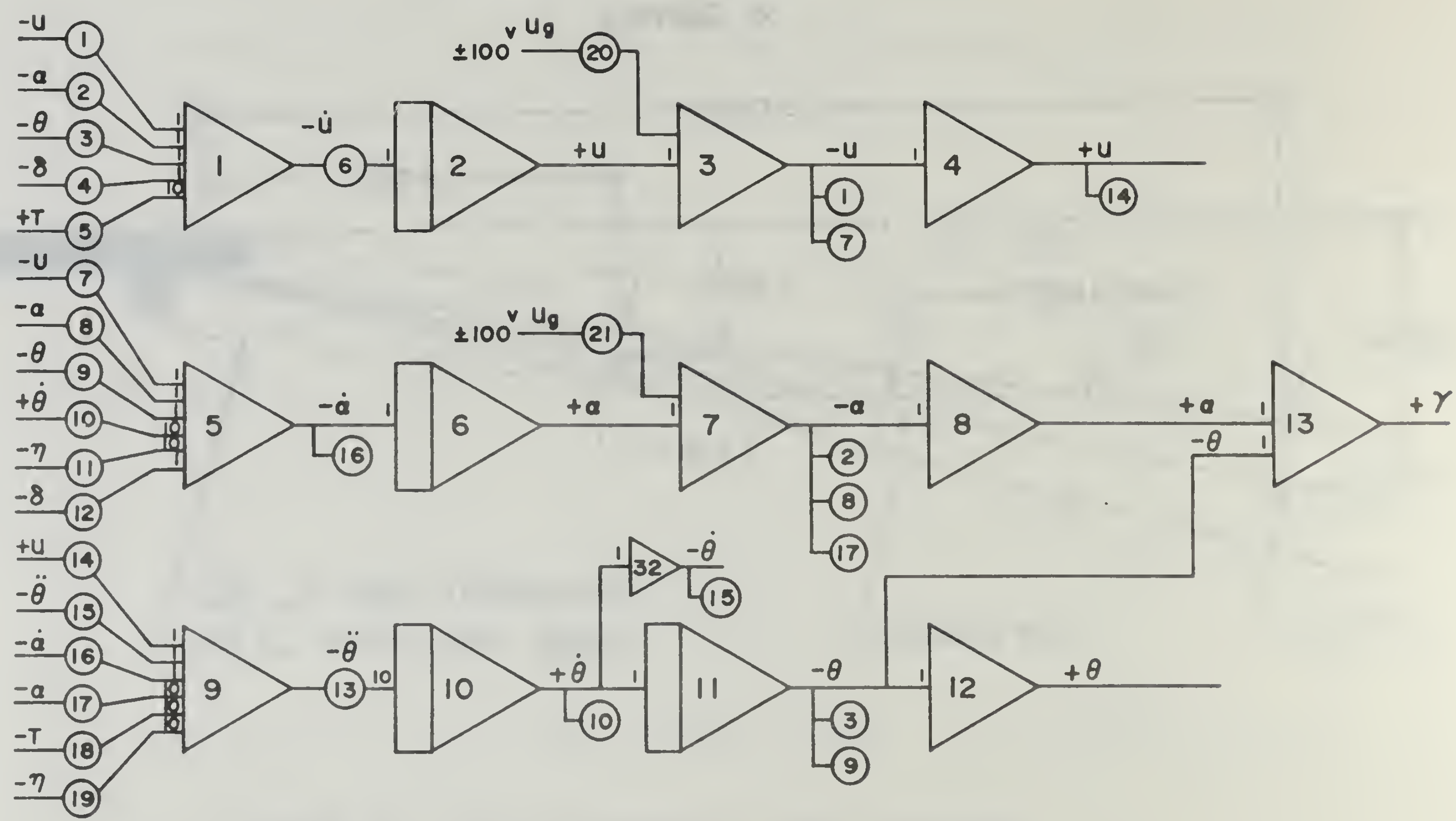

FIGURE 20 ANALOG DIAGRAM – BASIC AIRFRAME

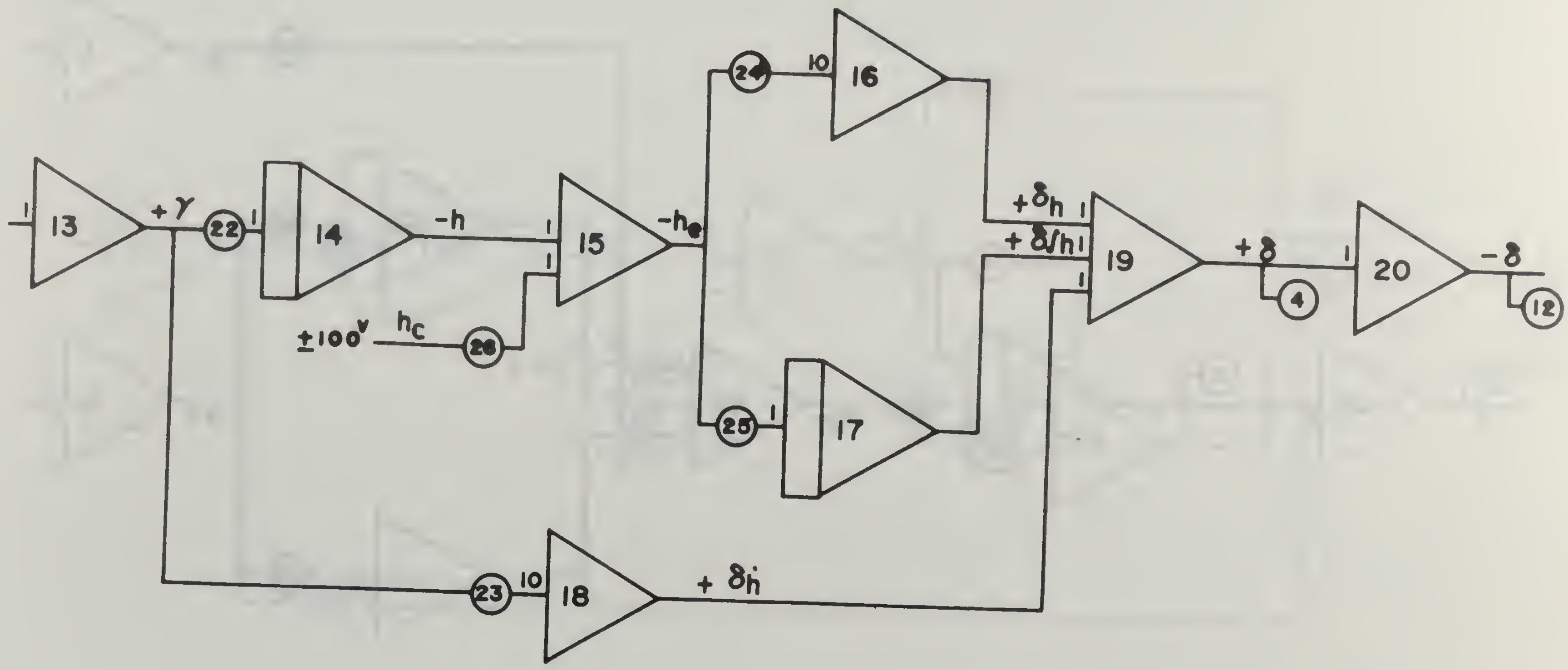

FIGURE 21

ANALOG DIAGRAM - DLC (AUTO)

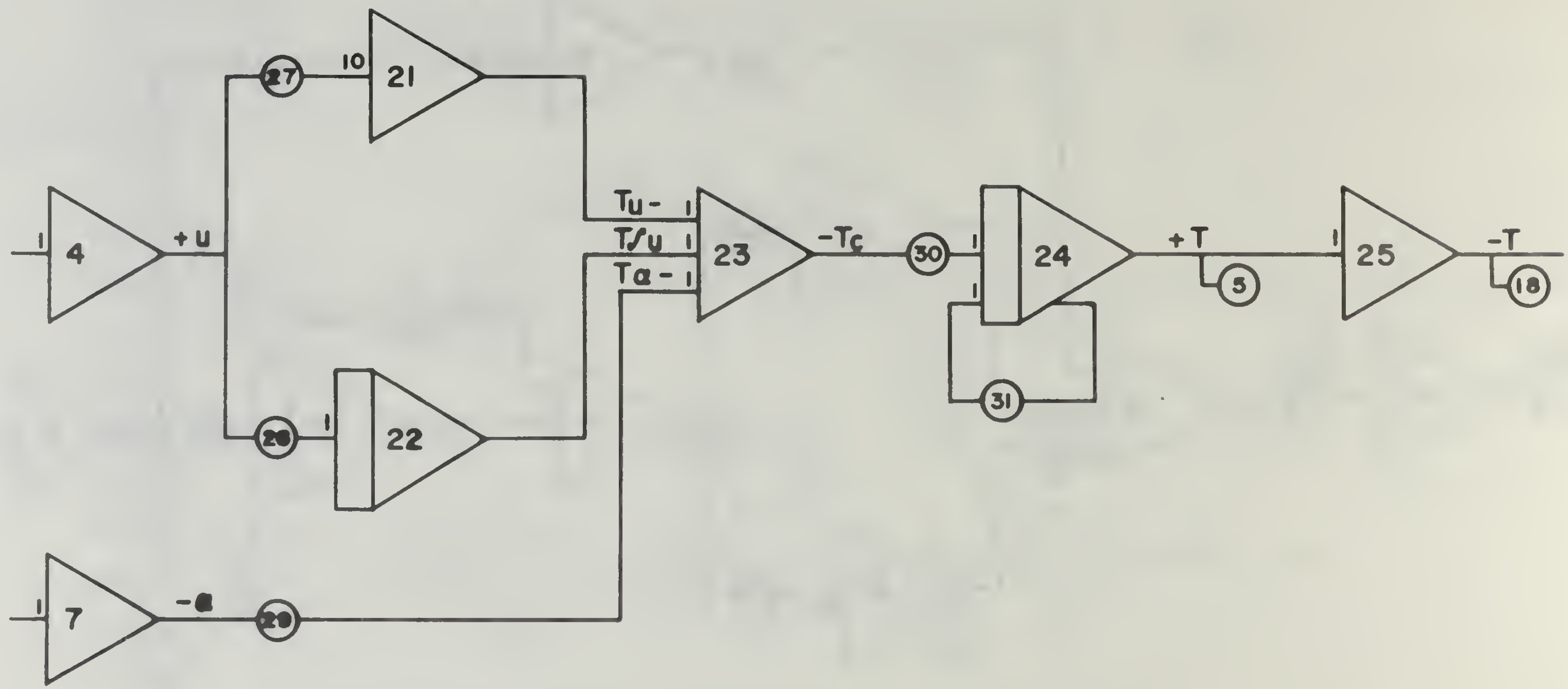

FIGURE 22

ANALOG DIAGRAM - APC

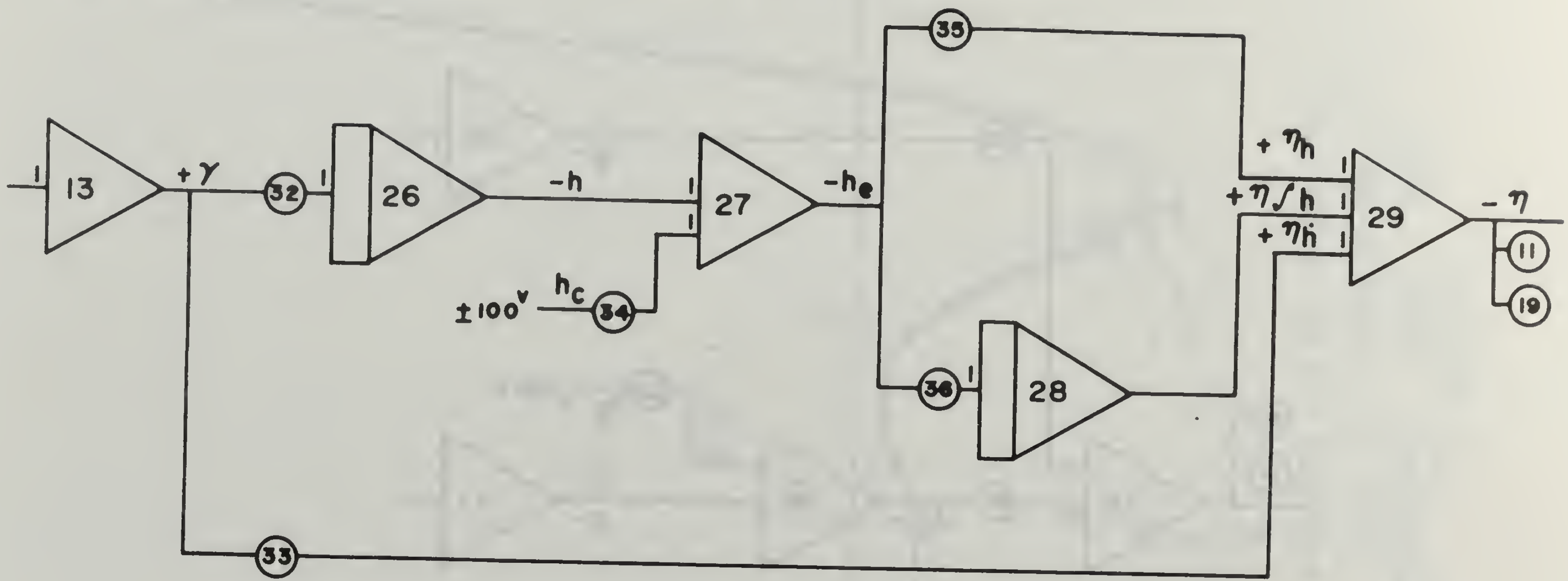

FIGURE 23

ANALOG DIAGRAM — EGSC (AUTO)

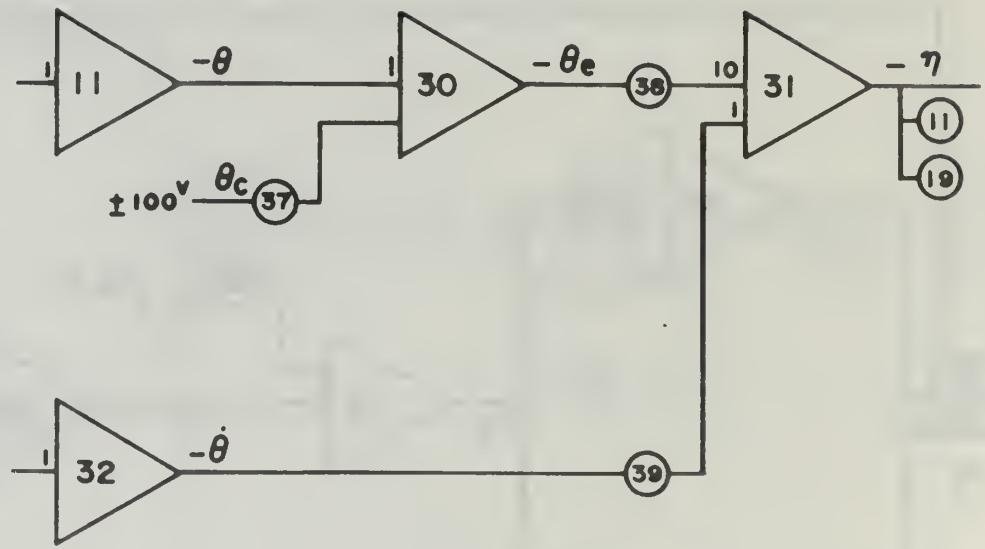

FIGURE 24

ANALOG DIAGRAM - PITCH CONTROL SYSTEM

FIGURE 25
APC GAIN OPTIMIZATION
U RESPONSE TO 5 KT TAIL GUST
Ku = 400 Ku Ki = VARIOUS Kα = 10,000

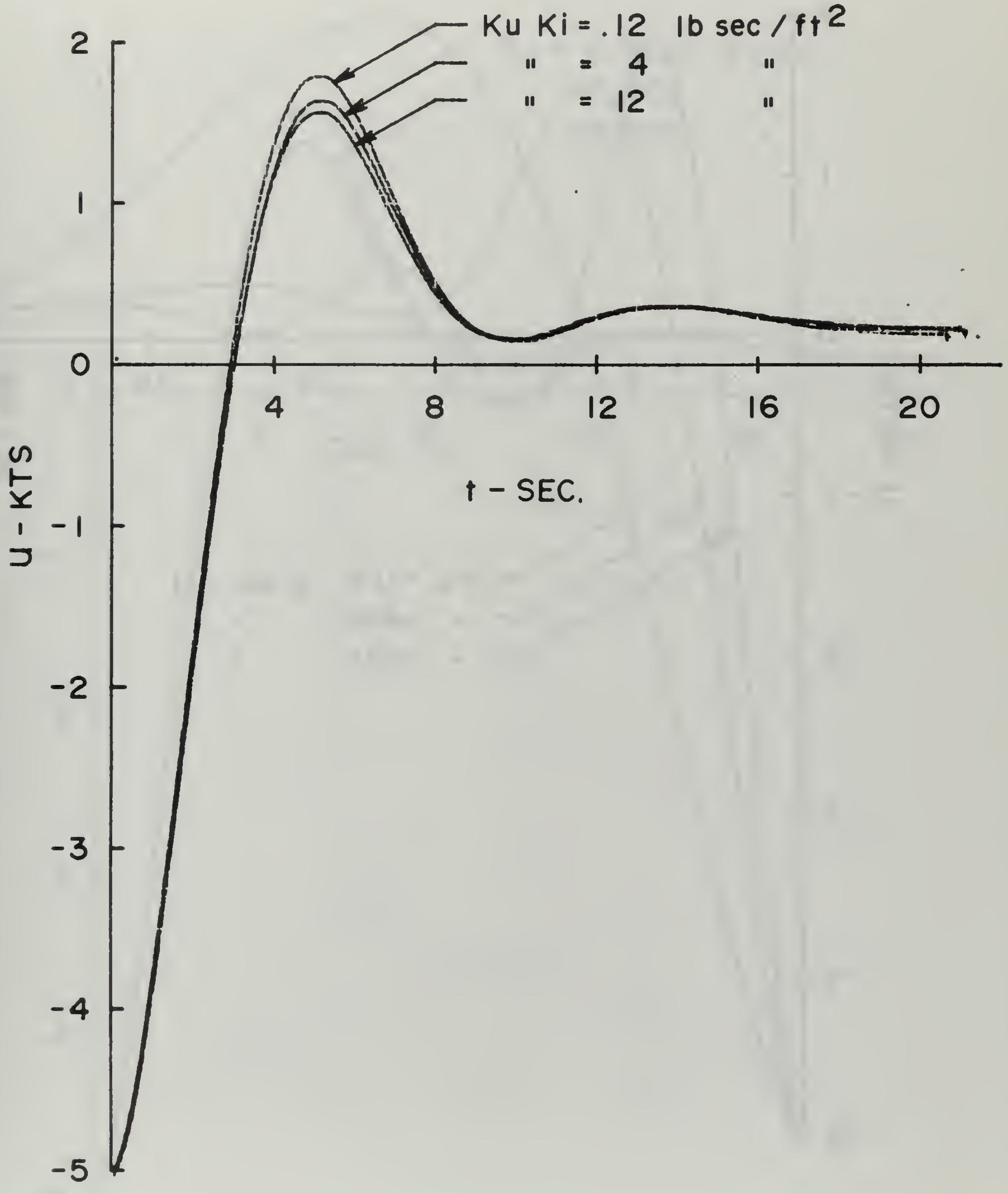

FIGURE 26
APC GAIN OPTIMIZATION
U RESPONSE TO 5KT TAIL GUST
Ku = VARIOUS KuKi = .12 Kα = 10,000

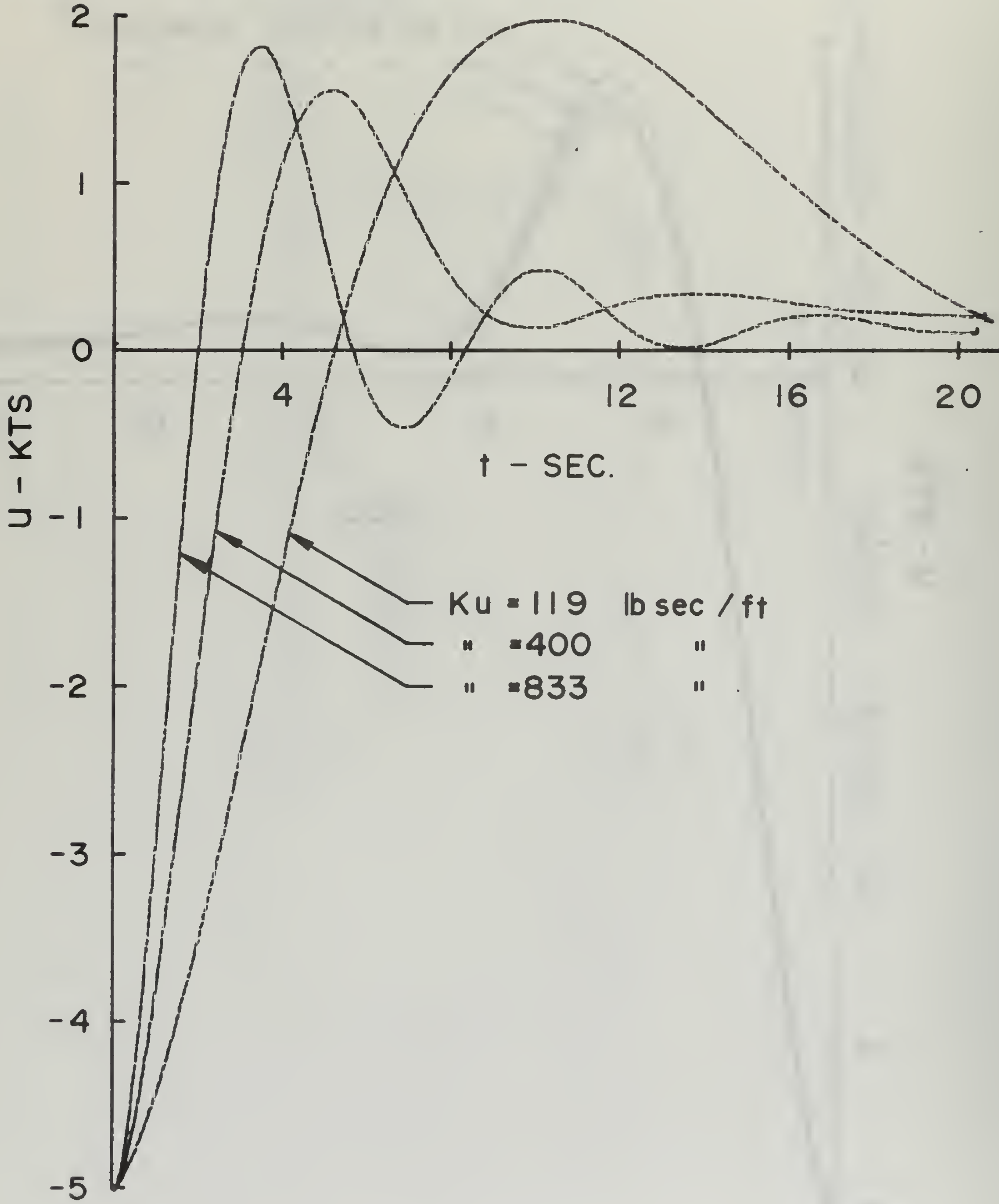

FIGURE 27

APC GAIN OPTIMIZATION

U RESPONSE TO 5KT TAIL GUST

$K_u = 400 \quad K_u K_i = .12 \quad K_\alpha$ = Various

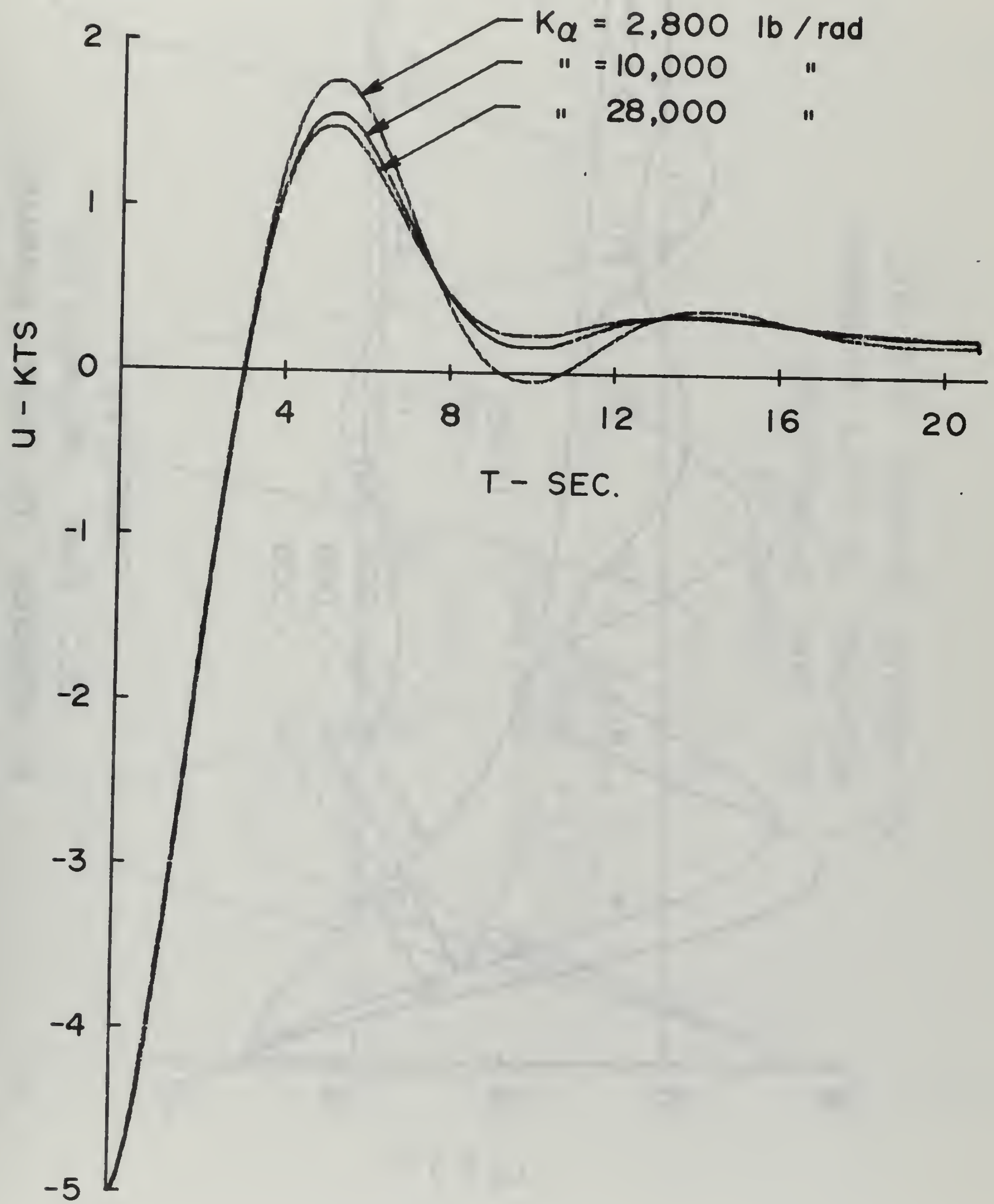

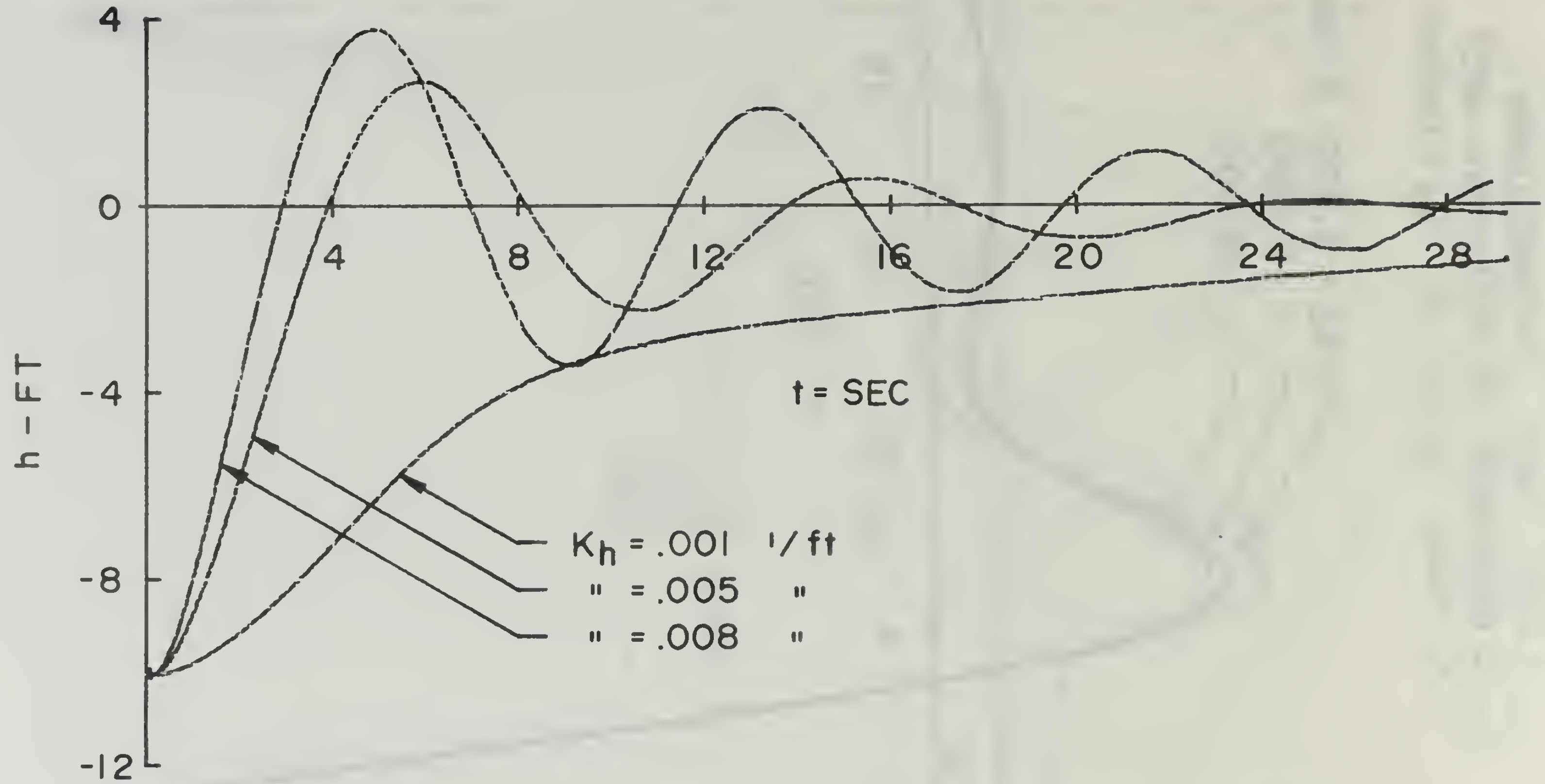

FIGURE 28

DLC GAIN OPTIMIZATION

h RESPONSE TO 10 FT. COMMAND

$K_{\dot{h}} = -.0073 \quad K_h = \text{VARIOUS} \quad K_h K_i = 10^{-5}$

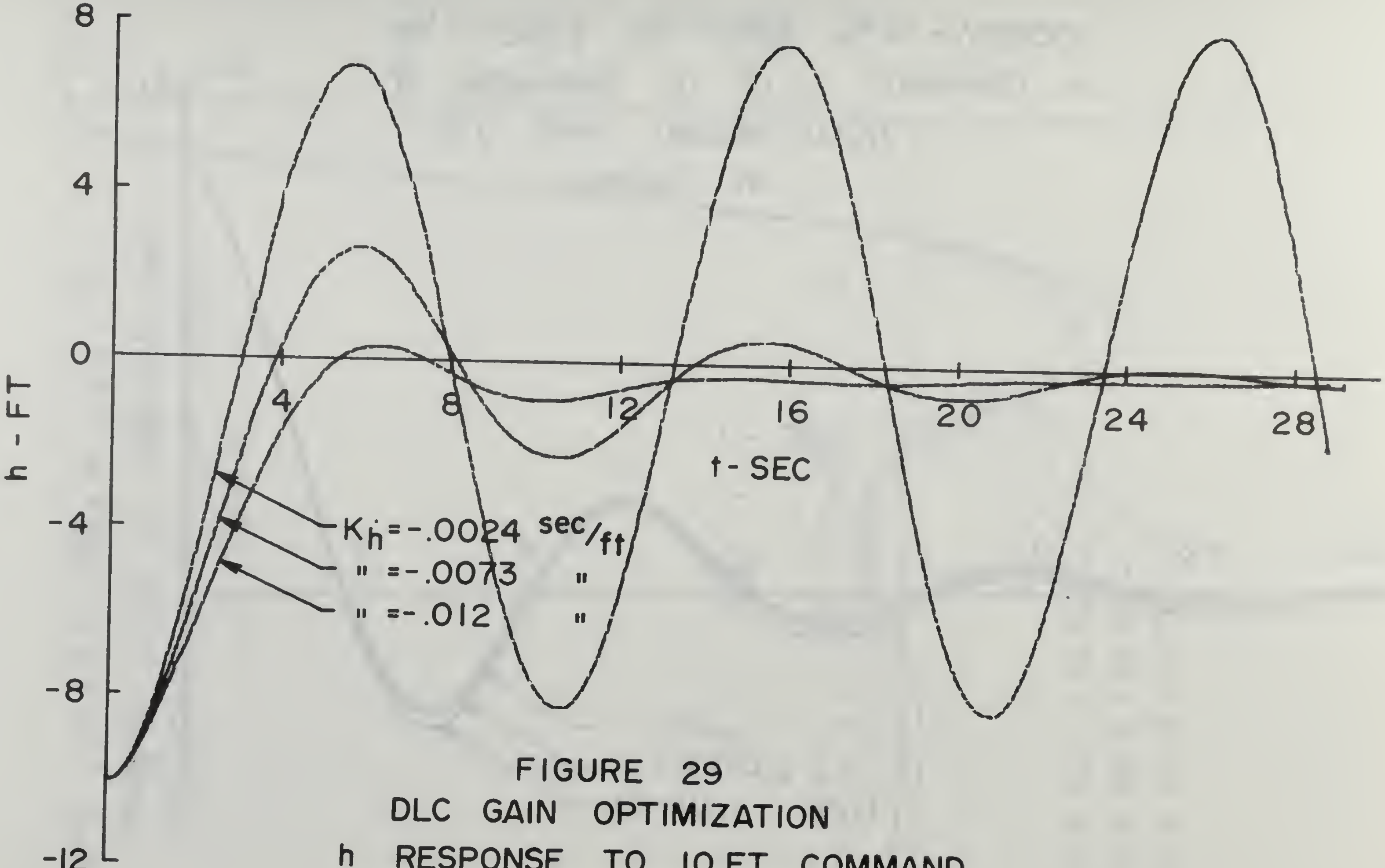

FIGURE 29
DLC GAIN OPTIMIZATION
h RESPONSE TO 10 FT. COMMAND
$K_{\dot{h}}$ = VARIOUS K_h = .005 $K_h K_i = 10^{-5}$

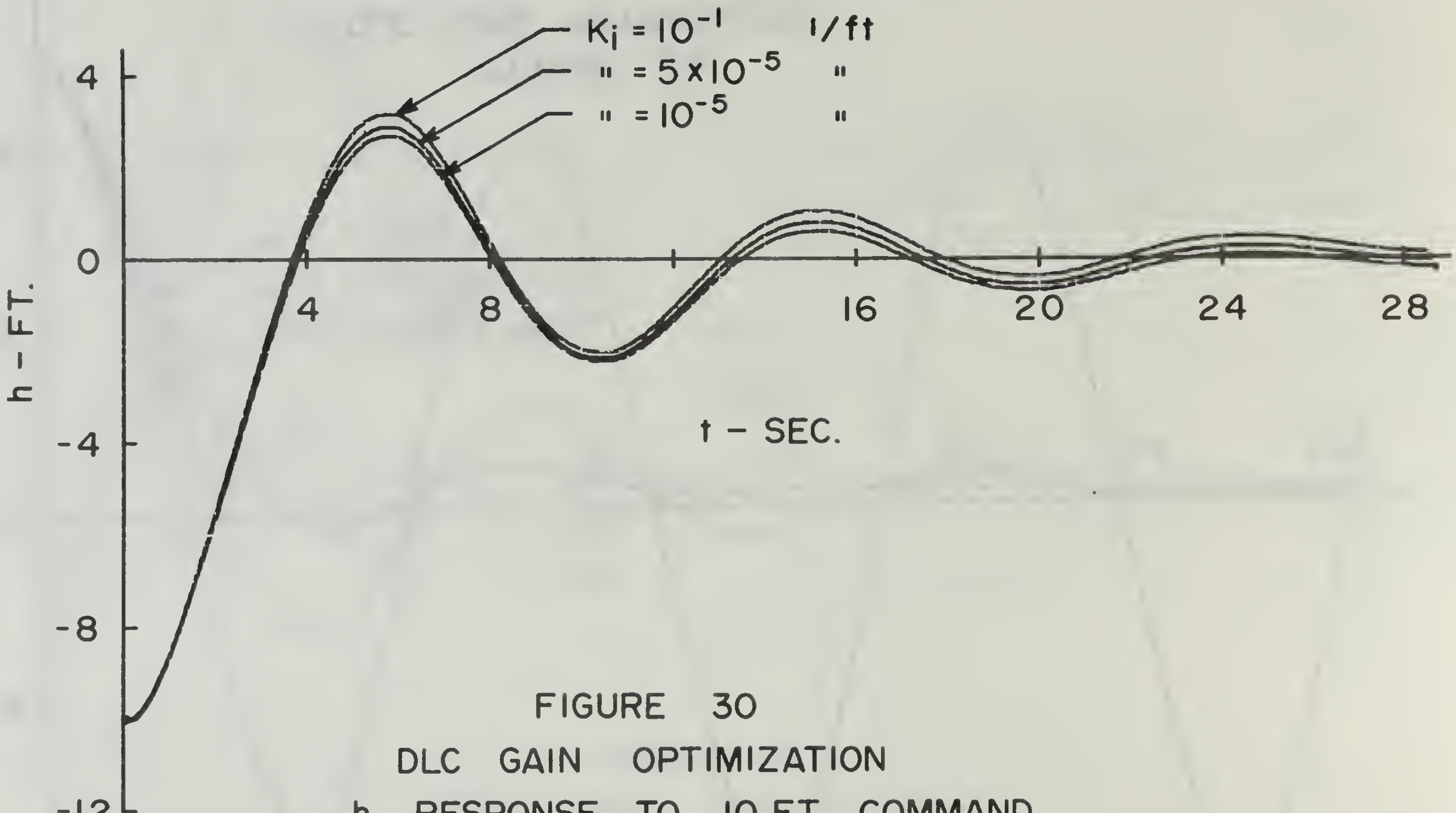

FIGURE 30

DLC GAIN OPTIMIZATION

h RESPONSE TO 10 FT. COMMAND

$K_{\dot{h}} = -.0073$ $K_h = .005$ $K_h K_i$ = VARIOUS

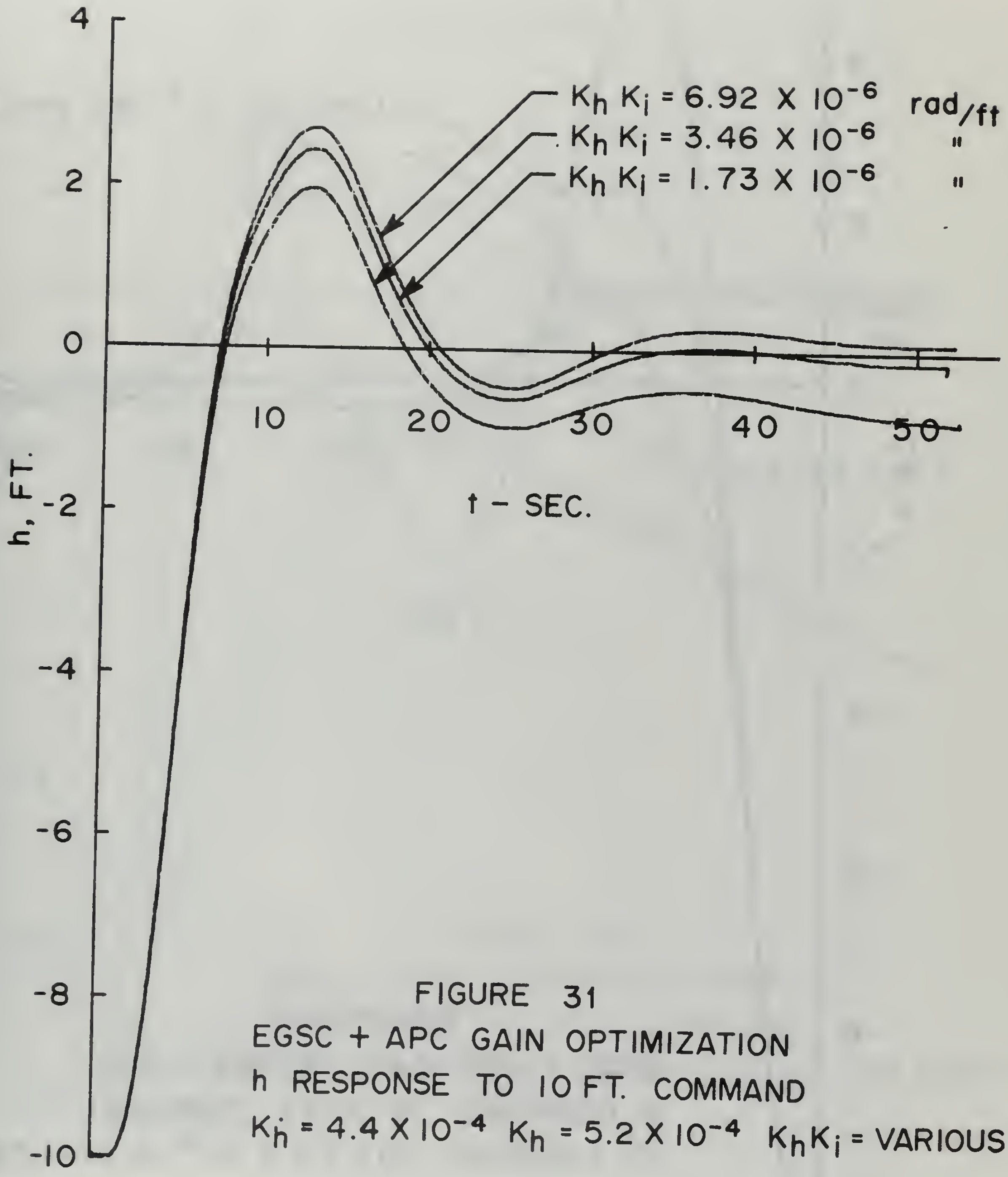

FIGURE 31

EGSC + APC GAIN OPTIMIZATION

h RESPONSE TO 10 FT. COMMAND

$K_{\dot{h}} = 4.4 \times 10^{-4}$ $K_h = 5.2 \times 10^{-4}$ $K_h K_i$ = VARIOUS

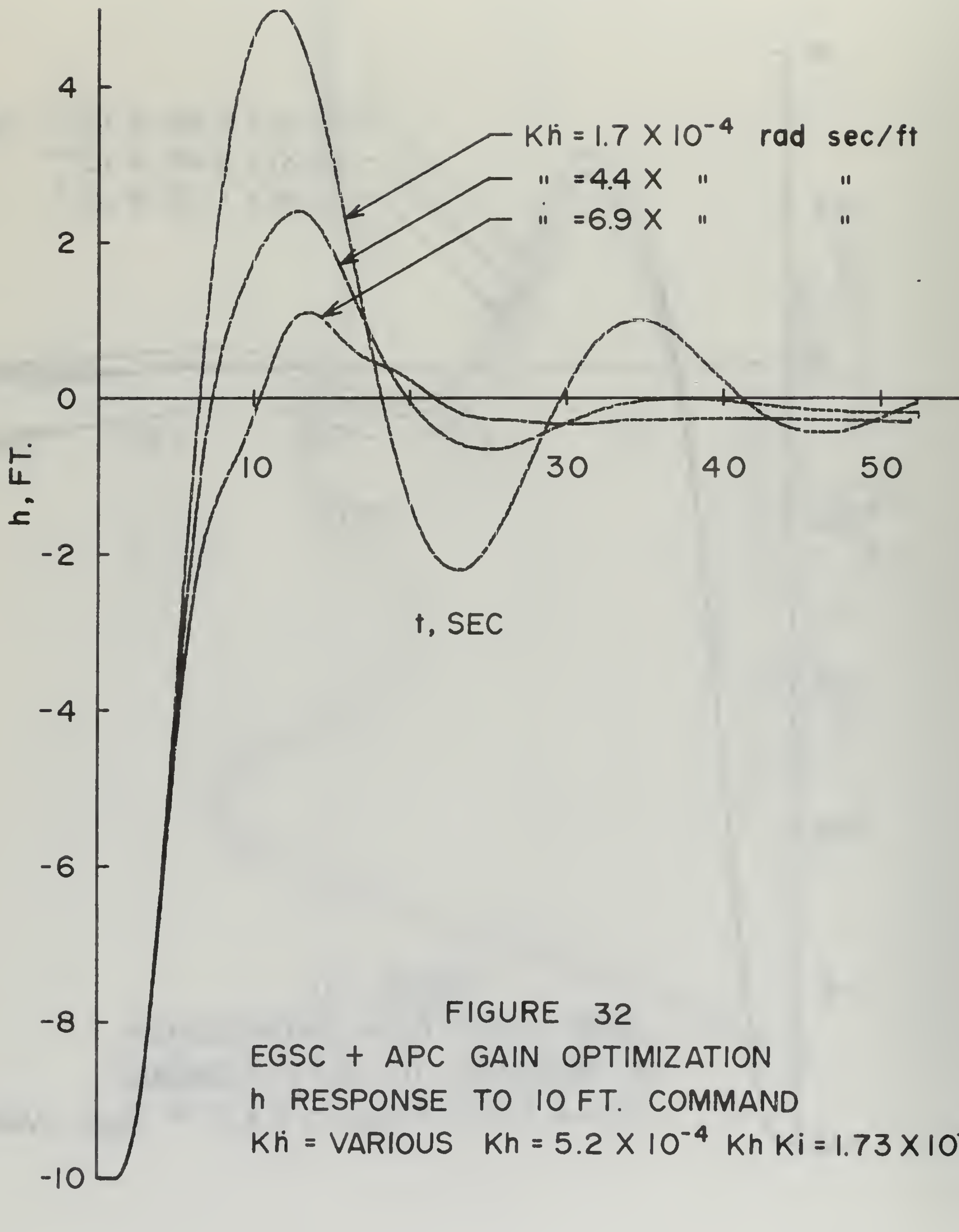

FIGURE 32

EGSC + APC GAIN OPTIMIZATION

h RESPONSE TO 10 FT. COMMAND

$K\ddot{h}$ = VARIOUS $K_h = 5.2 \times 10^{-4}$ $K_h K_i = 1.73 \times 10^{-6}$

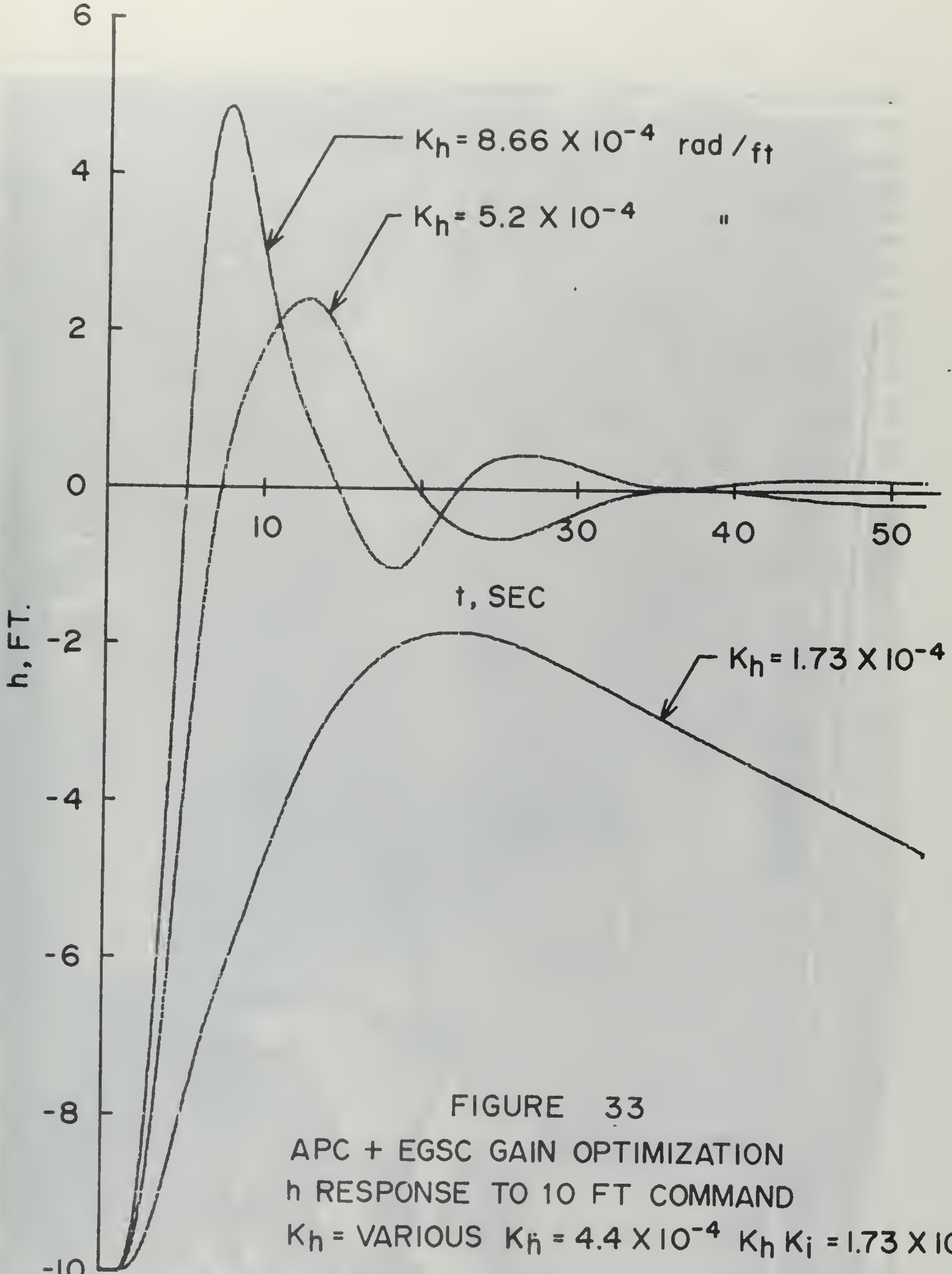

FIGURE 33

APC + EGSC GAIN OPTIMIZATION

h RESPONSE TO 10 FT COMMAND

K_h = VARIOUS $K_{\dot{h}} = 4.4 \times 10^{-4}$ $K_h K_i = 1.73 \times 10^{-6}$

FIGURE 34
GENERAL ARRANGEMENT

FIGURE 35
THROTTLE AND CONTROL STICK

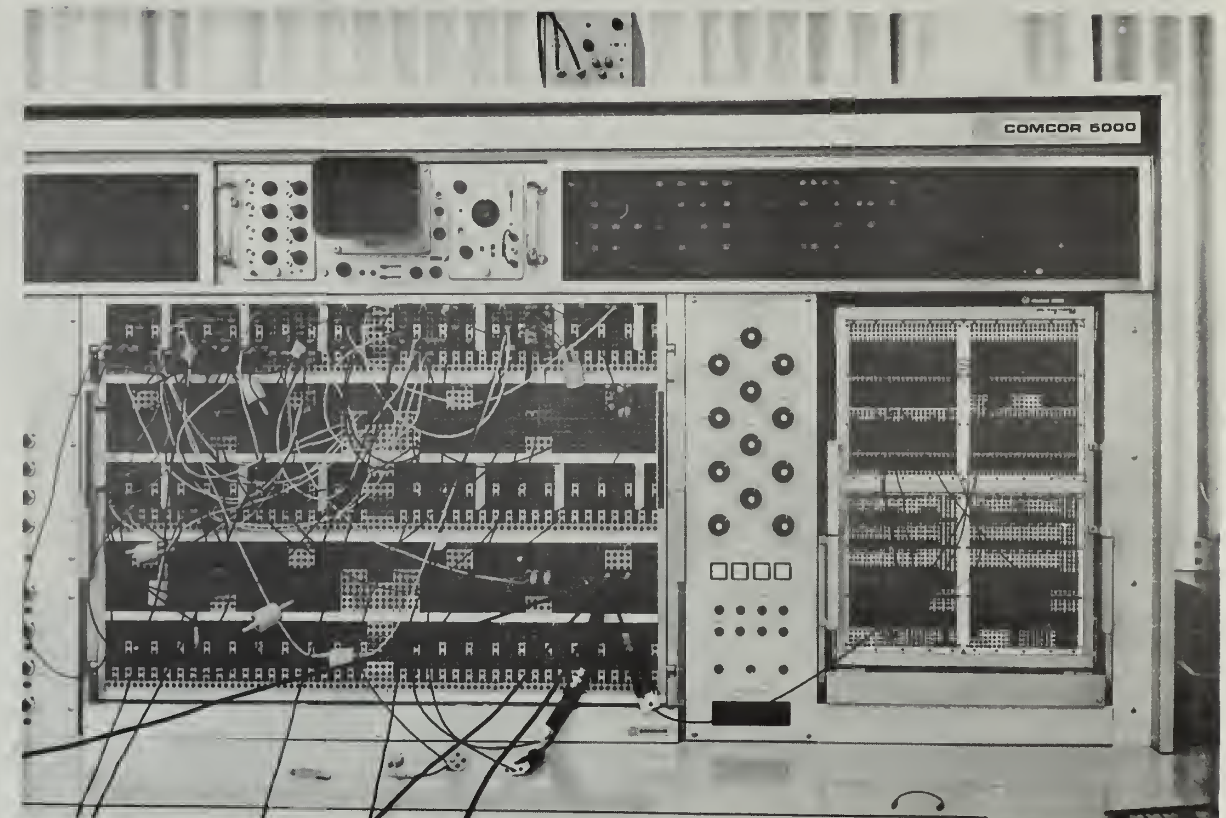

FIGURE 36

ANALOG COMPUTER PATCHBOARD

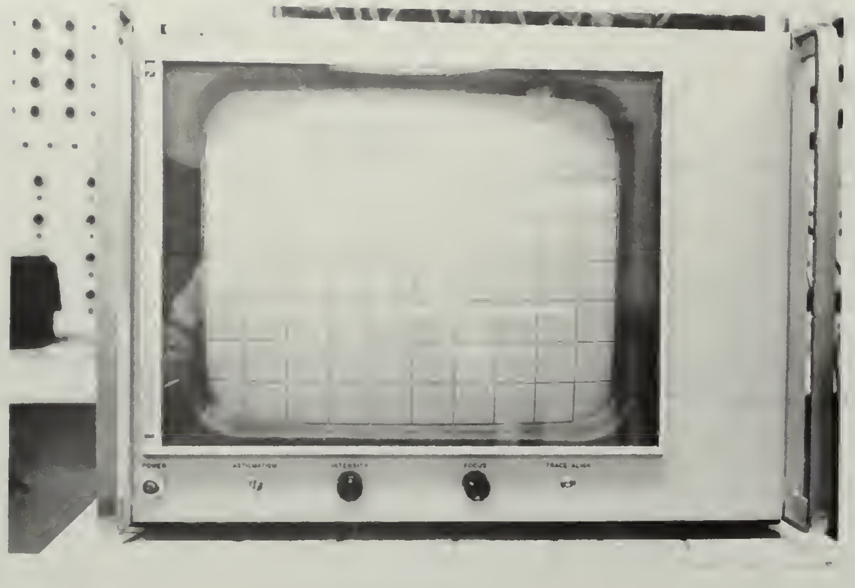

FIGURE 37a

PILOT'S VISUAL DISPLAY SHOWING
ON SPEED 2 FEET BELOW GLIDE SLOPE

FIGURE 37b

PILOT'S VISUAL DISPLAY SHOWING
2 KNOTS SLOW ON GLIDE SLOPE

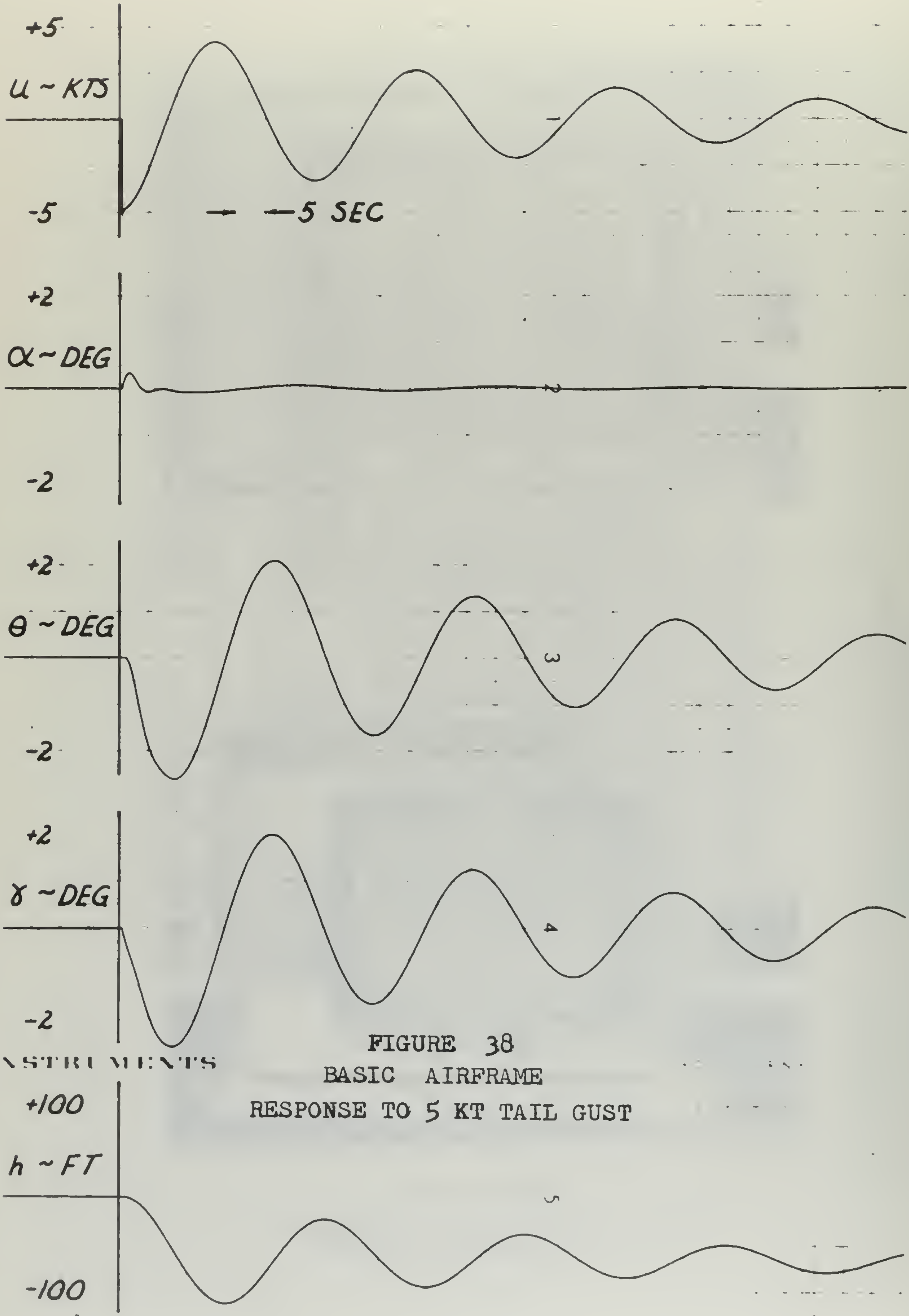

FIGURE 38
BASIC AIRFRAME
RESPONSE TO 5 KT TAIL GUST

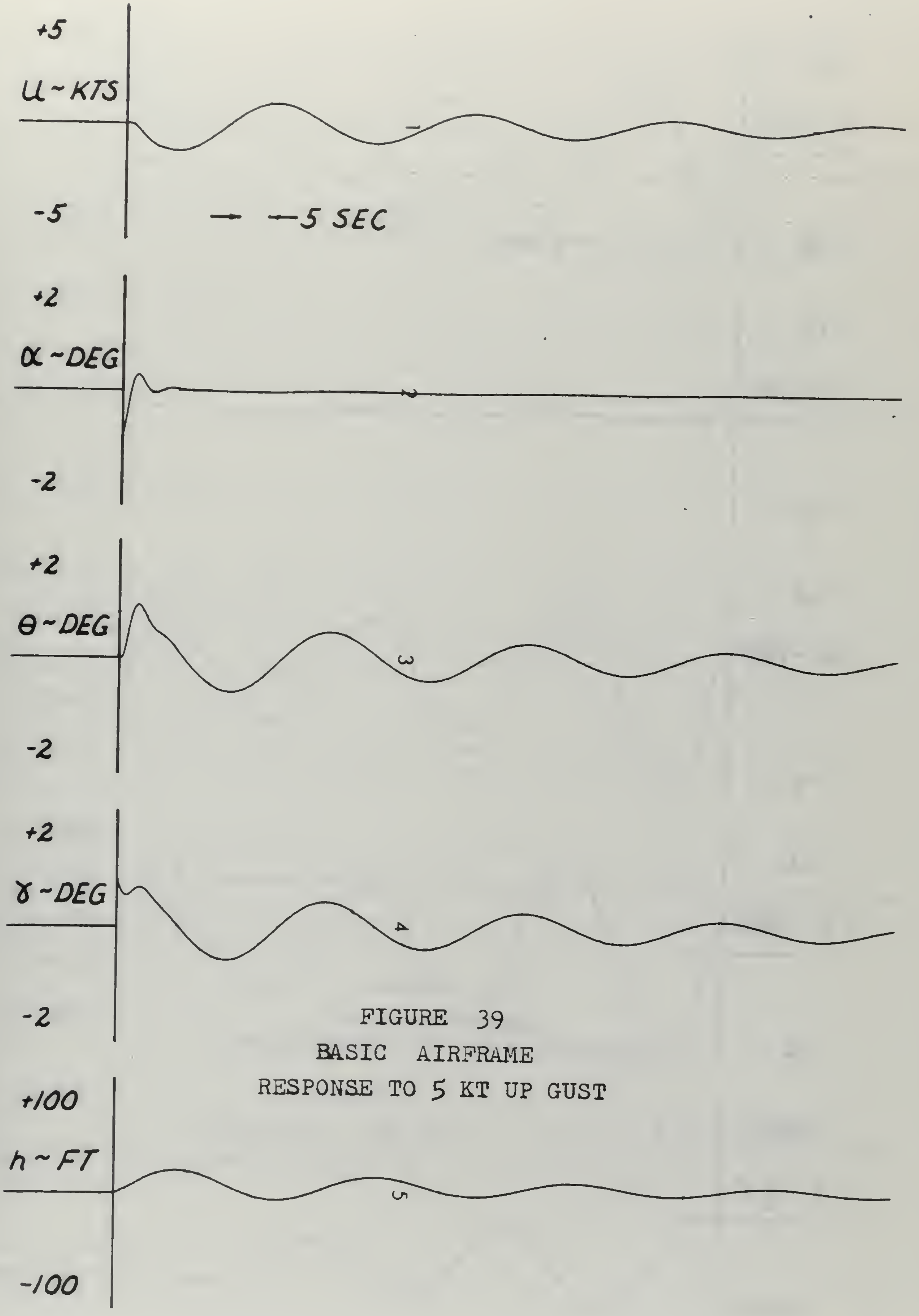

FIGURE 39
BASIC AIRFRAME
RESPONSE TO 5 KT UP GUST

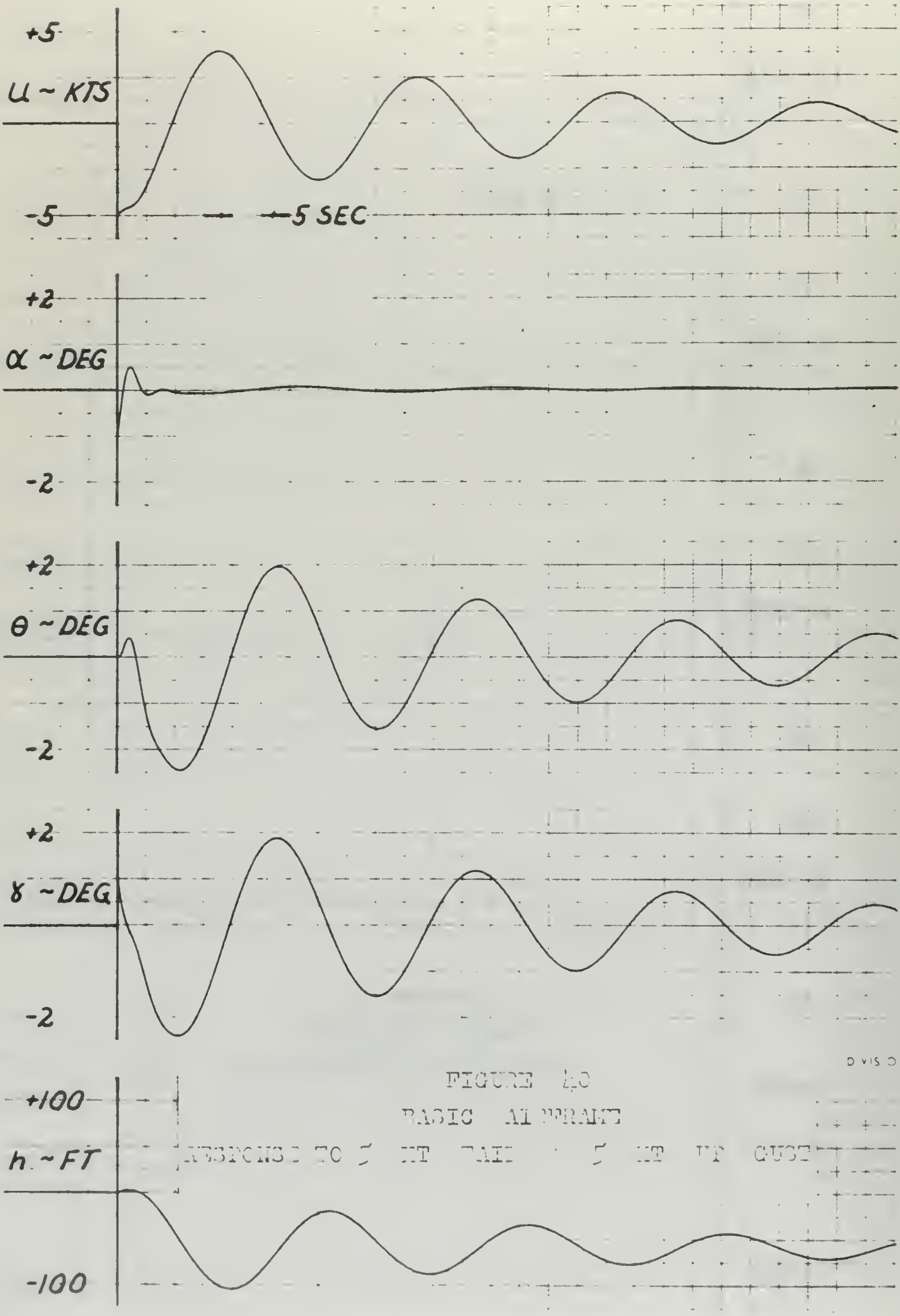

FIGURE 40
BASIC AIRFRAME
RESPONSE TO 5 KT TAIL 5 KT UP GUST

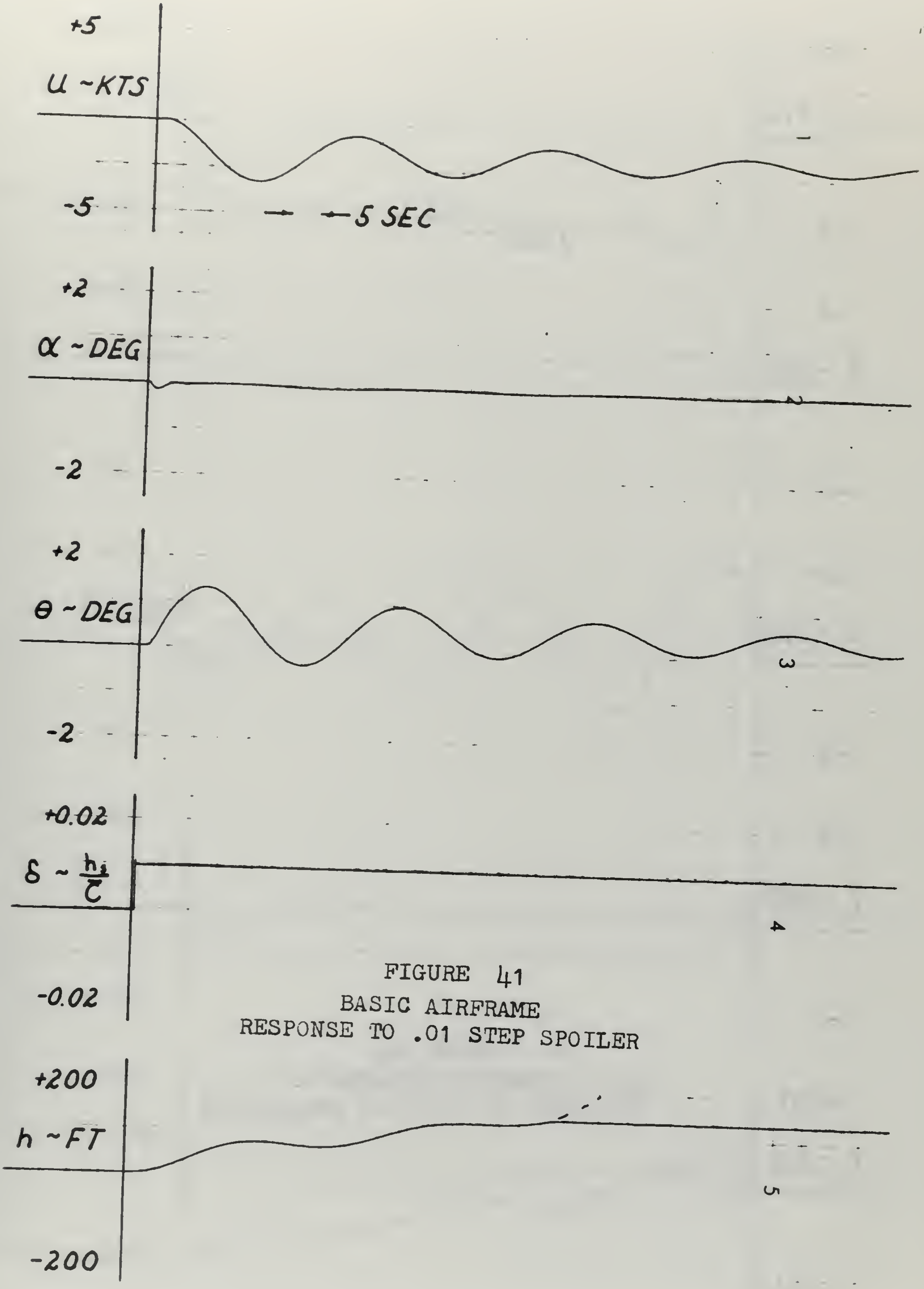

FIGURE 41
BASIC AIRFRAME
RESPONSE TO .01 STEP SPOILER

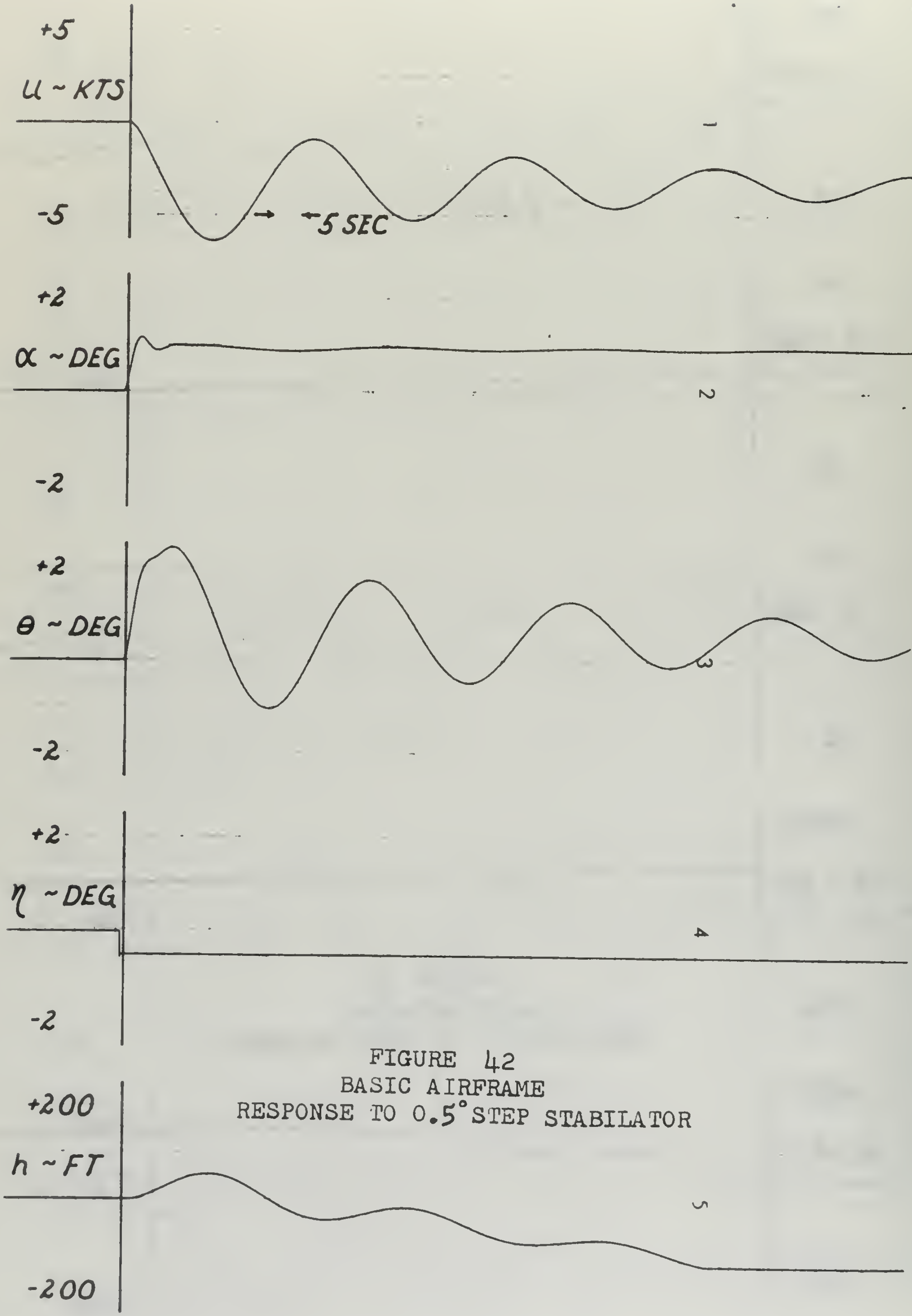

FIGURE 42
BASIC AIRFRAME
RESPONSE TO 0.5° STEP STABILATOR

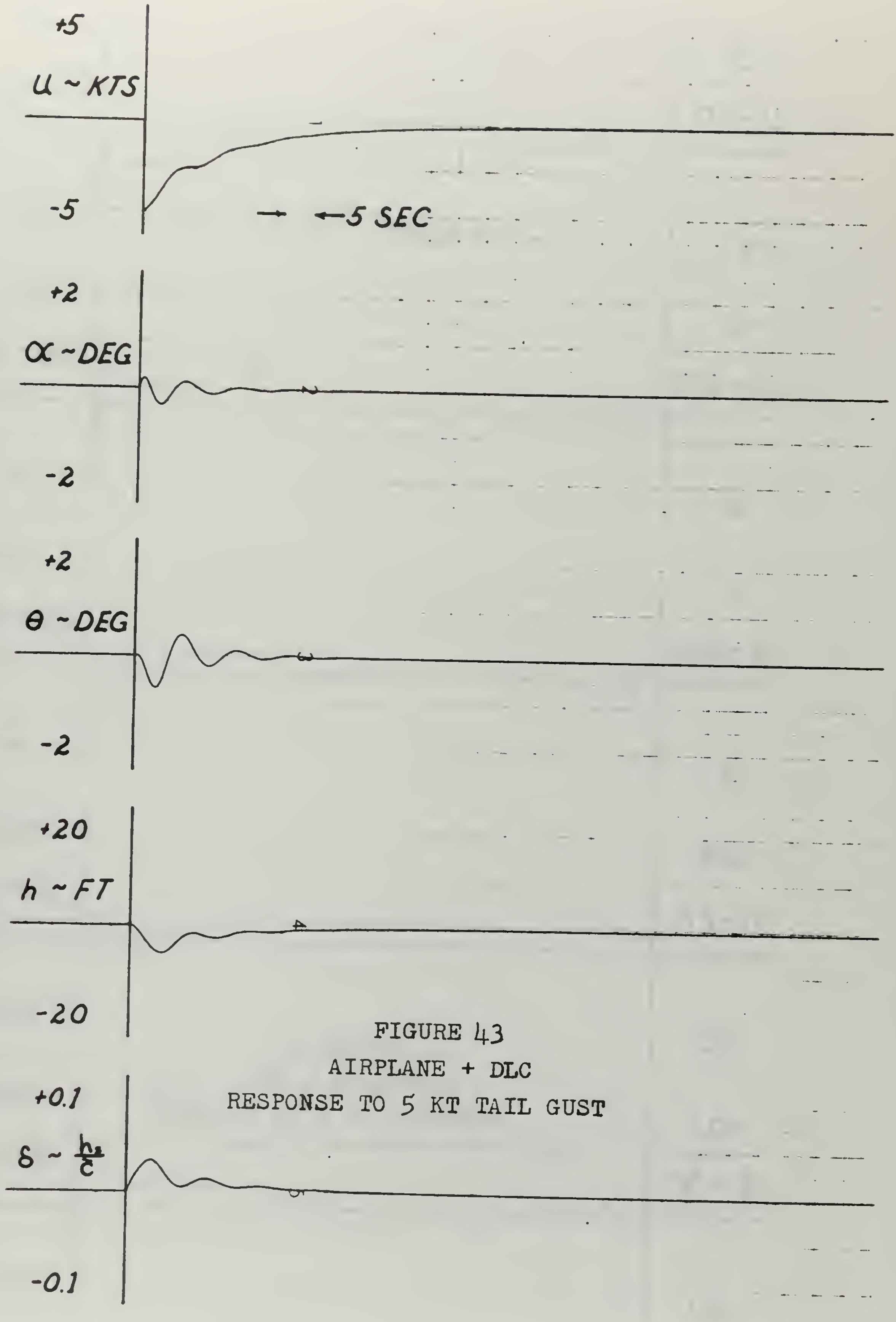

FIGURE 43
AIRPLANE + DLC
RESPONSE TO 5 KT TAIL GUST

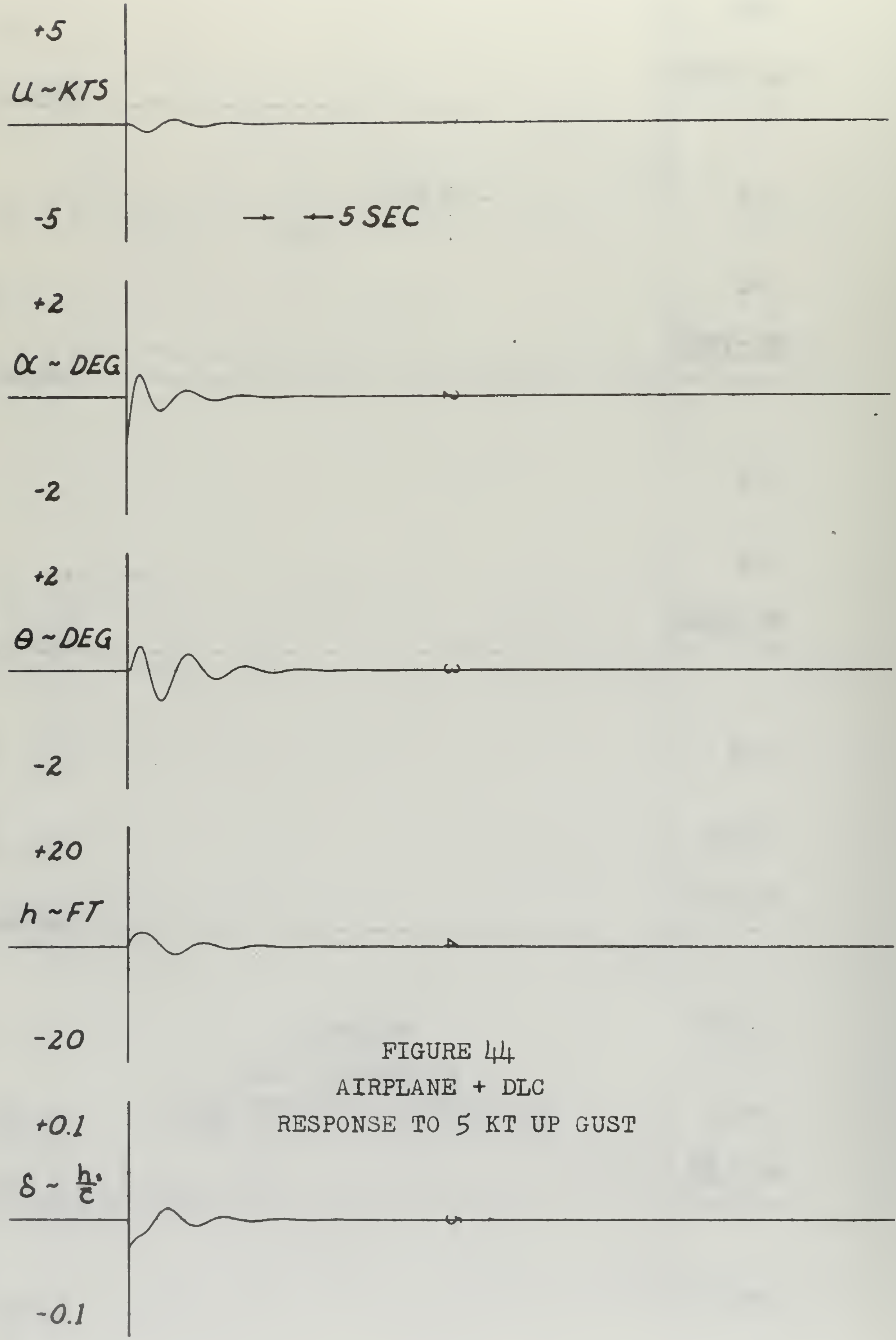

FIGURE 44
AIRPLANE + DLC
RESPONSE TO 5 KT UP GUST

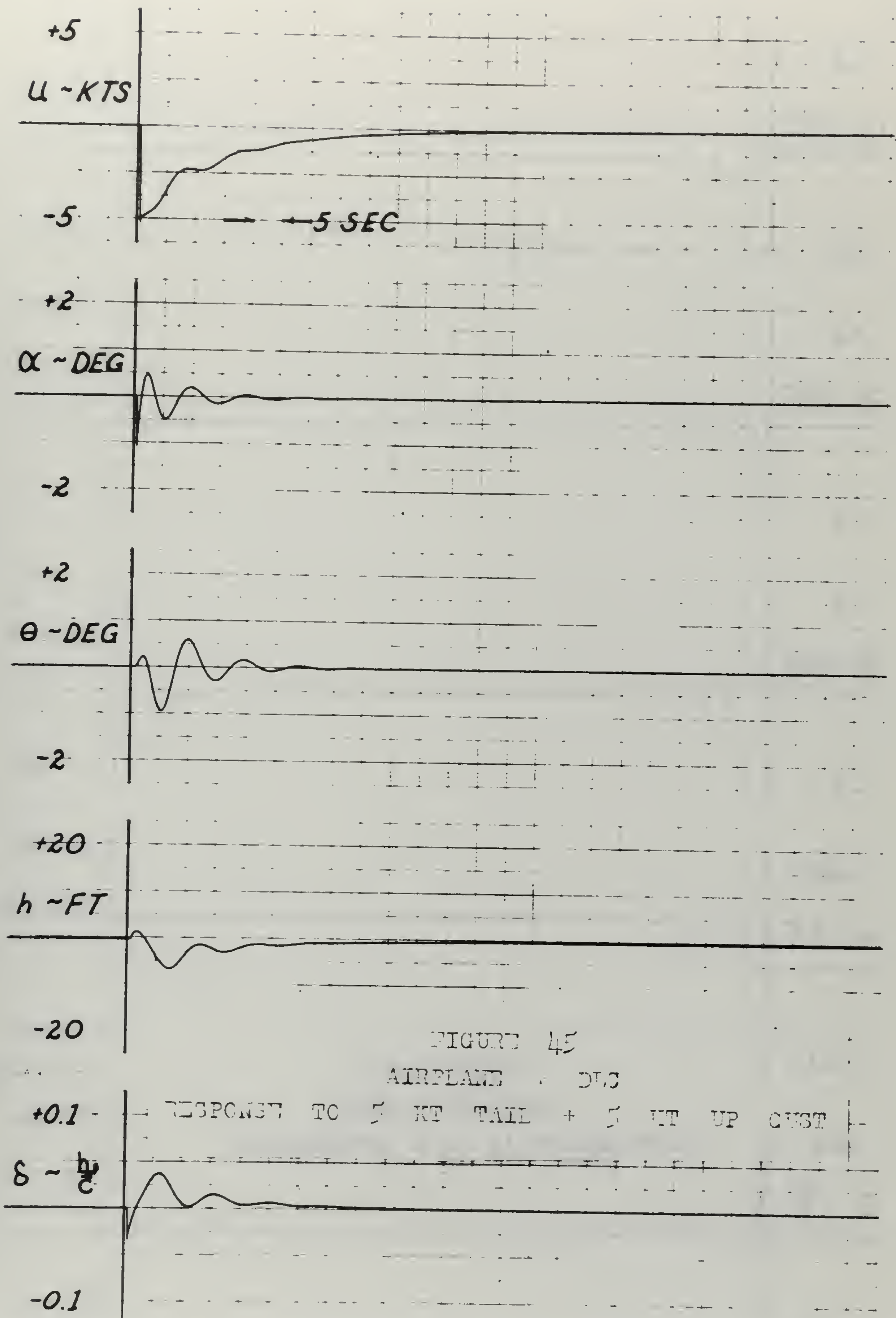

FIGURE 45
AIRPLANE + DLC
RESPONSE TO 5 KT TAIL + 5 FT UP GUST

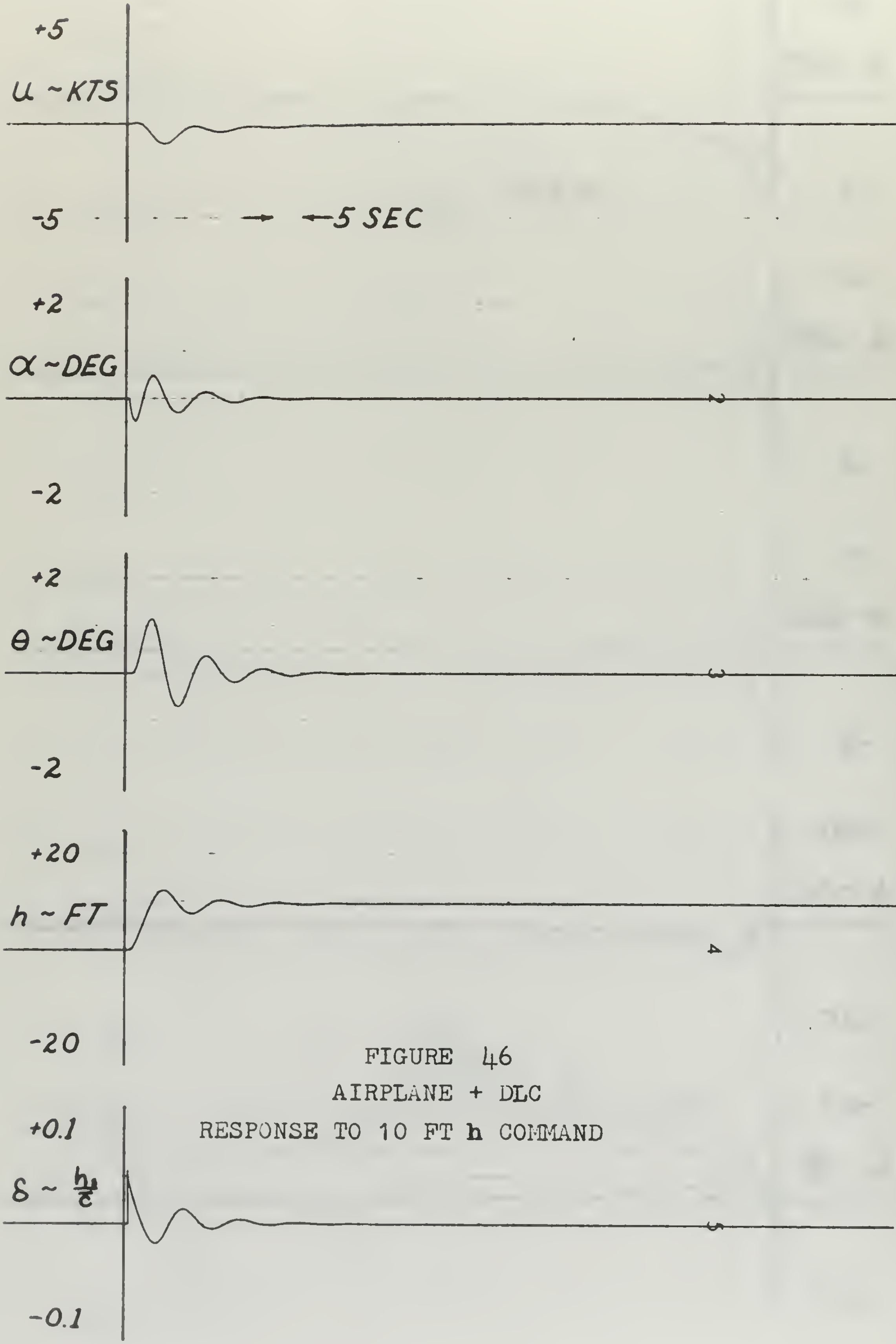

FIGURE 46
AIRPLANE + DLC
RESPONSE TO 10 FT h COMMAND

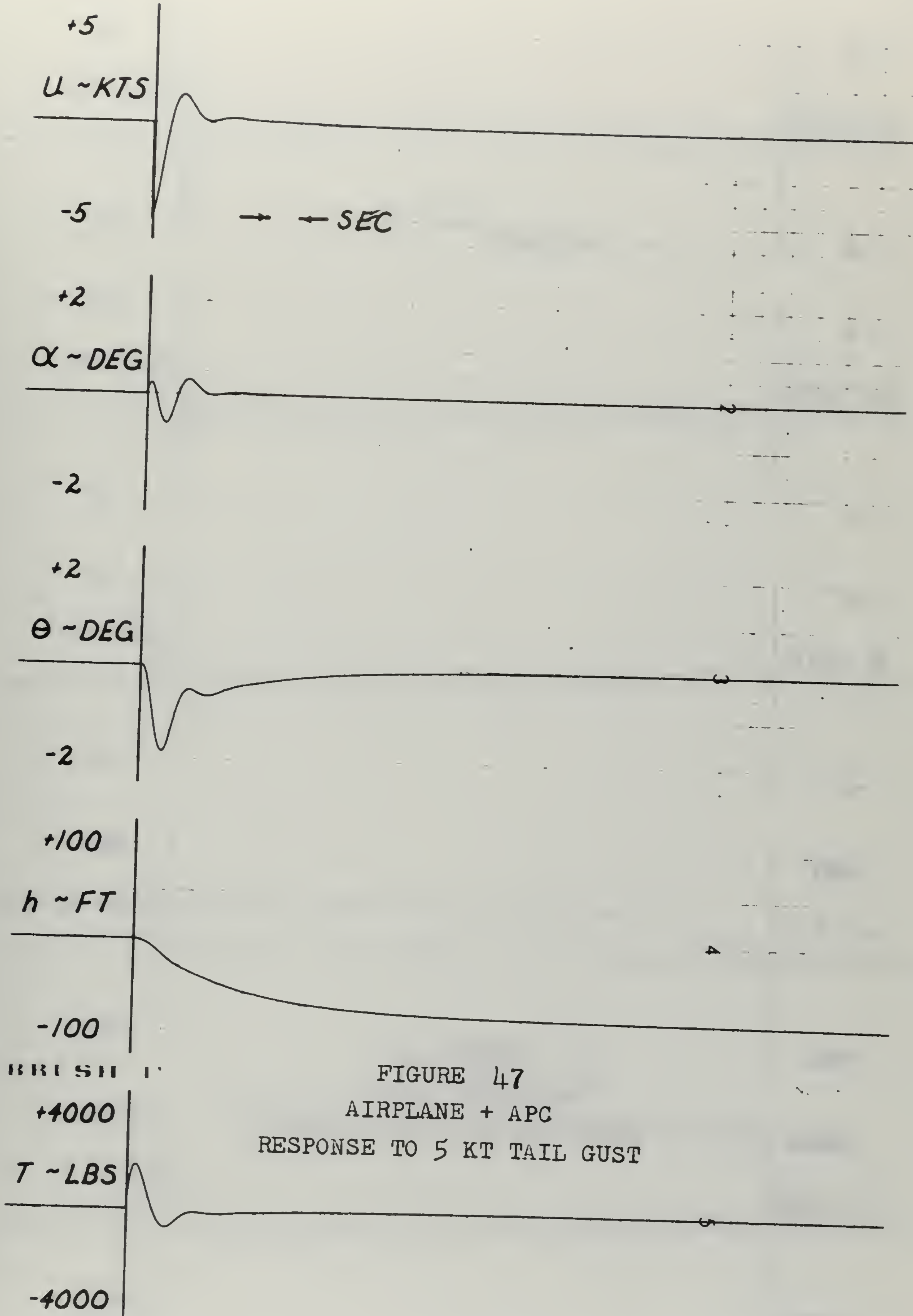

FIGURE 47
AIRPLANE + APC
RESPONSE TO 5 KT TAIL GUST

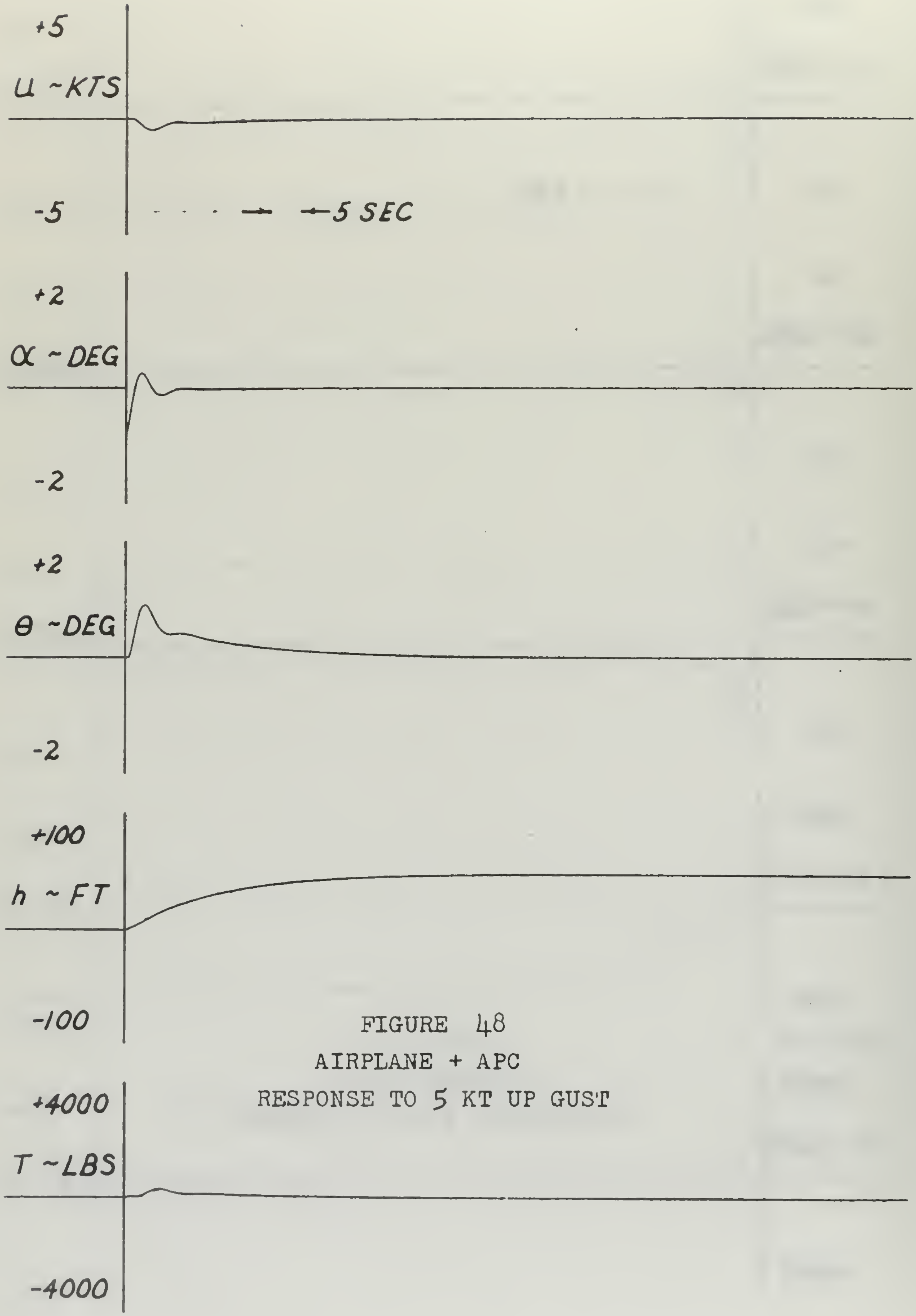

FIGURE 48
AIRPLANE + APC
RESPONSE TO 5 KT UP GUST

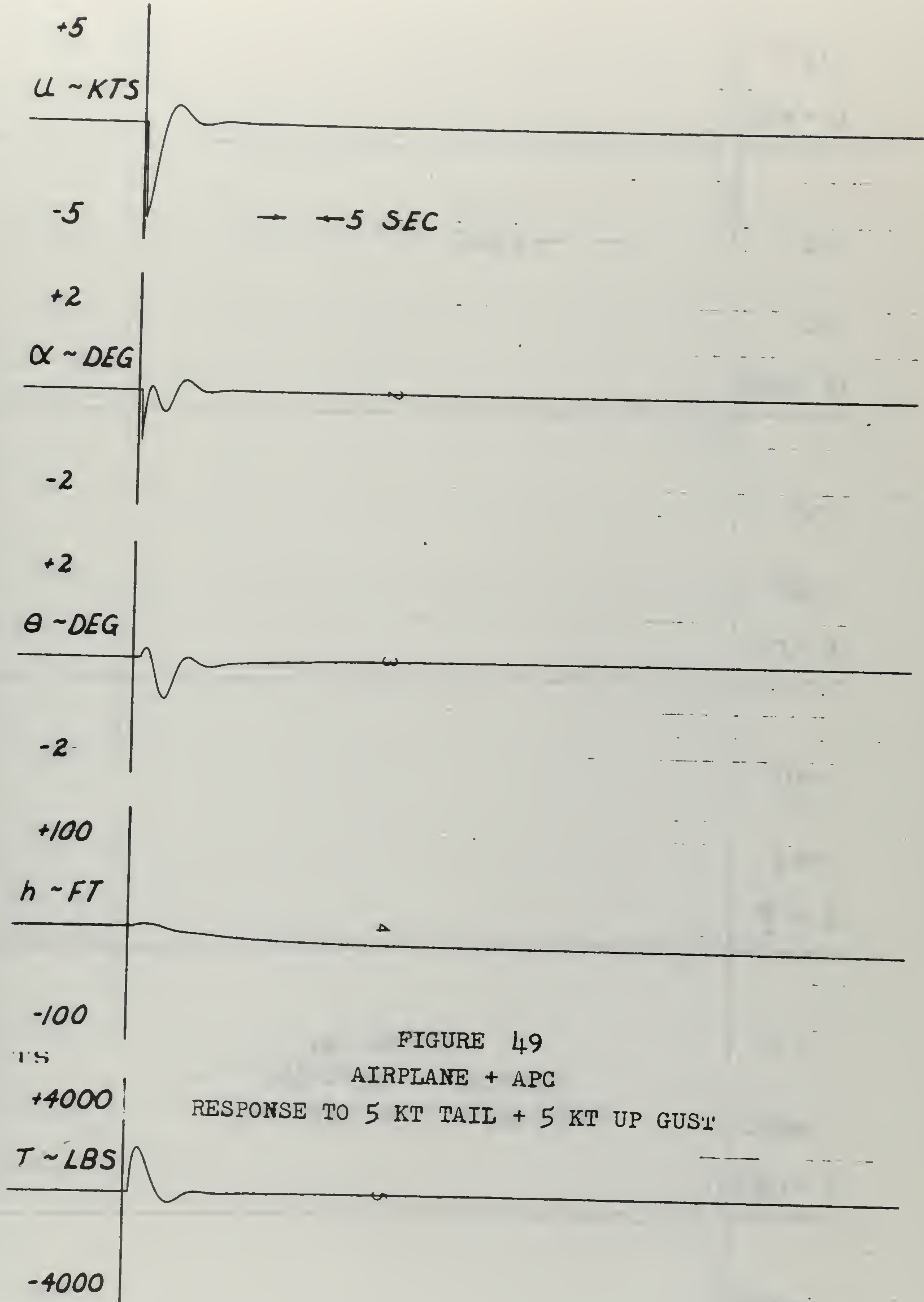

FIGURE 49
AIRPLANE + APC
RESPONSE TO 5 KT TAIL + 5 KT UP GUST

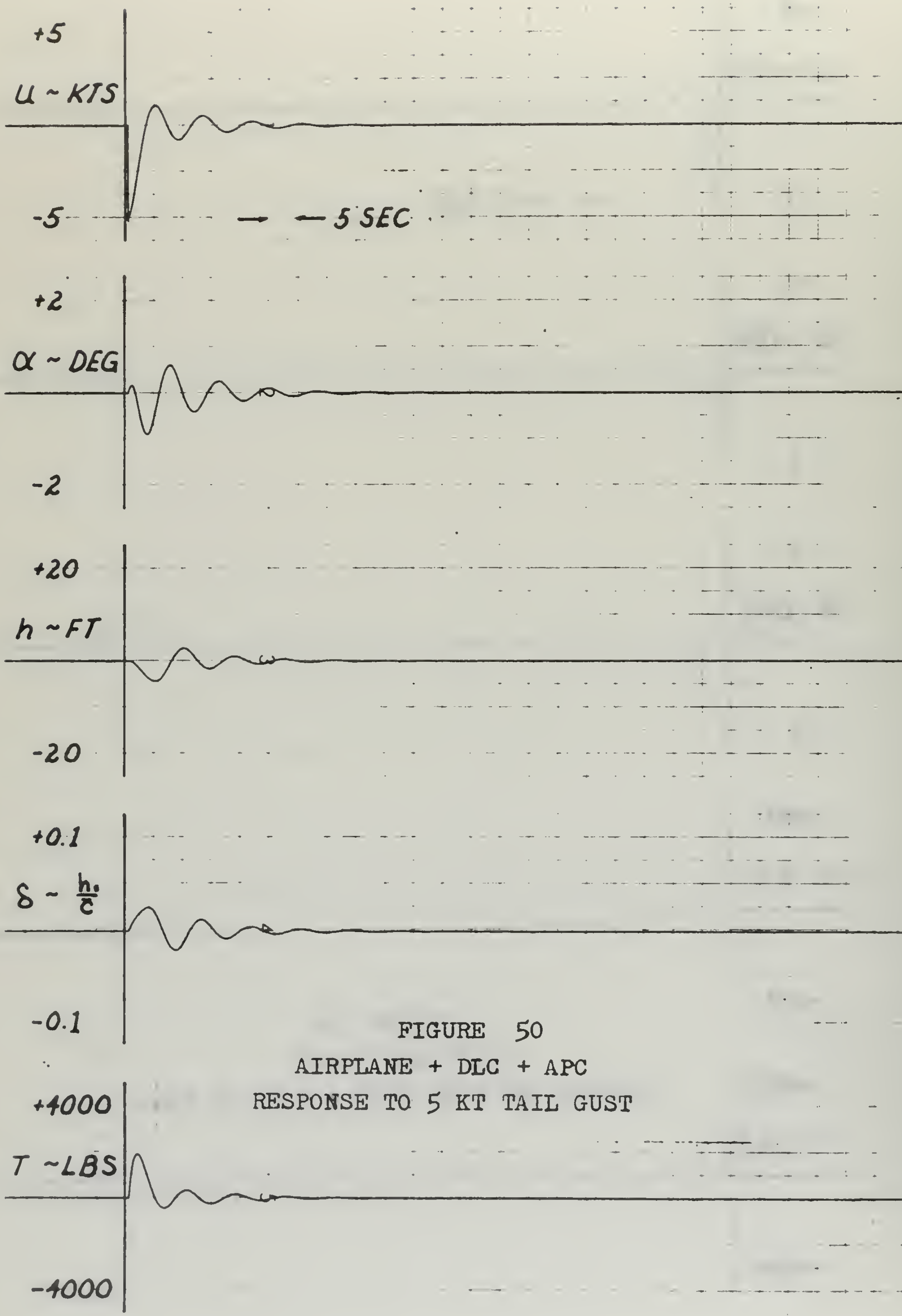

FIGURE 50
AIRPLANE + DLC + APC
RESPONSE TO 5 KT TAIL GUST

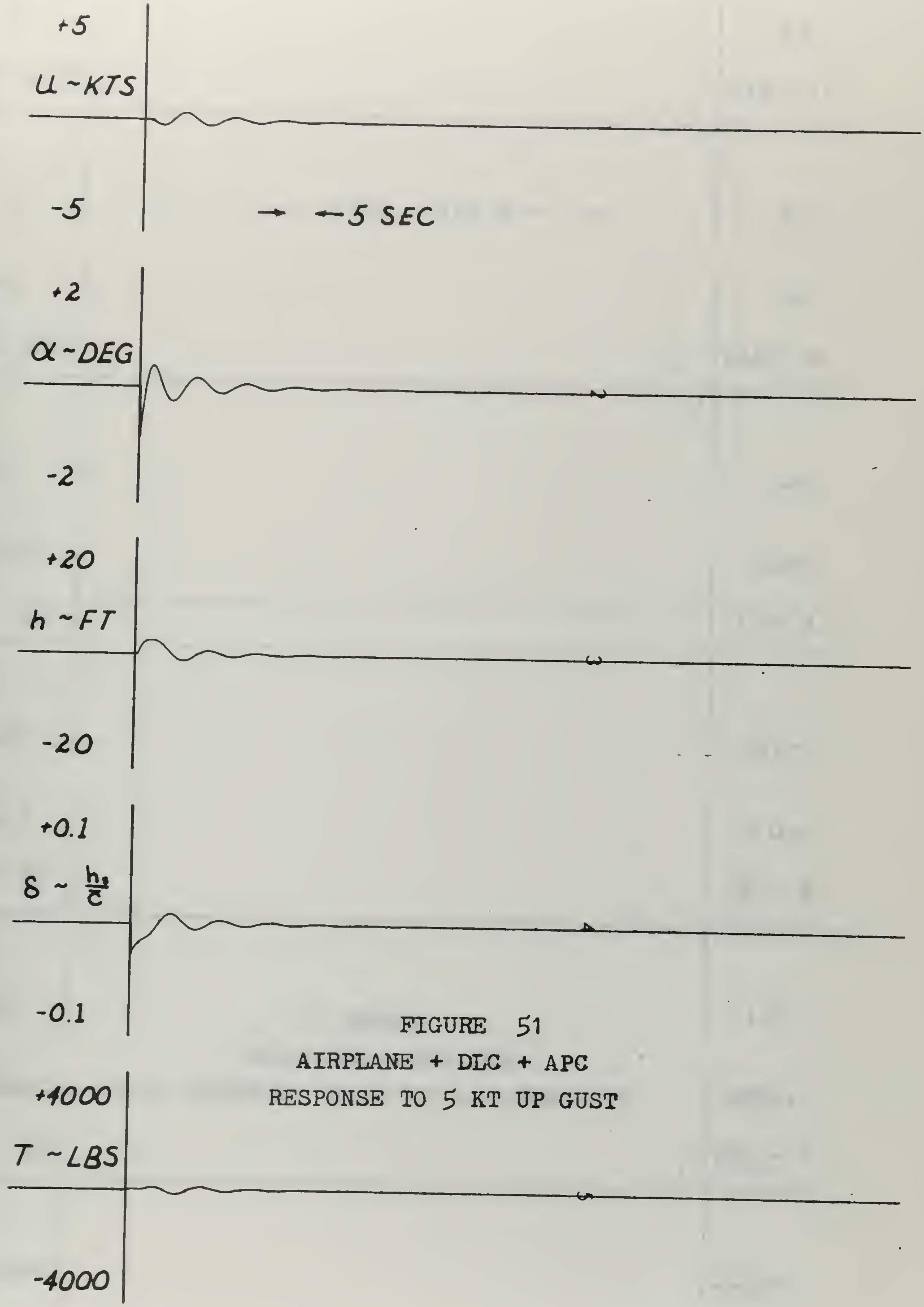

FIGURE 51
AIRPLANE + DLC + APC
RESPONSE TO 5 KT UP GUST

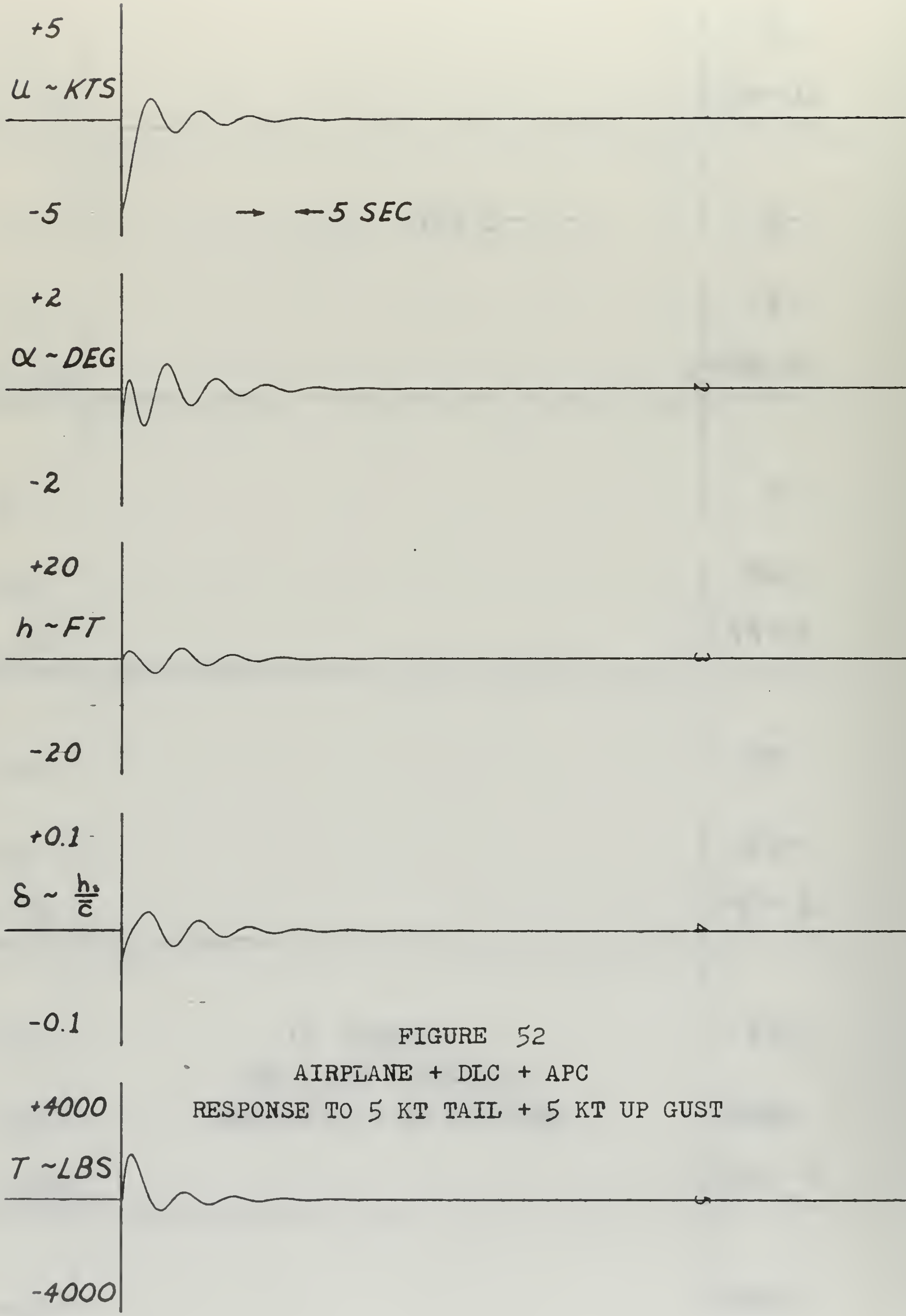

FIGURE 52

AIRPLANE + DLC + APC

RESPONSE TO 5 KT TAIL + 5 KT UP GUST

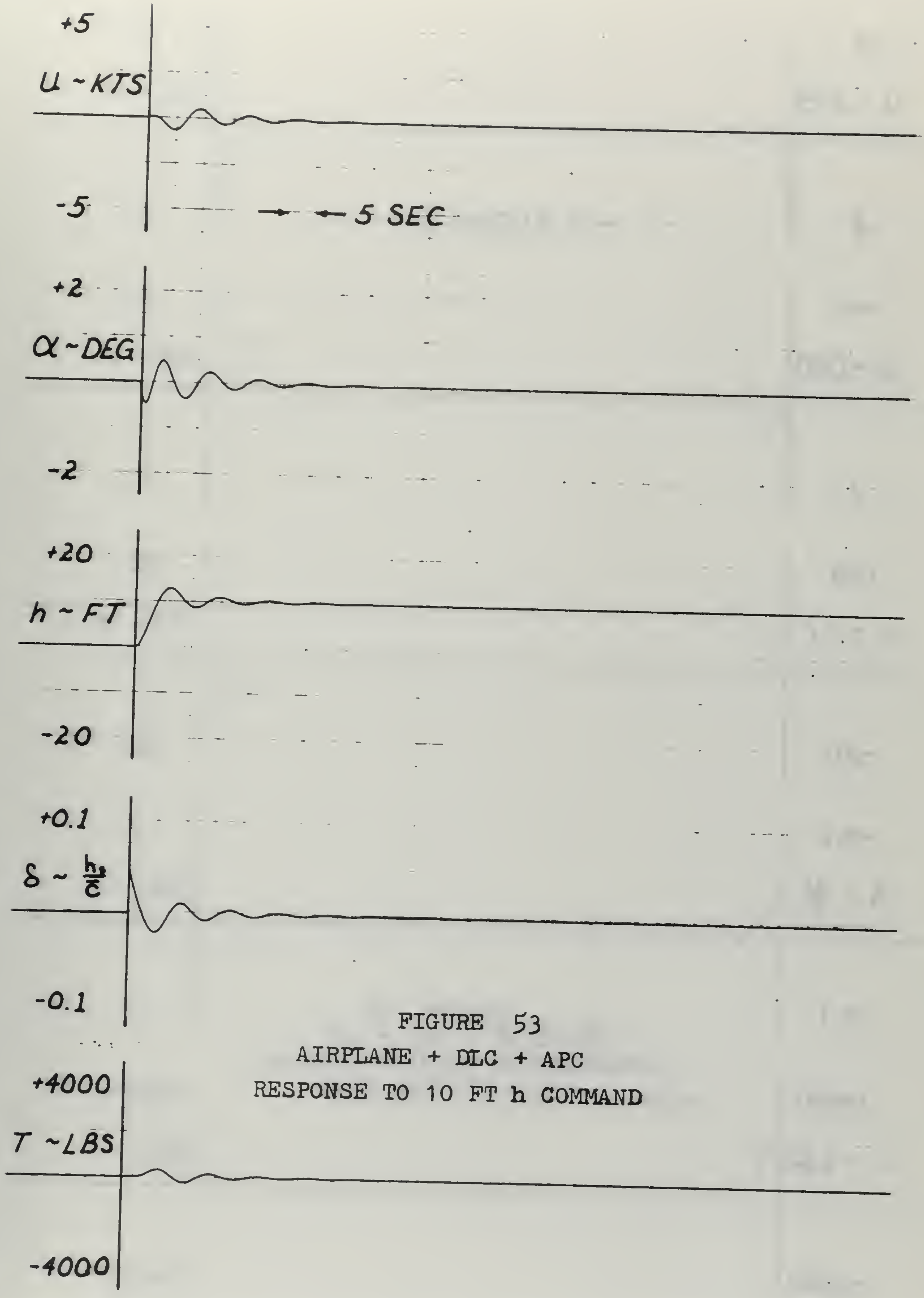

FIGURE 53
AIRPLANE + DLC + APC
RESPONSE TO 10 FT h COMMAND

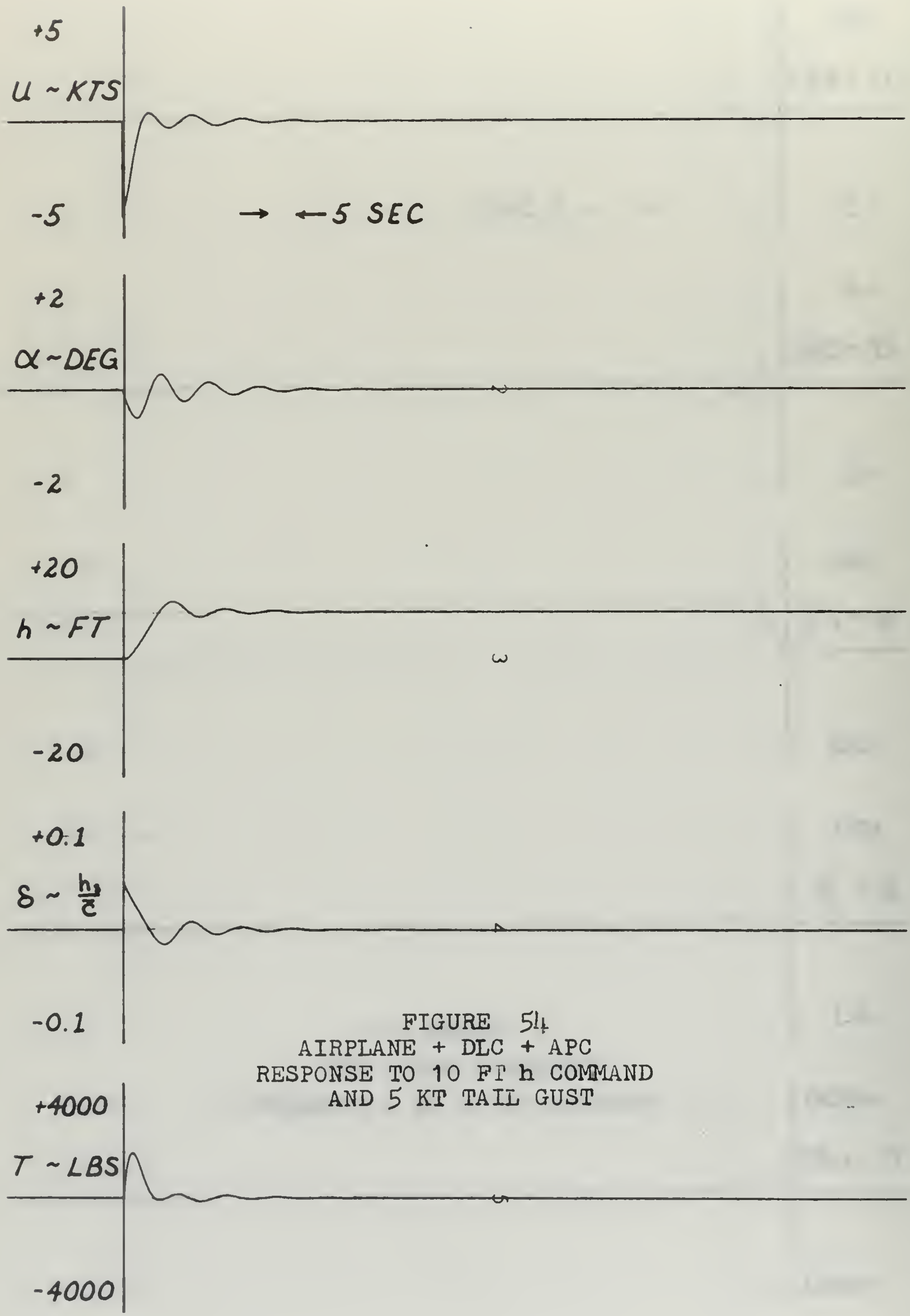

FIGURE 54
AIRPLANE + DLC + APC
RESPONSE TO 10 FT h COMMAND
AND 5 KT TAIL GUST

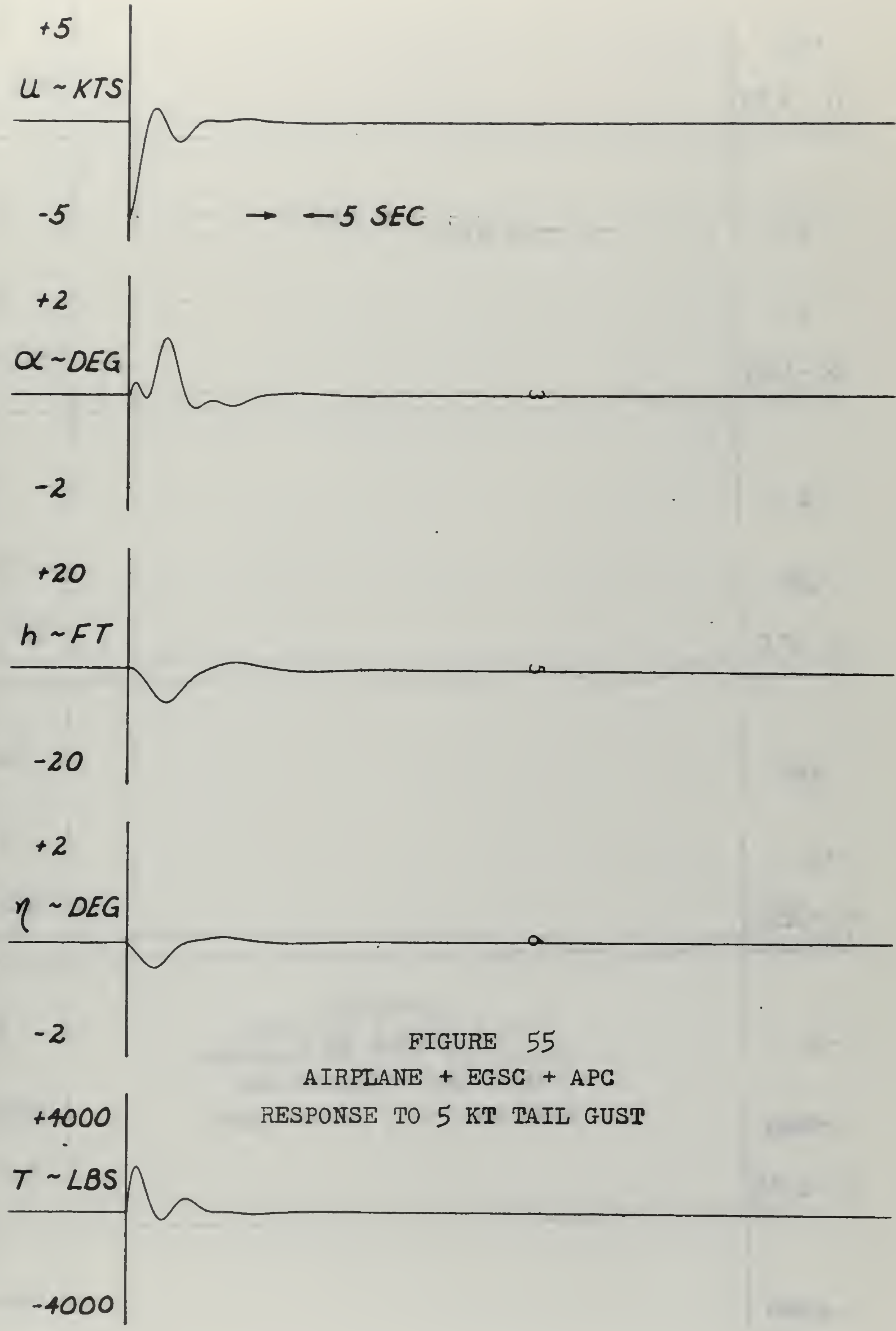

FIGURE 55
AIRPLANE + EGSC + APC
RESPONSE TO 5 KT TAIL GUST

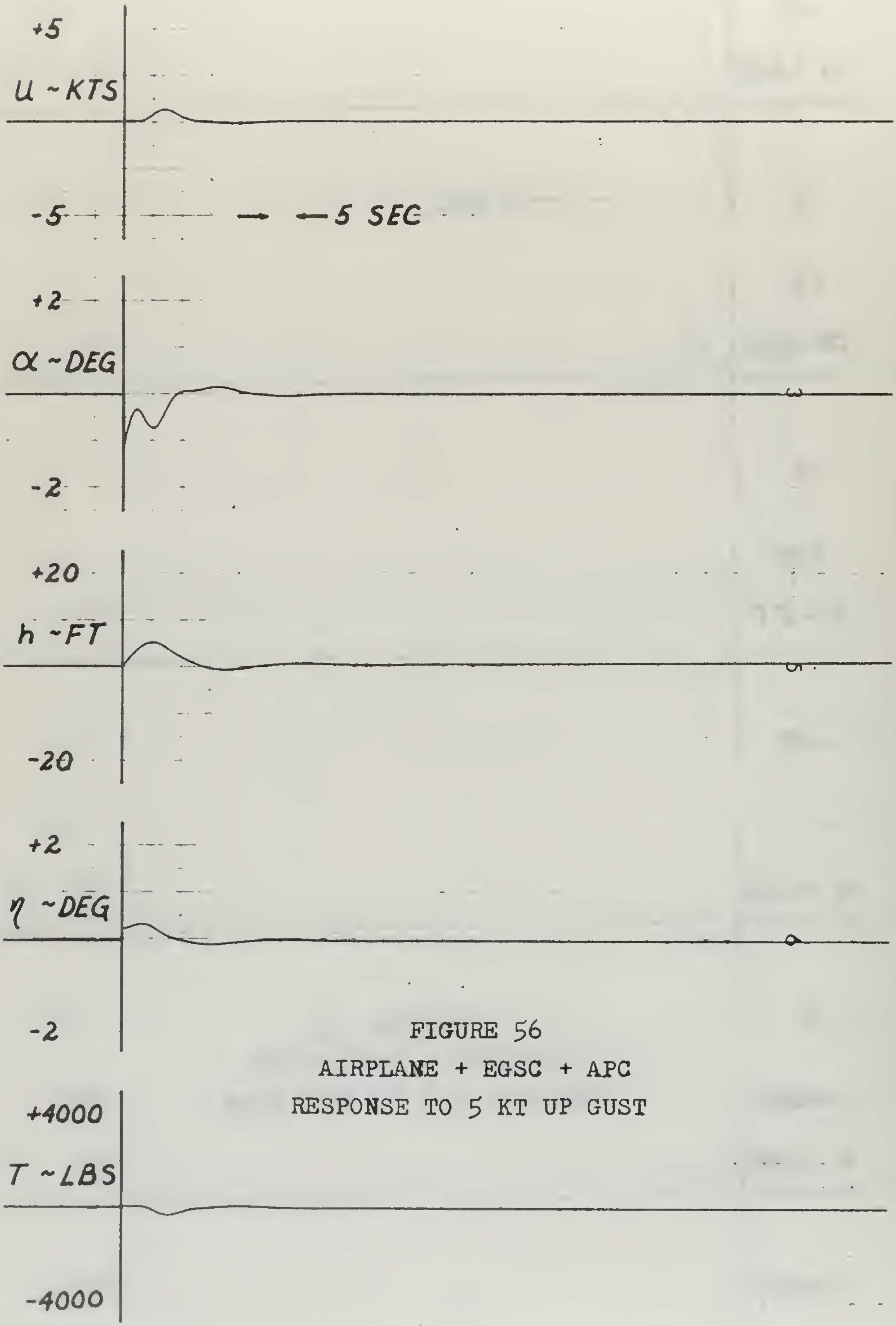

FIGURE 56
AIRPLANE + EGSC + APC
RESPONSE TO 5 KT UP GUST

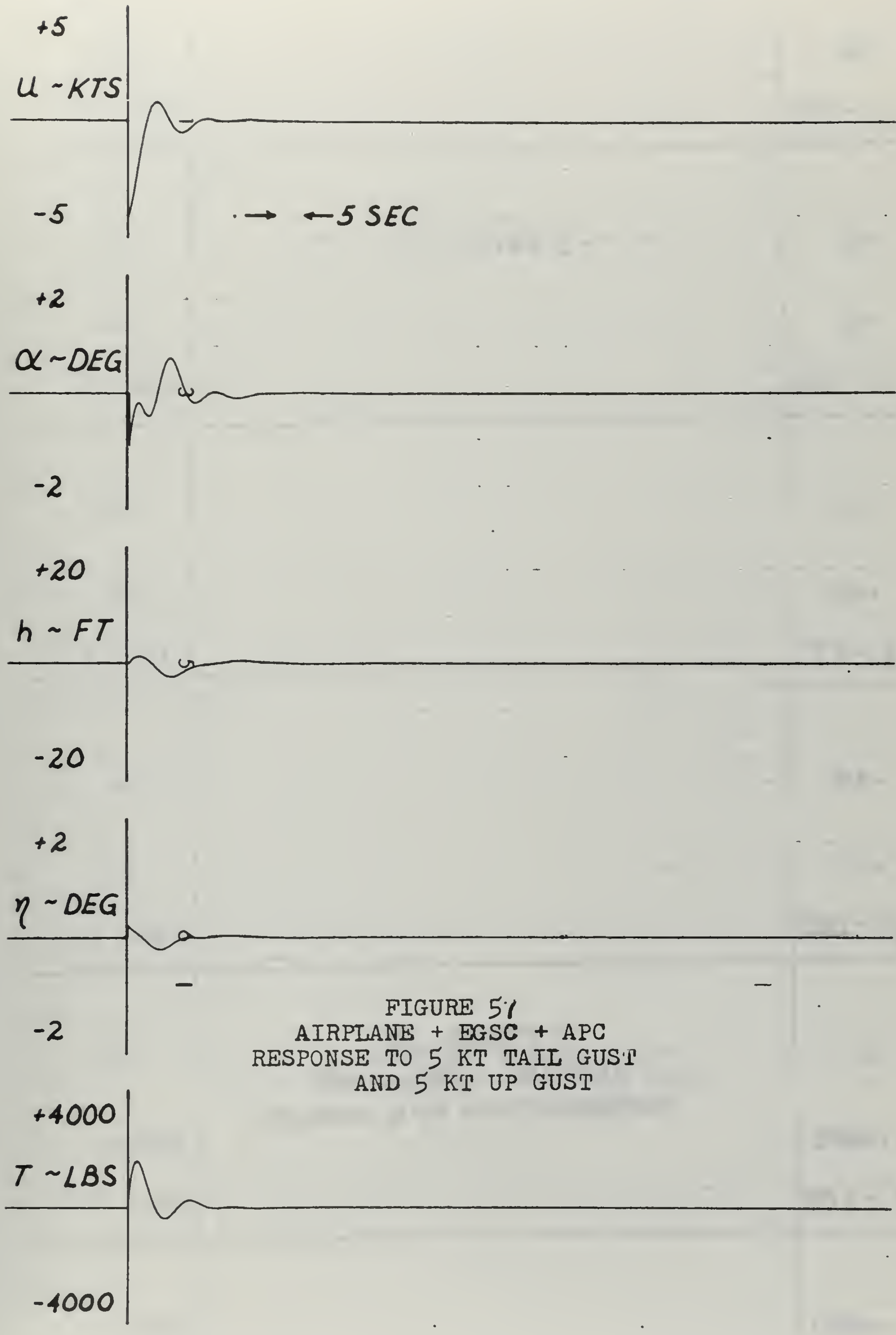

FIGURE 57
AIRPLANE + EGSC + APC
RESPONSE TO 5 KT TAIL GUST
AND 5 KT UP GUST

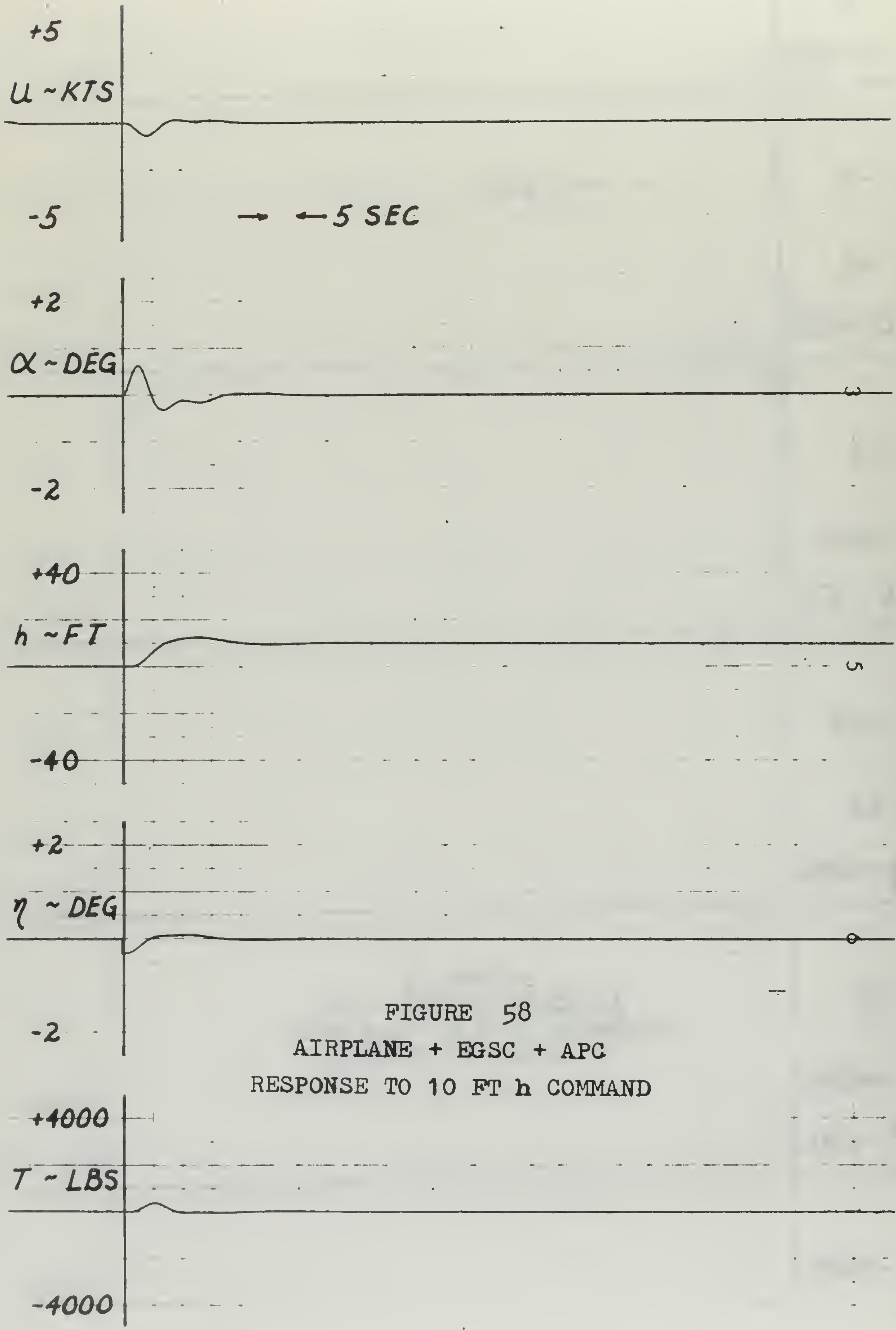

FIGURE 58
AIRPLANE + EGSC + APC
RESPONSE TO 10 FT h COMMAND

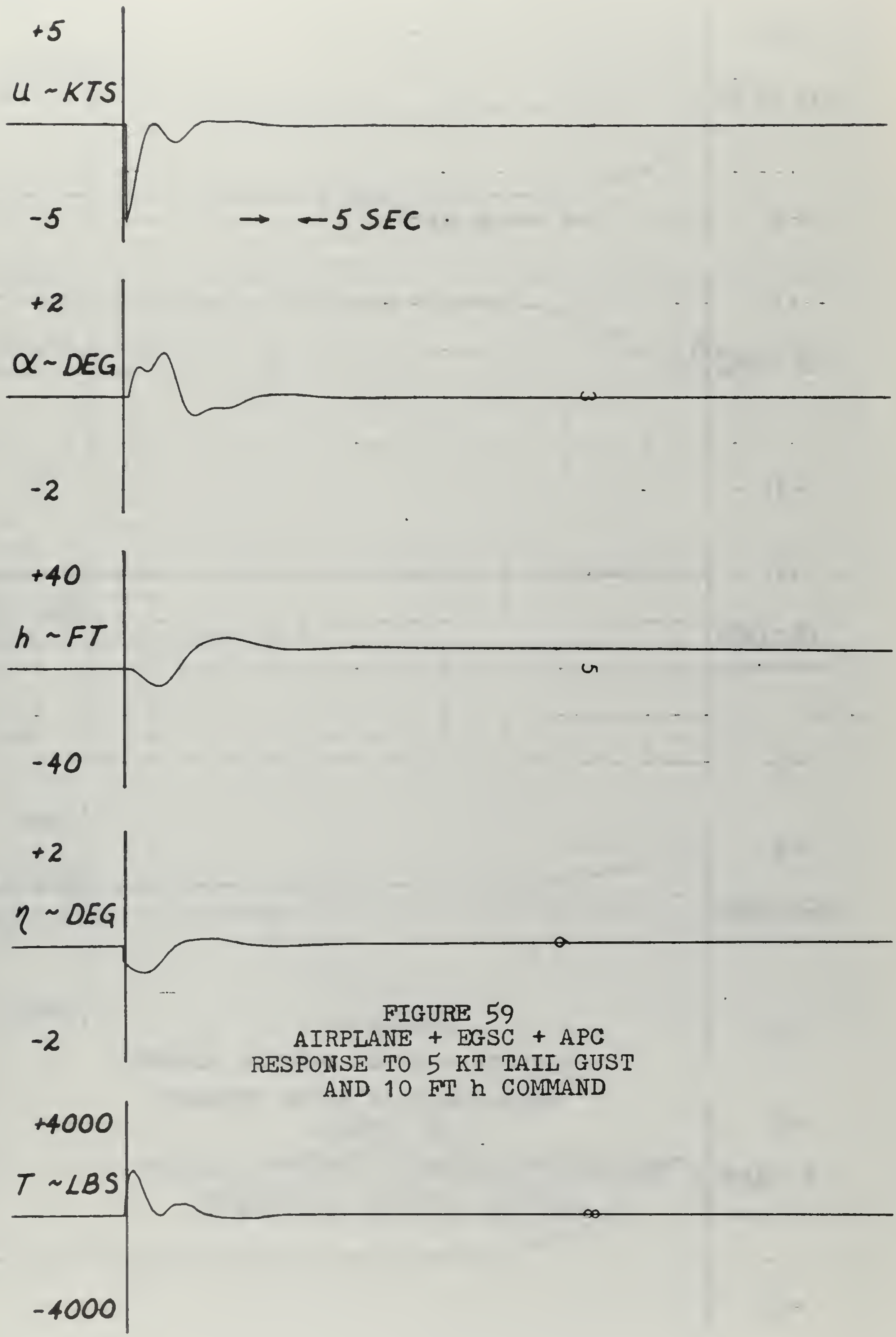

FIGURE 59
AIRPLANE + EGSC + APC
RESPONSE TO 5 KT TAIL GUST
AND 10 FT h COMMAND

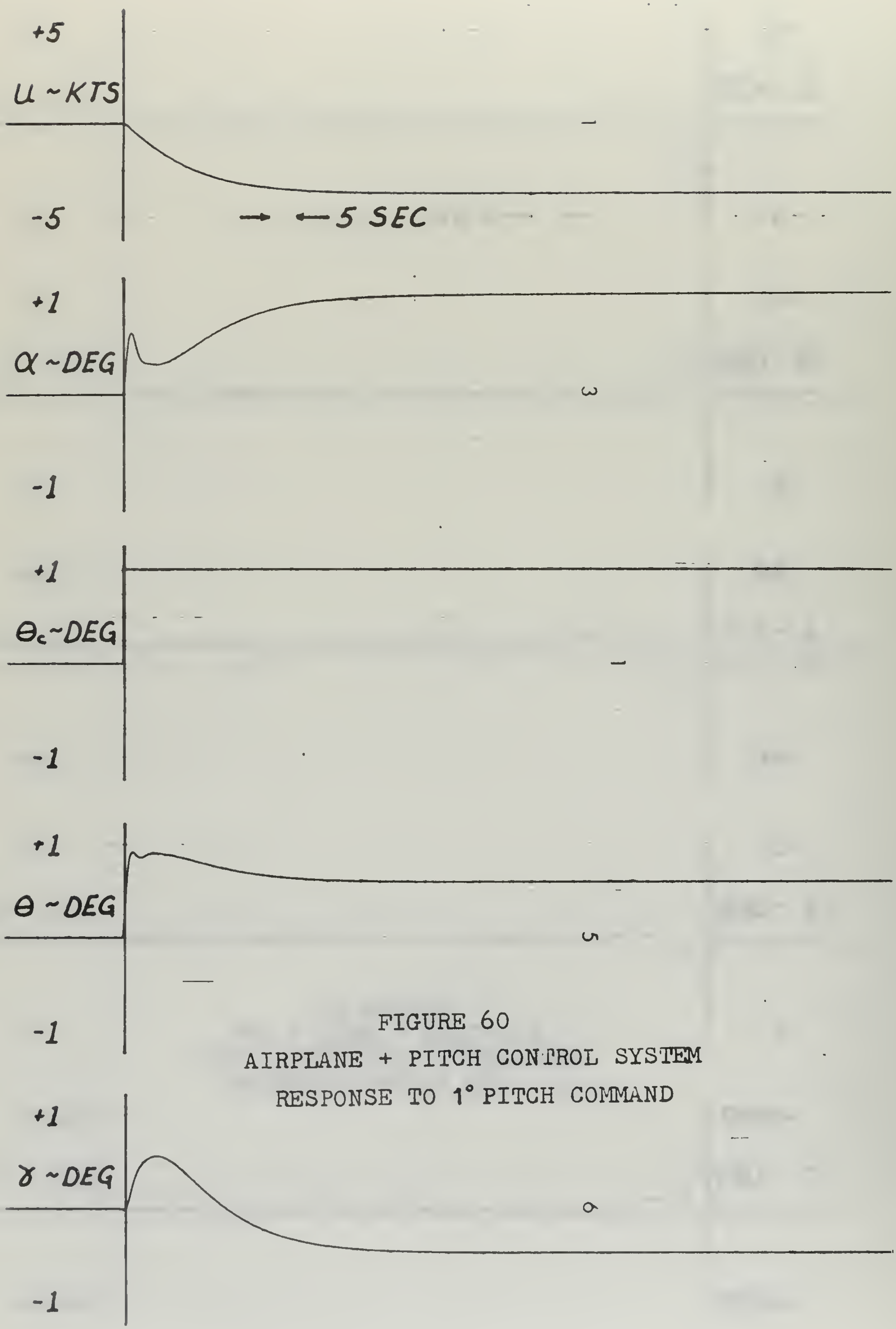

FIGURE 60
AIRPLANE + PITCH CONTROL SYSTEM
RESPONSE TO 1° PITCH COMMAND

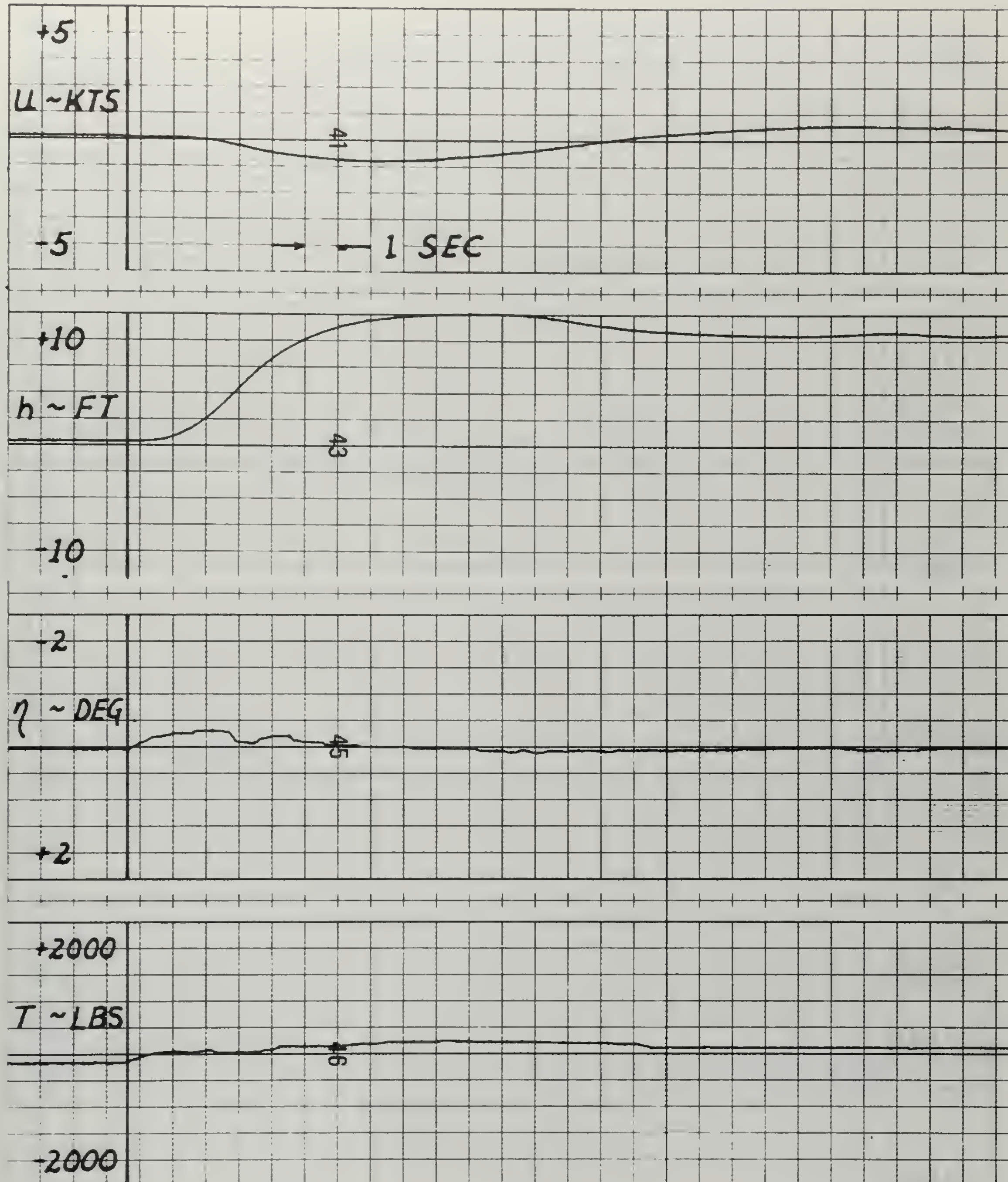

FIGURE 61
MANUAL THROTTLE + MANUAL STABILATOR
RESPONSE TO 10 FT h COMMAND

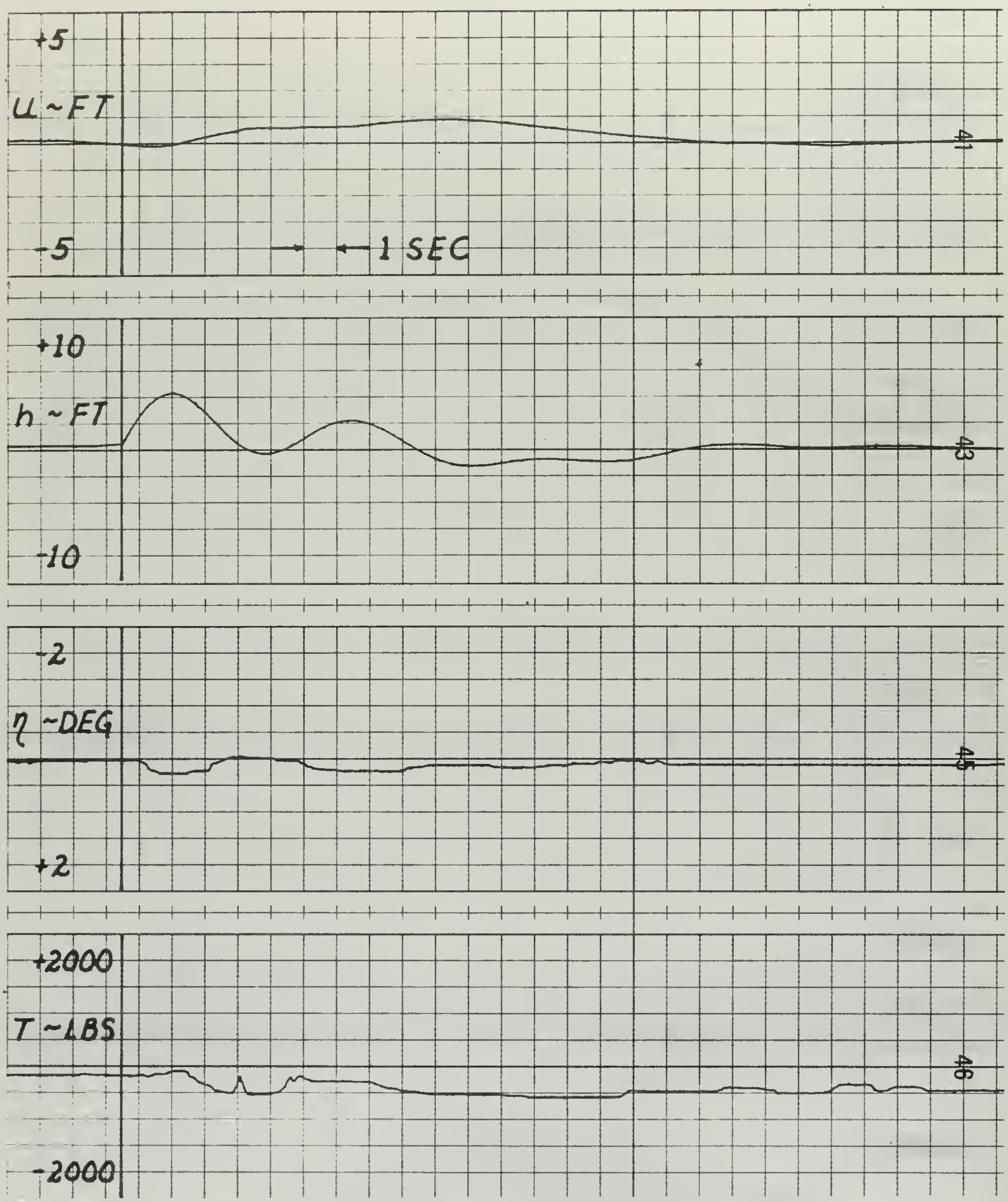

FIGURE 62
MANUAL THROTTLE + MANUAL STABILATOR
RESPONSE TO 5 KT UP GUST

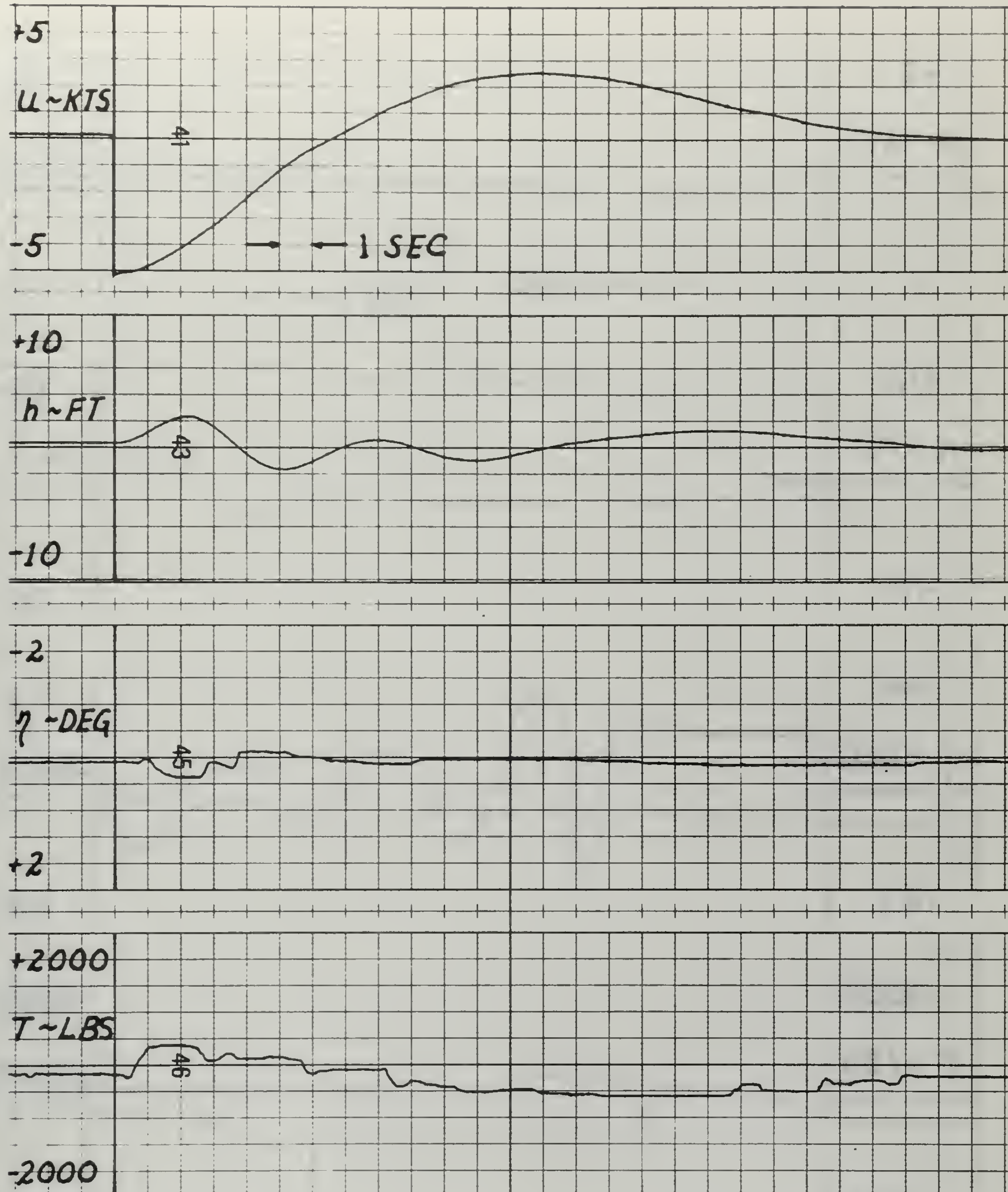

FIGURE 63

MANUAL THROTTLE + MANUAL STABILATOR

RESPONSE TO 5 KT TAIL GUST

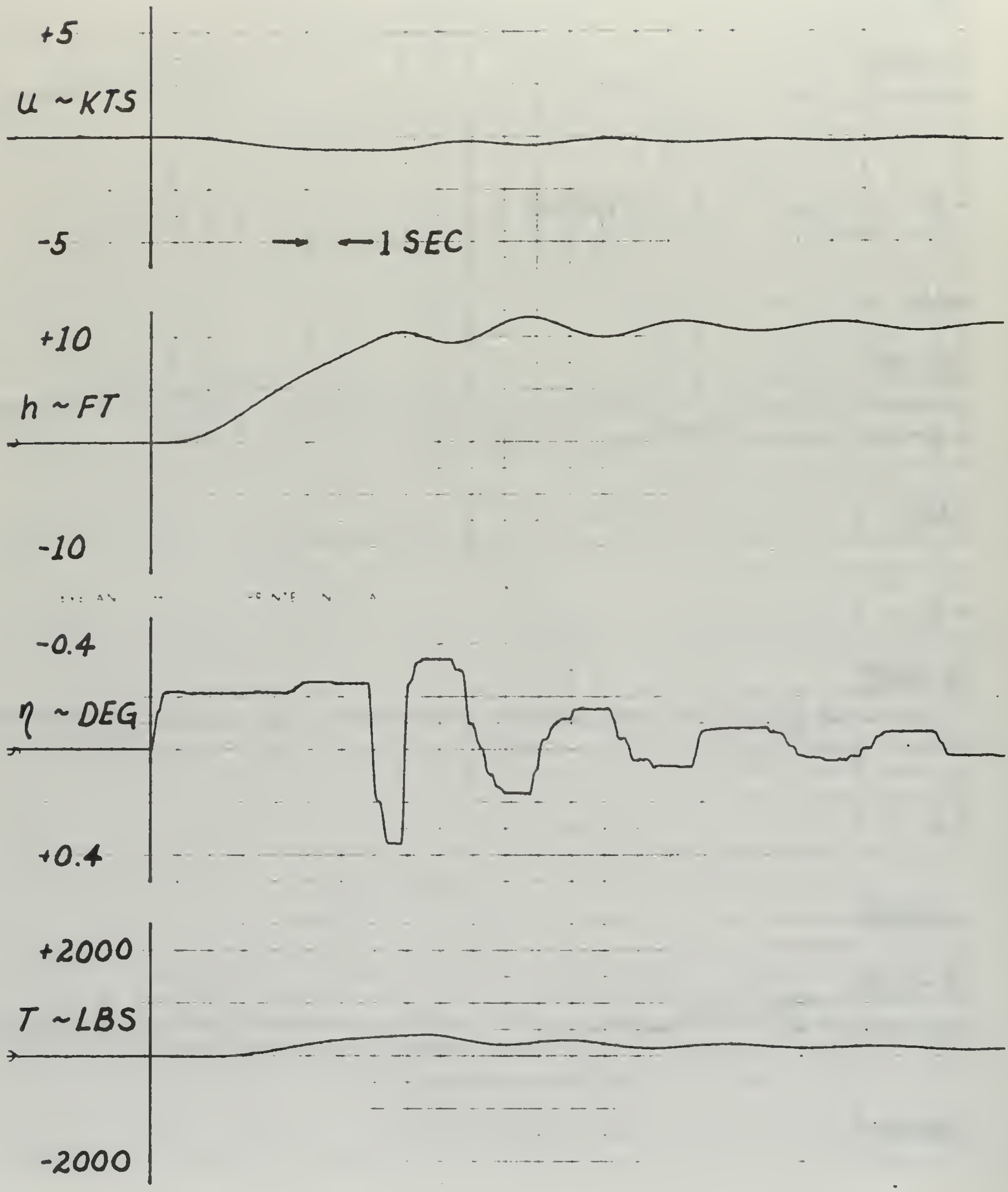

FIGURE 64
APC + MANUAL STABILATOR
RESPONSE TO 10 FT h COMMAND

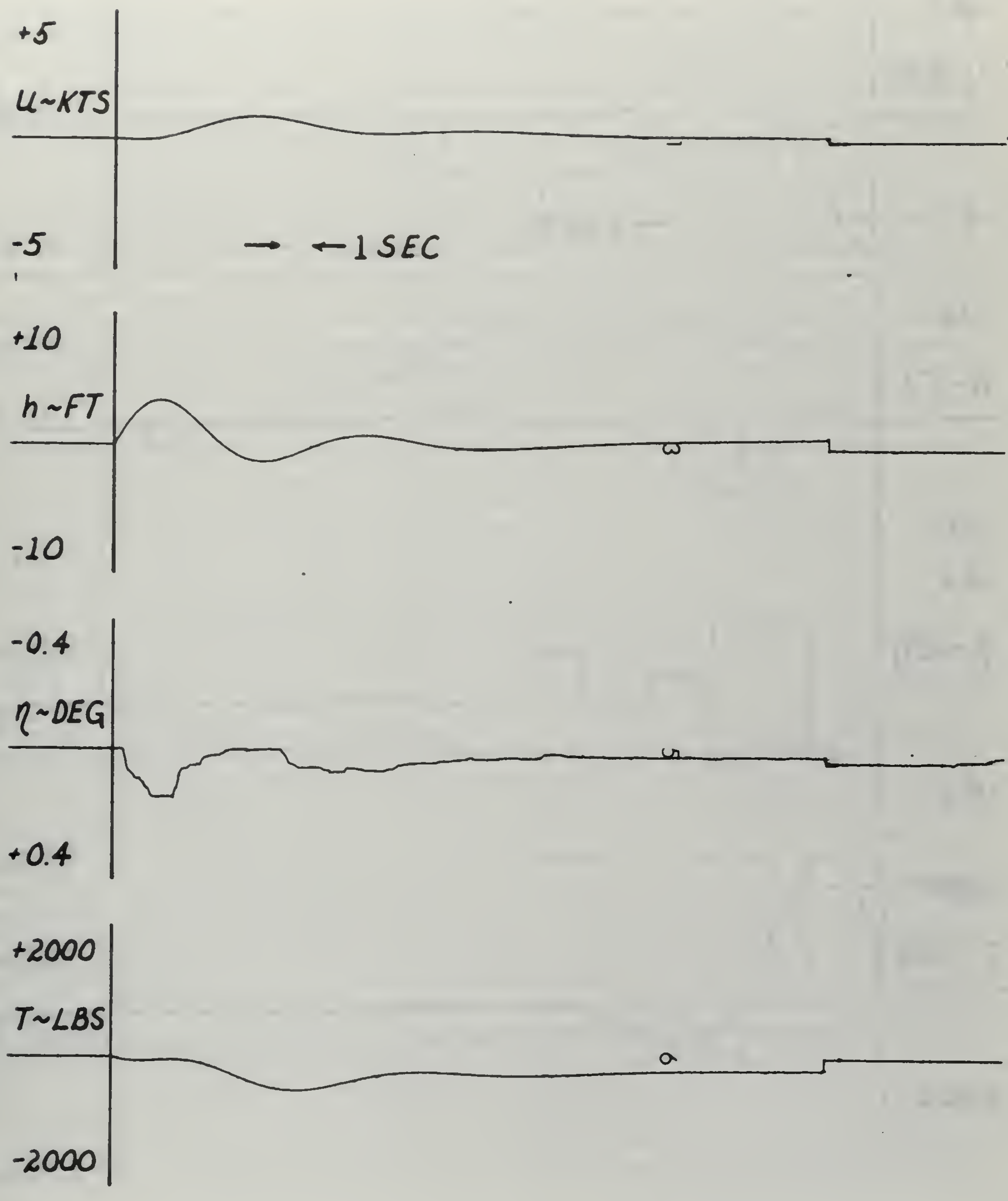

FIGURE 65
APC + MANUAL STABILATOR
RESPONSE TO 5 KT UP GUST

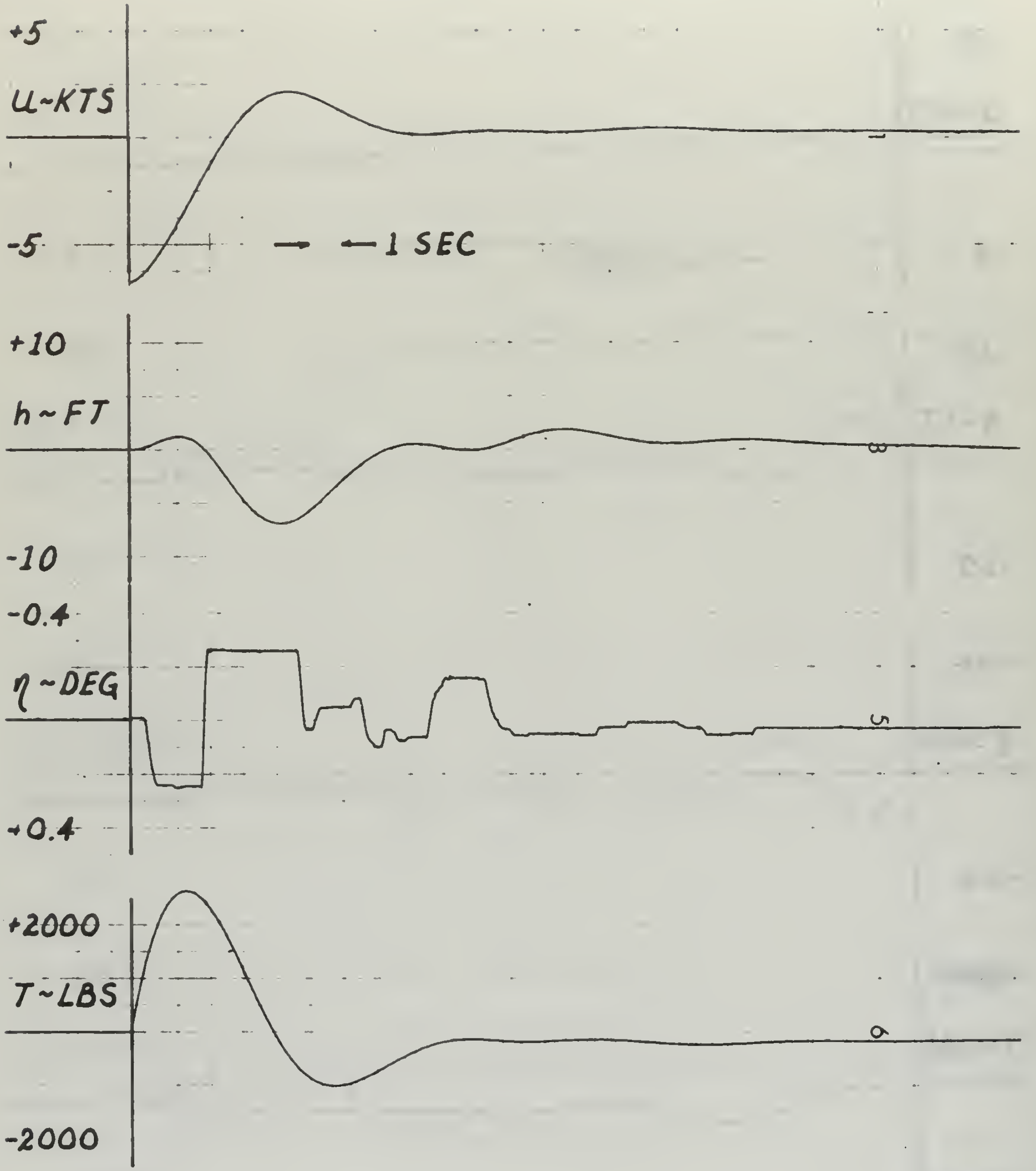

FIGURE 66
APC + MANUAL STABILATOR
RESPONSE TO 5 KT TAIL GUST

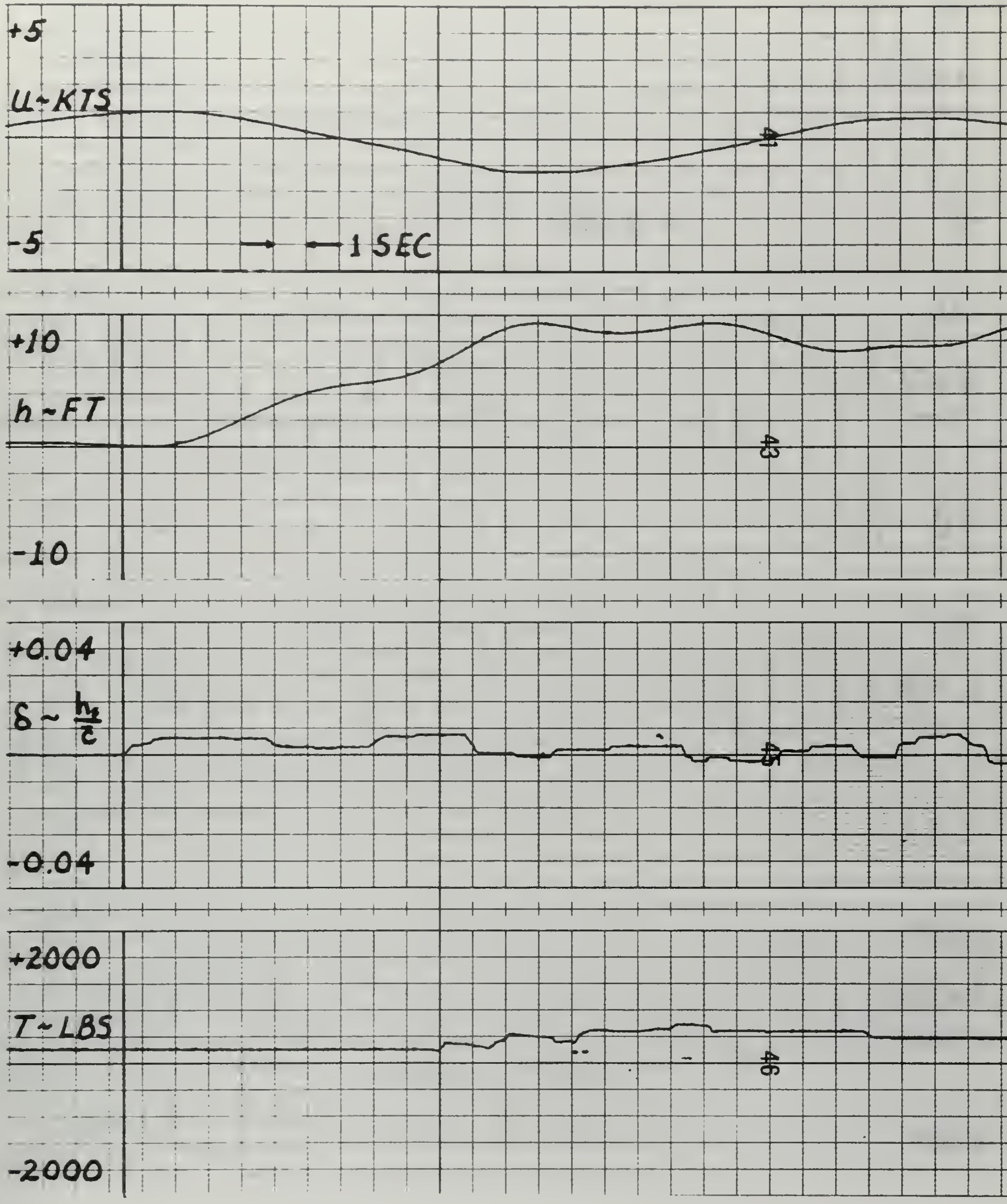

FIGURE 61
MANUAL THROTTLE + MANUAL SPOILERS
RESPONSE TO 10 FT h COMMAND

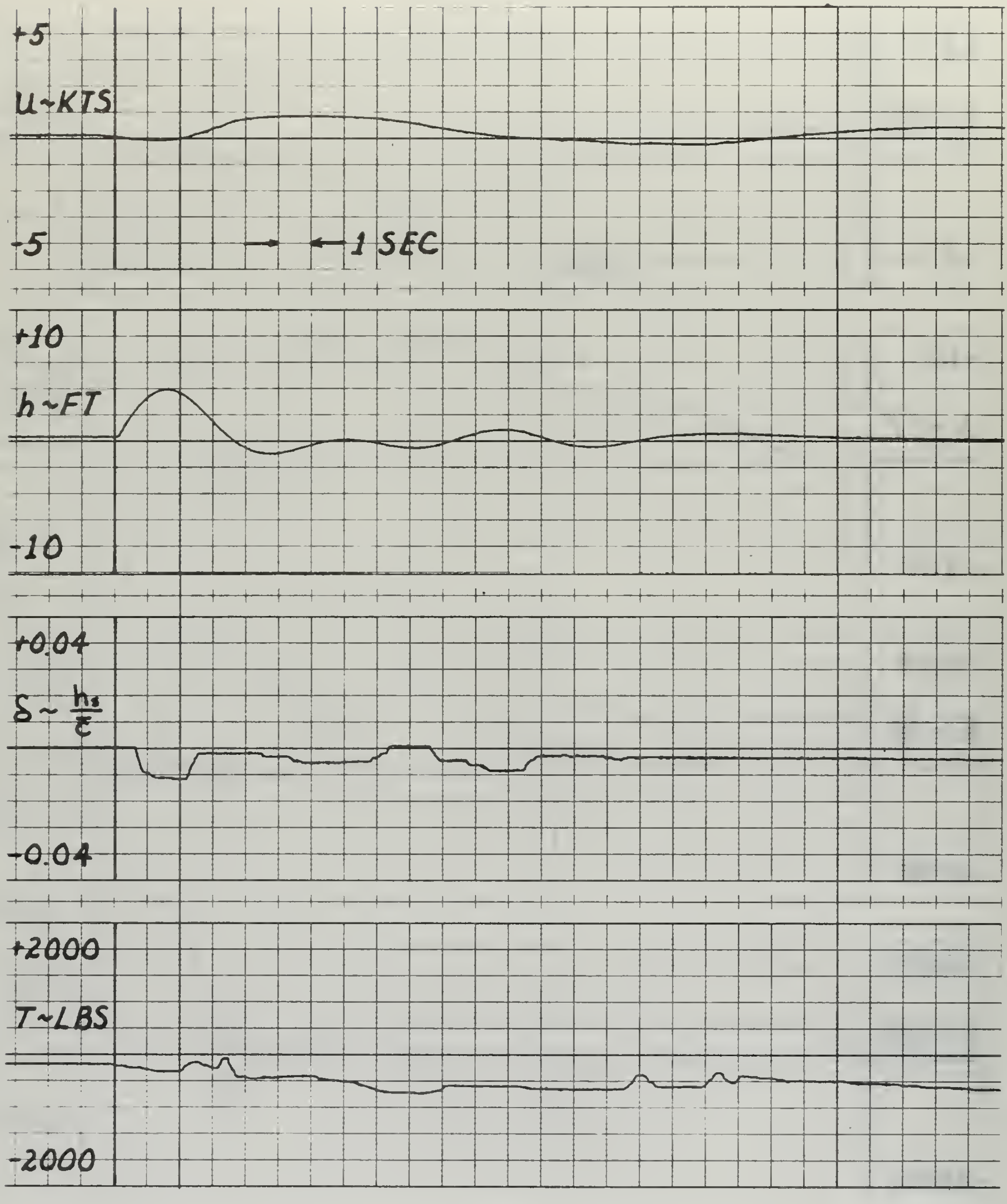

FIGURE 68
MANUAL THROTTLE + MANUAL SPOILERS
RESPONSE TO 5 KT UP GUST

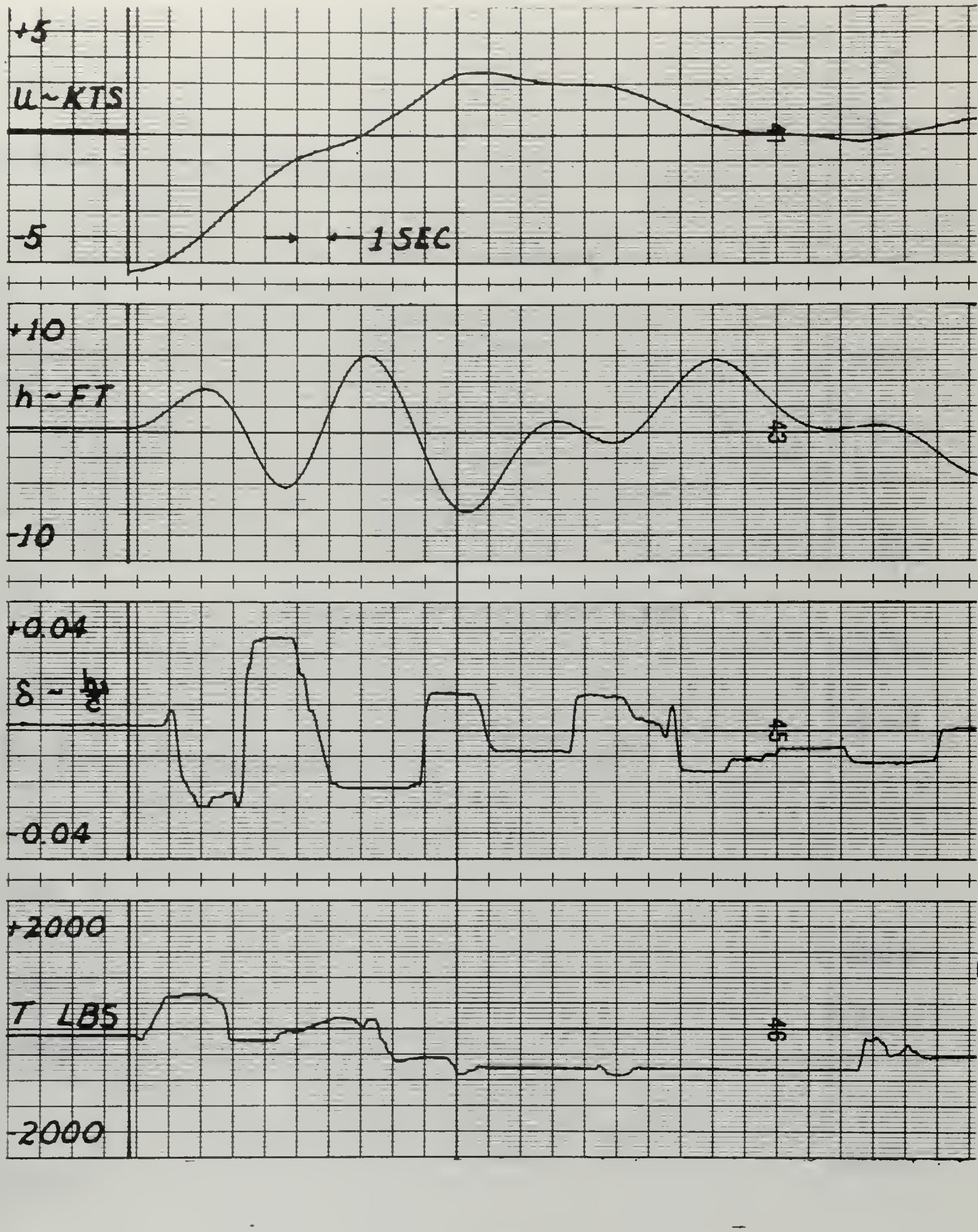

FIGURE 69
MANUAL THROTTLE + MANUAL SPOILERS
RESPONSE TO 5 KT TAIL GUST

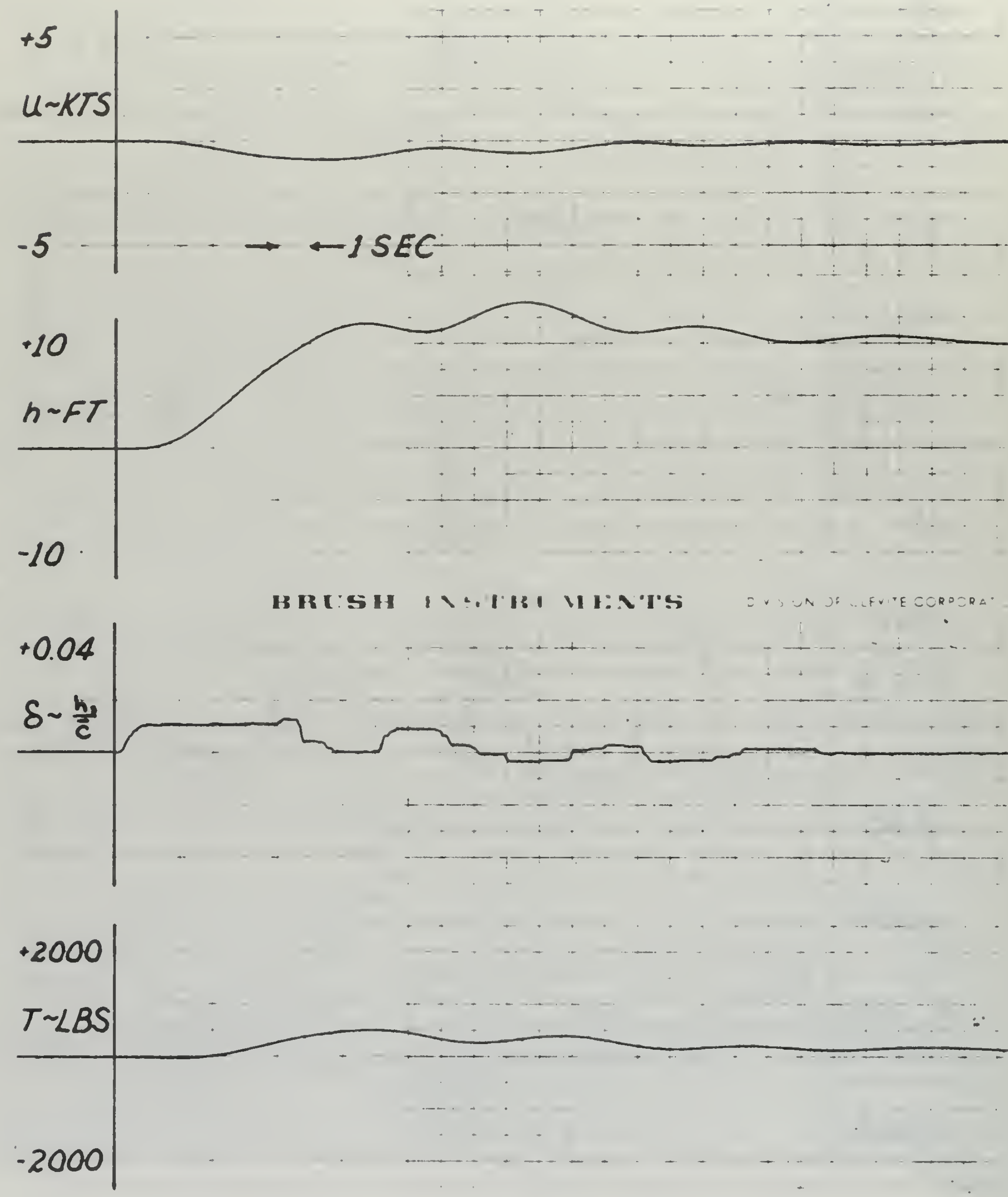

FIGURE 70

APC + MANUAL SPOILERS

RESPONSE TO 10 FT h COMMAND

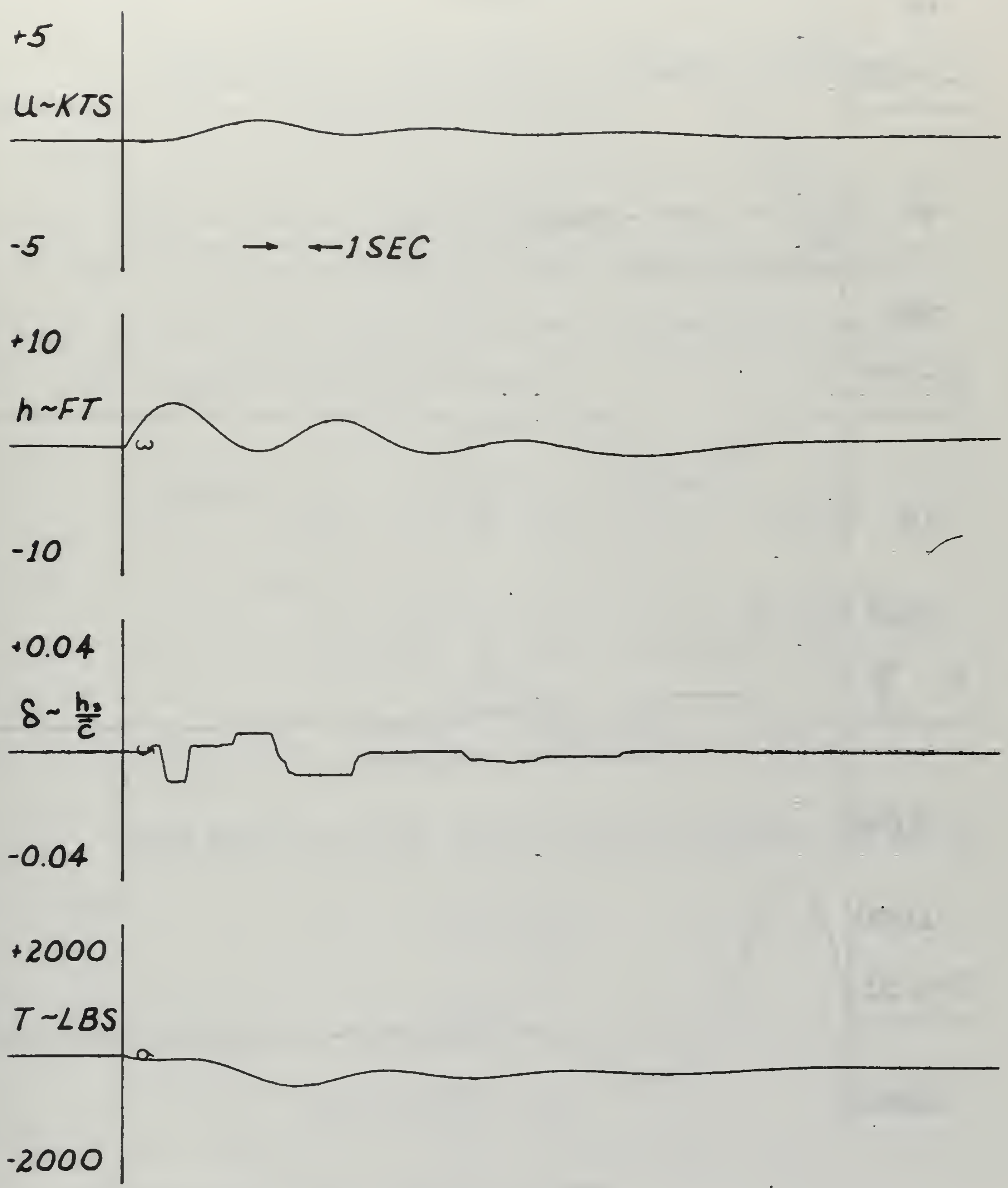

FIGURE 71
APC + MANUAL SPOILERS
RESPONSE TO 5 KT UP GUST

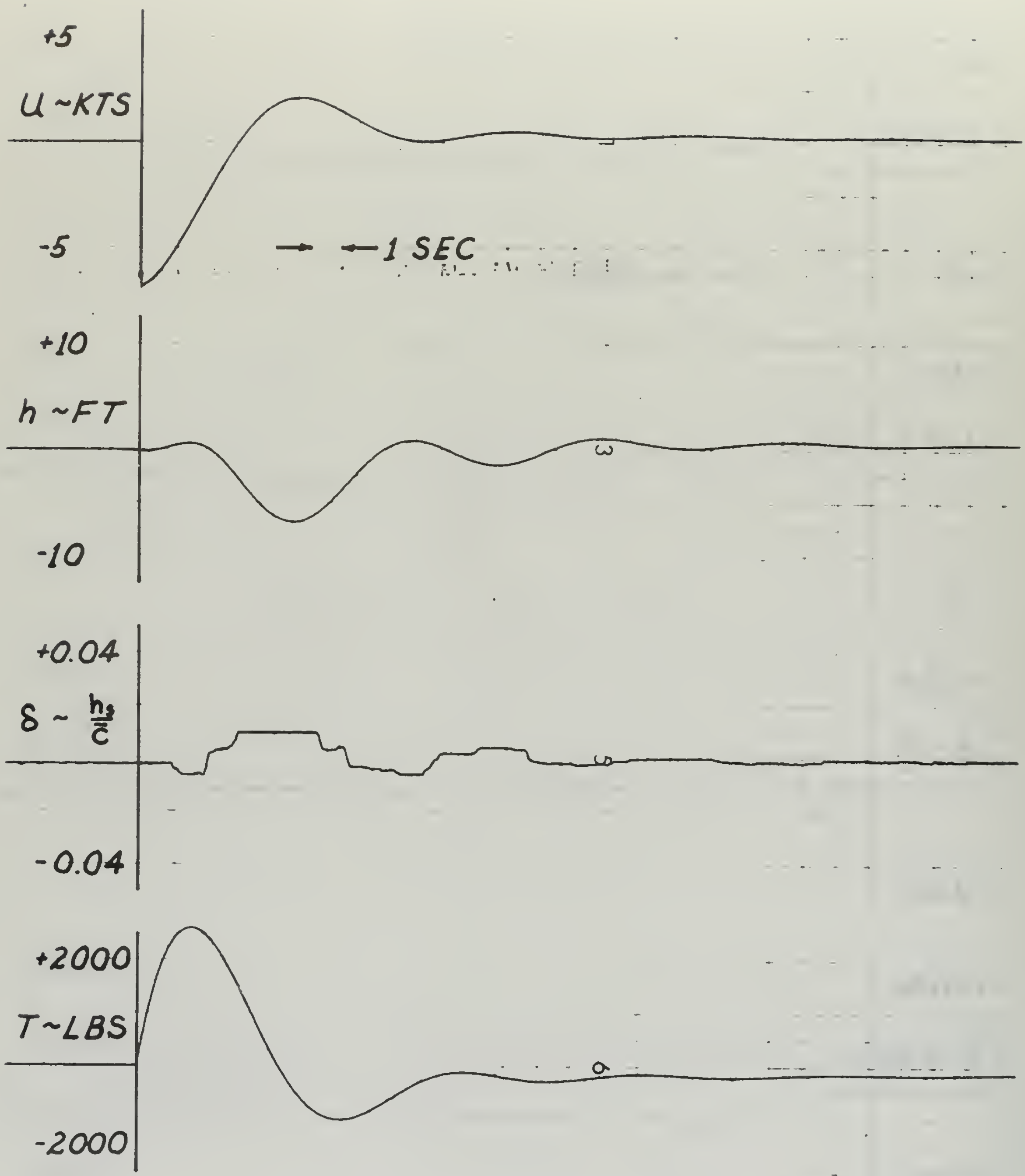

FIGURE 72
APC + MANUAL SPOILERS
RESPONSE TO 5 KT TAIL GUST

APPENDIX

DETERMINATION OF LOOP GAINS FOR AUTOMATIC SYSTEMS

APC

For the purpose of determining approximate loop gains, the inner loop of the APC system was first analyzed independently of the rest of the system. Referring to Figure 12, a simplified inner loop was constructed, Figure 73.

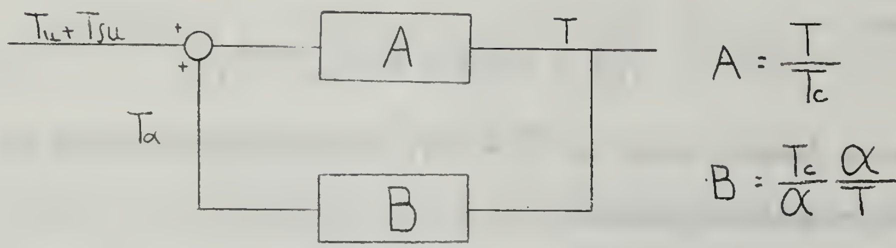

FIGURE 73

Inner Loop, APC System

From Figure 73, using the short period assumption for the α loop,

$$T_c = \frac{T}{A}$$

$$TB = T_\alpha$$

$$T_\alpha + T_u + T_{ju} = T_c$$

Combining these three equations yielded

$$T_u + T_{ju} + TB = \frac{T}{A}$$

Replacing A and B by their respective transfer functions from Table VIII and neglecting the engine time lag in order to reduce the characteristic equation to an easily handled second order function,

$$\frac{T}{T_u + T_{\zeta u}} = \frac{s^2 + 0.806s + 1.281}{s^2 + 0.806s + 1.281 + 4.55\times10^{-6} K_\alpha}$$

The characteristic equation is then,

$$s^2 + 0.806s + 1.281 + 4.55\times10^{-6} K_\alpha = 0$$

from which,

$$2\zeta\omega_n = 0.806$$

and

$$\omega_n^2 = 1.281 + 4.55\times10^{-6} K_\alpha$$

For a damping ratio of ζ = 0.5, simultaneous solution of these two equations yielded,

$$K_\alpha = -1.485\times10^{5}\ \text{lbs/rad}$$

The inner loop of the APC system was then reduced to the single transfer function below.

$$\frac{T}{T_{\zeta u} + T_u} = \frac{s^2 + 0.806s + 1.281}{s^2 + 0.806s + 0.65}$$

For the analysis of the overall loop, $T_{\zeta u}$ was neglected since it is small compared to T_u. A simplified loop, derived from Figure 12, was used for the analysis. The simplified loop is shown in Figure 74.

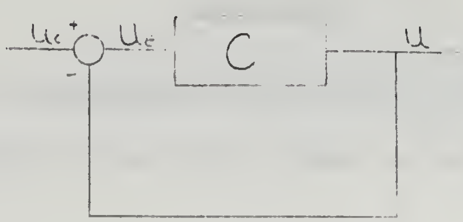

$$C = \frac{T_c}{u_e}\,\frac{T}{T_u}\,\frac{u}{T}$$

FIGURE 74
Outer Loop, APC System

Using the phugoid assumption for $\frac{u}{T}$, the simplified transfer function for the APC was derived in the following manner,

$$u_e = \frac{u}{C}$$

$$u_c - u = u_e$$

The result of combining these two equations was,

$$\frac{u}{u_c} = \frac{1}{1 + C}$$

Insertion of values for the transfer functions in C from Table VIII and from the inner loop analysis gave

$$\frac{u}{u_c} = \frac{.00145K_u s^3 + .00117K_u s^2 + .00186 s}{s^4 + (.866 + .00145K_u)s^3 + (.743 + .00117K_u)s^2 + (.068 + .00186K_u)s + .023}$$

from which the characteristic equation is

$$s^4 + (.866 + .00145K_u)s^3 + (.743 + .00117K_u)s^2 + (.068 + .00186K_u)s + .023 = 0$$

A digital computer program was used to make a root locus plot of the characteristic equation, Figure 15. From this plot, for a damping ratio of 0.5, an estimate for K_u of 42 lb sec/ft was found.

DLC

The DLC system was analyzed in a manner similar to the above. The short period assumption was used throughout and the integration loop was neglected. The simplified inner loop block diagram, taken from Figure 13, is shown in Figure 75.

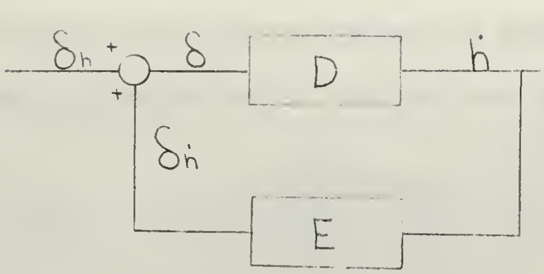

$$D = \frac{\dot h}{\delta} \qquad E = \frac{\delta_{\dot h}}{\dot h}$$

FIGURE 75

Inner Loop, DLC System

From Figure 75, the following analysis was made

$$\delta = \frac{\dot h}{D}$$

$$\delta_{\dot h} = \dot h E$$

$$\delta_h + \delta_{\dot h} = \delta$$

These three equations were combined to form

$$\frac{\dot h}{\delta_h} = \frac{D}{1 - DE}$$

Incorporation of numerical values from Table VIII for D and E resulted in,

$$\frac{\dot h}{\delta} = \frac{234(.36\Delta^2 + .134\Delta + .41}{\Delta^3 + (.806 - 84.3K_{\dot h})\Delta^2 + (1.281 + 31.4K_{\dot h})\Delta - 96K_{\dot h}}$$

From this, the inner loop characteristic is

$$\Delta^3 + (.806 - 84.3K_{\dot h})\Delta^2 + (1.281 + 31.4K_{\dot h})\Delta - 96K_{\dot h} = 0$$

The root locus plot for this characteristic equation is found in Figure 16. For a damping ratio of 0.8, the resulting $K_{\dot h}$ was found to be -0.003 sec/ft. The resulting transfer function for the inner loop is

$$\frac{\dot h}{\delta_h} = \frac{234(.36\Delta^2 + .134\Delta + .41)}{\Delta^3 + 1.06\Delta^2 + 1.38 + .288}$$

The simplified block diagram for the DLC system was derived from Figure 13 and is shown in Figure 76.

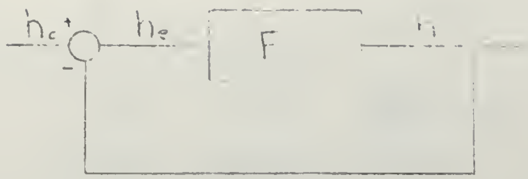

$$F = \frac{\delta_h}{h_e}\,\frac{\dot{h}}{\delta_h}\,\frac{h}{\dot{h}}$$

FIGURE 76

Outer Loop, DLC System

Analysis of Figure 76 yielded

$$h_e = \frac{h}{F}$$

$$h_c - h = h_e$$

from which

$$\frac{h}{h_c} = \frac{F}{1+F}$$

The transfer function for the DLC system is then,

$$\frac{h}{h_c} = \frac{234\,K_h(.36s^2+.134s+.41)}{s^4+1.06s^3+(1.38+84.3K_h)s^2+(.288+31.4K_h)s+96K_h}$$

from which the characteristic equation is

$$s^4+1.06s^3+(1.38+84.3K_h)s^2+(.288+31.4K_h)s+96K_h = 0$$

Root locus analysis of this function yielded a value of 0.005 for K_h .

PCS

Figure 77 shows the block diagram for the simple Pitch Control System. This system was used to demonstrate the lack of feasibility of conventional elevator, without speed control, as a means of automatic glide slope control.

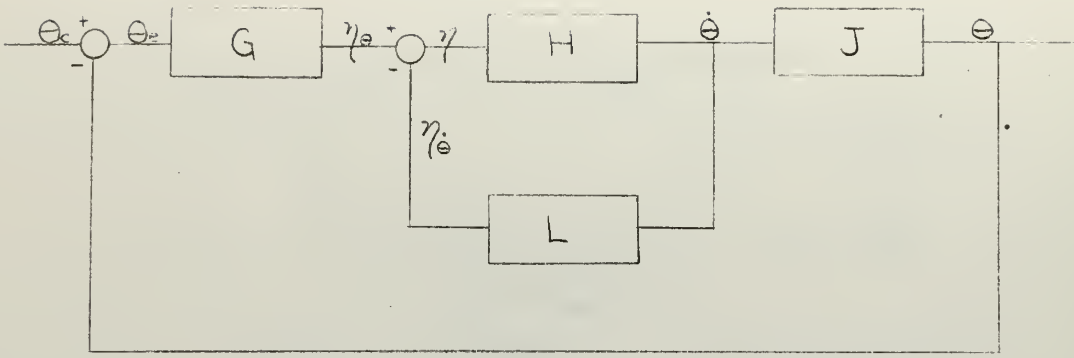

$$G = K_\theta \qquad L = K_{\dot{\theta}} \qquad H = \frac{\dot{\theta}}{\eta} \qquad J = \frac{\theta}{\dot{\theta}}$$

FIGURE 77

Simplified PCS System

Using the short period assumption for $\frac{\dot{\theta}}{\eta}$, the following analysis was made

$$\begin{bmatrix} s - Z_w & -s \\ -U(M_w + sM_{\dot{w}}) & s^2 - M_q s \end{bmatrix} \begin{bmatrix} \alpha \\ \theta \end{bmatrix} \quad \begin{bmatrix} \frac{Z_\eta}{U} \\ M_\eta \end{bmatrix} \Big[\eta \Big]$$

from which

$$\frac{\theta}{\eta} = \frac{-(2.25 s + .867)}{s(s^2 + .806 s + 1.281)}$$

and

$$\frac{\dot{\theta}}{\eta} = \frac{s\theta}{\eta} = \frac{-(2.25 s + .867)}{s^2 + .806 s + 1.281}$$

Referring to Figure 77, the inner loop transfer function is

$$\frac{\dot{\theta}}{\eta_\theta} = \frac{H}{1 + HL}$$

from which

$$\frac{\dot{\theta}}{\eta_\theta} = \frac{-(2.25 s + .867)}{s^2 + (.806 + 2.25 K_{\dot{\theta}}) s + (1.281 - .867 K_{\dot{\theta}})}$$

The characteristic equation for the inner loop is

$$s^2 + (.806 + 2.25 K_{\dot{\theta}}) s + (1.281 - .867 K_{\dot{\theta}}) = 0$$

From the characteristic equation,

$$\omega_n^2 = 1.281 - .867\,K_{\dot\theta}$$
$$2\zeta\omega_n = .806 - 2.25\,K_{\dot\theta}$$

When these two equations were combined, the result was a quadratic equation in $K_{\dot\theta}$.

Solution of this equation yielded,

$$K_{\dot\theta} = +.989,\ -.667 \text{ (dimensionless)}$$

Returning to the characteristic equation, it was seen that, for the system to be stable,

$$.806 - 2.25\,K_{\dot\theta} > 0$$

and

$$1.281 - .867\,K_{\dot\theta} > 0$$

These two inequalities imply that

$$K_{\dot\theta} < .36$$

Therefore the correct value for $K_{\dot\theta}$ is -0.677. The resulting transfer function for the $\dot\theta$ loop is,

$$\frac{\dot\theta}{\eta} = \frac{-(2.25s + .867)}{s^2 + 2.326s + 1.858}$$

Also

$$\frac{\theta}{\eta} = \frac{-(2.25s + .867)}{s(s^2 + 2.326s + 1.858)}$$

The simplified block diagram for the PCS outer loop is shown in Figure 78.

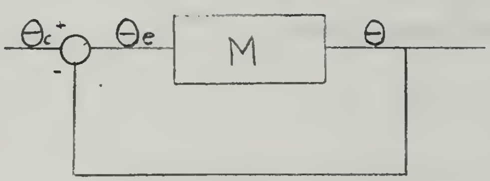

$$M = \frac{\eta}{\theta_e}\frac{\theta}{\eta} = K_\theta \frac{\theta}{\eta}$$

FIGURE 78

Simplified Block Diagram, PCS Outer Loop

Analysis of this loop yielded the result,

$$\frac{\Theta}{\Theta_c} = \frac{1}{1+M}$$

from which

$$\frac{\Theta}{\Theta_c} = \frac{-(2.25 K_\Theta s + .867 K_\Theta)}{s^3 + 2.326 s^2 + (1.858 - 2.25 K_\Theta) s - .867 K_\Theta}$$

The characteristic equation is

$$s^3 + 2.326 s^2 + (1.858 - 2.25 K_\Theta) s - .867 K_\Theta = 0$$

The root locus analysis of this characteristic function resulted in the choice of $K_\Theta = -1.3$ for a damping ratio of $\zeta = 0.5$. The root locus plot for the outer loop of the PCS system is shown in Figure 79.

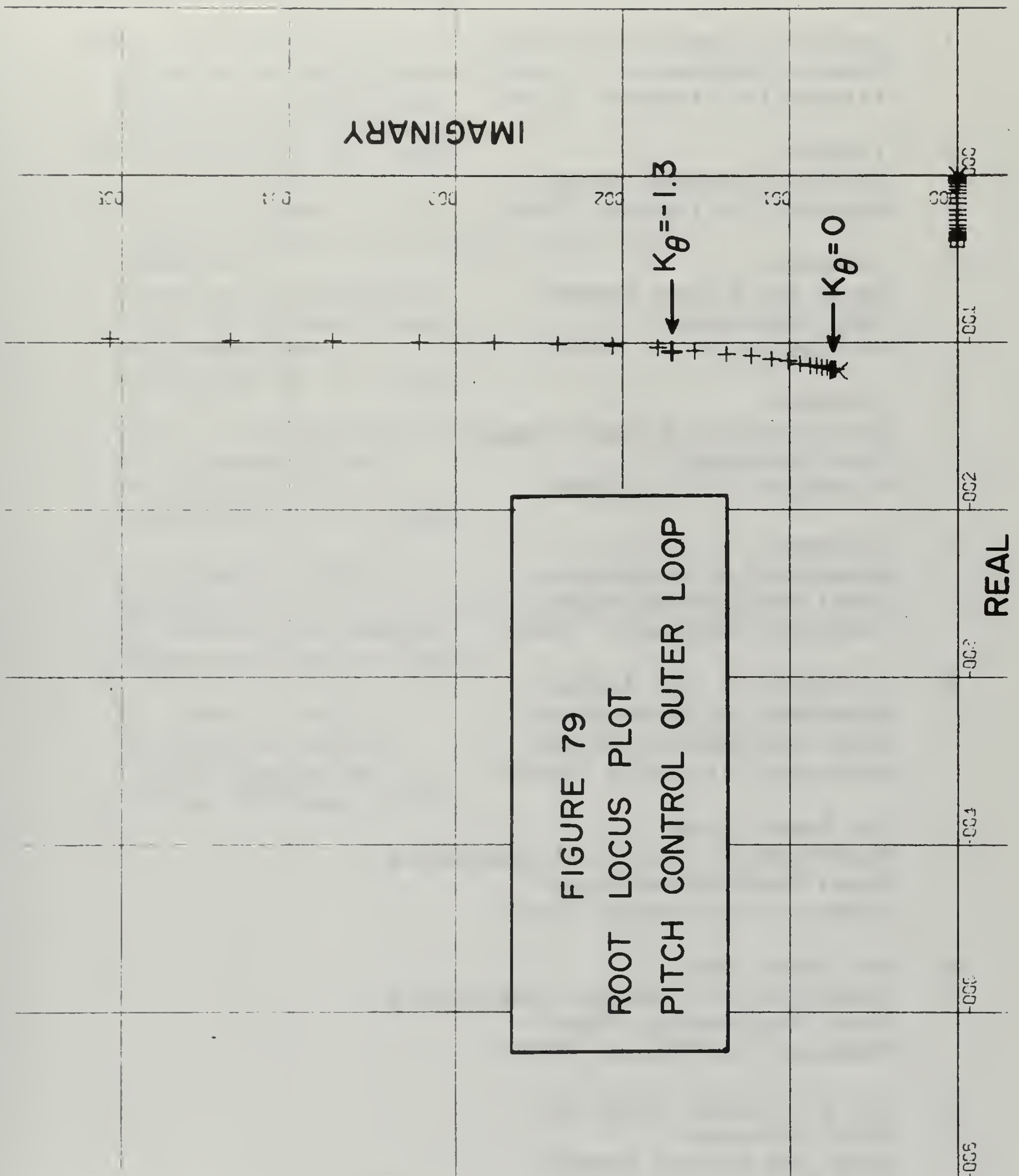

FIGURE 79
ROOT LOCUS PLOT
PITCH CONTROL OUTER LOOP

INITIAL DISTRIBUTION LIST

		No. Copies
1.	Defense Documentation Center Cameron Station Alexandria, Virginia 22314	20
2.	Library Naval Postgraduate School Monterey, California 93940	2
3.	Commander Naval Air Systems Command Navy Department Washington, D. C. 20360	1
4.	Commander Naval Ordnance Systems Command Navy Department Washington, D. C. 20360	1
5.	Chairman Department of Aeronautics Naval Postgraduate School Monterey, California 93940	3
6.	Professor E. John Andrews Department of Aeronautics Naval Postgraduate School Monterey, California 93940	1
7.	Mr. Robert Limes Department of Electrical Engineering Naval Postgraduate School Monterey, California 93940	1
8.	Dr. George Rahe Department of Electrical Engineering Naval Postgraduate School Monterey, California 93940	1
9.	Dr. E. S. Lamar (Code 03C) Chief Scientist Naval Air Systems Command Navy Department Washington, D. C. 20360	1

10. Dr. F. I. Tanczos (Code 03B) 1
Naval Air Systems Command
Navy Department
Washington, D. C. 20360

11. Mr. G. L. Desmond 1
Aerodynamics and Structures Admin. (Code 320)
Research and Technology
Naval Air Systems Command
Washington, D. C. 20360

12. Mr. K. G. Orman 1
Command Control and Guidance Administrator
(COde 360)
Research and Technology
Naval Air Systems Command
Navy Department
Washington, D. C. 20360

13. Office of Naval Research 1
Air Programs Office
Navy Department
Washington, D. C. 20360

14. Lt. Robert C. Lloyd 6
VA-125
U. S. Naval Air Station
Lemoore, California 93245

15. Lt. James K. Swift 6
c/o Mr. E. E. Klebba
1710 Nottingham Rd.
Lansing, Michigan 48910

DOCUMENT CONTROL DATA - R & D

Security classification of title, body of abstract and indexing annotation must be entered when the overall report is classified)

1 ORIGINATING ACTIVITY (Corporate author)

Naval Postgraduate School
Monterey, California 93940

2a. REPORT SECURITY CLASSIFICATION

Unclassified

2b. GROUP

3 REPORT TITLE

Analog Simulation of Automatic Glide Slope Control Using Wing Lift Spoilers as Direct Lift Control

4 DESCRIPTIVE NOTES (Type of report and inclusive dates)

Aeronautical Engineer Thesis, June 1968

5 AUTHOR(S) (First name, middle initial, last name)

Robert C. Lloyd
James K. Swift

6. REPORT DATE	7a. TOTAL NO. OF PAGES	7b. NO. OF REFS
June 1968	146	19

8a. CONTRACT OR GRANT NO.	9a. ORIGINATOR'S REPORT NUMBER(S)
b. PROJECT NO	
c.	9b. OTHER REPORT NO(S) (Any other numbers that may be assigned this report)
d.	

10. DISTRIBUTION STATEMENT

[redacted]

11. SUPPLEMENTARY NOTES	12. SPONSORING MILITARY ACTIVITY
	Naval Postgraduate School Monterey, California 93940

13. ABSTRACT

The use of wing lift spoilers as a means of changing lift without changing angle of attack was studied for use in the landing approach task. The vehicle used was the F-8 type fighter. Automatic glide slope controllers were proposed using an elevator glide slope coupler in conjunction with an automatic power compensator for comparison with an automatic direct lift control system. The system gains were optimized for gust disturbances and initial offsets from glide slope. An analog computer simulation program including a manual control phase was used to determine arbitrary measures of effectiveness of the proposed systems.

14 KEY WORDS	LINK A		LINK B		LINK C	
	ROLE	WT	ROLE	WT	ROLE	WT
Automatic Glide Slope Control						
Direct Lift Control						
Glide Slope Control						
Lift Control						
Wing Lift Spoilers						

DD FORM 1 NOV 65 1473 (BACK)
S/N 0101-807-6821

A-31409

[redacted]